1976

Electron Impact Excitation Studies in Rare Gases

Kim Hwa Tan
University of Windsor

1976

Electron Impact Excitation Studies in Rare Gases

Kim Hwa Tan
University of Windsor

29239

National Library of Canada | Bibliothèque nationale du Canada | CANADIAN THESES ON MICROFICHE | *THÈSES CANADIENNES SUR MICROFICHE*

NAME OF AUTHOR/*NOM DE L'AUTEUR* Kim Hwa Tan

TITLE OF THESIS/*TITRE DE LA THÈSE* Electron impact excitation studies in rare gases

UNIVERSITY/*UNIVERSITÉ* University of Windsor, Windsor, Ontario

DEGREE FOR WHICH THESIS WAS PRESENTED/ *GRADE POUR LEQUEL CETTE THÈSE FUT PRÉSENTÉE* Ph.D.

YEAR THIS DEGREE CONFERRED/*ANNÉE D'OBTENTION DE CE DEGRÉ* 1976

NAME OF SUPERVISOR/*NOM DU DIRECTEUR DE THÈSE* Dr. J. W. McConkey

Permission is hereby granted to the NATIONAL LIBRARY OF CANADA to microfilm this thesis and to lend or sell copies of the film.

The author reserves other publication rights, and neither the thesis nor extensive extracts from it may be printed or otherwise reproduced without the author's written permission.

L'autorisation est, par la présente, accordée à la BIBLIOTHÈQUE NATIONALE DU CANADA de microfilmer cette thèse et de prêter ou de vendre des exemplaires du film.

L'auteur se réserve les autres droits de publication; ni la thèse ni de longs extraits de celle-ci ne doivent être imprimés ou autrement reproduits sans l'autorisation écrite de l'auteur.

DATED/*DATÉ* May 7th, 1976 SIGNED/*SIGNÉ* K. Tan

PERMANENT ADDRESS/*RÉSIDENCE FIXÉ* 1775 McKay Ave. Windsor, ONTARIO.
N9B 3P3

NL-91 (11-73)

ELECTRON IMPACT EXCITATION STUDIES IN RARE GASES

by

Kim Hwa Tan

A Dissertation
submitted to the Faculty of Graduate Studies
through the Department of
Physics in Partial Fulfillment
of the requirements for the Degree
of Doctor of Philosophy at
The University of Windsor

Windsor, Ontario, Canada

1976

Approved by,

Dr. J. W. McConkey
(Chairman)

Dr. R. Helbing

Dr. A. van Wijngaarden

TO MY WIFE AND PARENTS

ABSTRACT

Absolute cross-sections for electron impact excitation of the 4s, 4s', 5s, 3d, 4d, 3d' and 4d' configurations of Ar^+ from the ground state of Ar are presented by studying the vacuum UV photon decay of the states. Polarization free measurements were achieved by orientating the exciting electron beam at an angle of 55° to the optic axis of the detecting monochromator and at 45° to the plane containing the entrance slit and the optic axis. Absolute intensity calibration was achieved using the well known resonance lines of He and Ne as standards.

The high energy behavior of the excitation functions demonstrated the two electron nature of the excitation. Where cascade could be satisfactorily taken into account, excitation of states with the same orbital angular momentum and multiplicity is according to their statistical weights. Some significant discrepancies are exposed between theoretically calculated and experimentally measured relative transition probabilities. Configuration interaction effects are demonstrated to exist and in a number of instances are quantitatively investigated.

Electron - photon angular correlations and polarization correlations were measured for He and Ar atoms in the 2^1P and $4s'\ ^1P_1 + 4s\ ^3P_1$ states respectively. The ratio of the differential cross-sections for exciting the degenerate magnetic sublevels, λ , and the relative phase of the corresponding excitation amplitudes, $|\chi|$, for various incident electron energies and for electrons scattered at an angle of 42^o have been obtained. A co-axial cylindrical energy analyser and a double reflection vacuum UV polarizer were developed for this experiment.

ACKNOWLEDGEMENTS

It is a pleasure to acknowledge the constant guidance and supervision of Dr. J. W. McConkey throughout the entire period of this work, and in the preparation of the manuscript.

I would also like to thank Dr. A. Crowe, Dr. J. Fryar, Dr. P. S. Farago, Dr. P. J. O. Teubner and Mr. G. Allcock for their help and many useful discussions.

The financial support from Windsor University, which made this study possible, is gratefully acknowledged. The equipment used was purchased with the aid of grants from the National Research Council of Canada.

TABLE OF CONTENTS

LIST OF TABLES

LIST OF FIGURES

INTRODUCTION

Polarization free measurements of the vacuum U-V excitation cross sections of the atmosphere gases by electron impact have been carried out in this laboratory for several years.

Experimental and theoretical studies of excitation and ionization of atoms by electron impact is partly motivated by requirements for cross section data in laser physics, plasma physics, atmospheric physics and astrophysics. Excitation of Ar by electron impact in the vacuum U-V is especially interesting in that a wide range of physical phenomena may be observed. Associated experiments in this laboratory have looked at structure in the total ionization cross section of argon by electron impact, Ar^+ ion angular distributions following the ionization process, autoionization effects, differential elastic scattering and excitation of the resonance lines.

The present study is divided into two parts. In one we report measurements made on the excitation of the argon atom to various configurations of the ion and particular attention is paid to the role of configuration interaction in this

process and to associated cascade processes. Absolute apparent cross sections for electron impact excitation are presented and should be valuable in clarifying the relative importance of various processes occurring in the Ar^+ laser and also for calibration purposes in vacuum U-V spectroscopy. In addition, the measurements provide much important new data on relative transition probabilities. This should be a stimulus to theoreticians to improve on existing rather inaccurate calculations.

In the second part we report coincidence measurements involving inelastically scattered electrons and emitted photons. These measurements are used to obtain individual scattering amplitudes for exciting the different magnetic sublevels of the excited state as well as the phase between the corresponding excitation amplitudes. These collision parameters of the electron atom excitation can be linked with the orientation and alignment parameters of the excited atom. A special cylindrical mirror analyser was developed for this work together with a special U-V polarizer. This type of data provides the most sensitive test of current theories of atomic excitation.

PART I

Simultaneous Ionization And Excitation Of Ar By Electrons.

CHAPTER I

Review Of Previous Work

This review will give a short account of the experimental and theoretical work done by different workers on the excitation and ionization of Ar by electron impact, including cross-section measurements, the cascading problem, life time measurements, transition probability determinations and configuration-interaction effects. The main emphasis will be on discussion of the results obtained, the discrepancies between different workers and on comparison with theories.

I. Excitation of Ar^+

Figure 1.1 is a simplified term diagram of Ar^+, the excited states of Ar^+ combine optically with the $3s^2\ 3p^5$ ground state of Ar^+ yielding radiation in the vacuum U-V spectral region below 1000 Å. The first excited state of Ar^+ is the $3s3p^6\ ^2S_{\frac{1}{2}}$ level, corresponding to the ejection from the ground state ($3s^2\ 3p^6$) atom of an inner shell 3s electron. This state combines with both of the ionic ground states ($3s^2\ 3p^5\ P_{\frac{1}{2}}, {}_{\frac{3}{2}}$) and the transitions yield radiation at 920Å and 932 Å. The excitation of the higher excited states of Ar^+ involves an outer shell ionization and excitation process involving two electrons. The present work deals with this later type of process. There have been no previous vacuum U-V measurements of these states reported. Some of them are however,

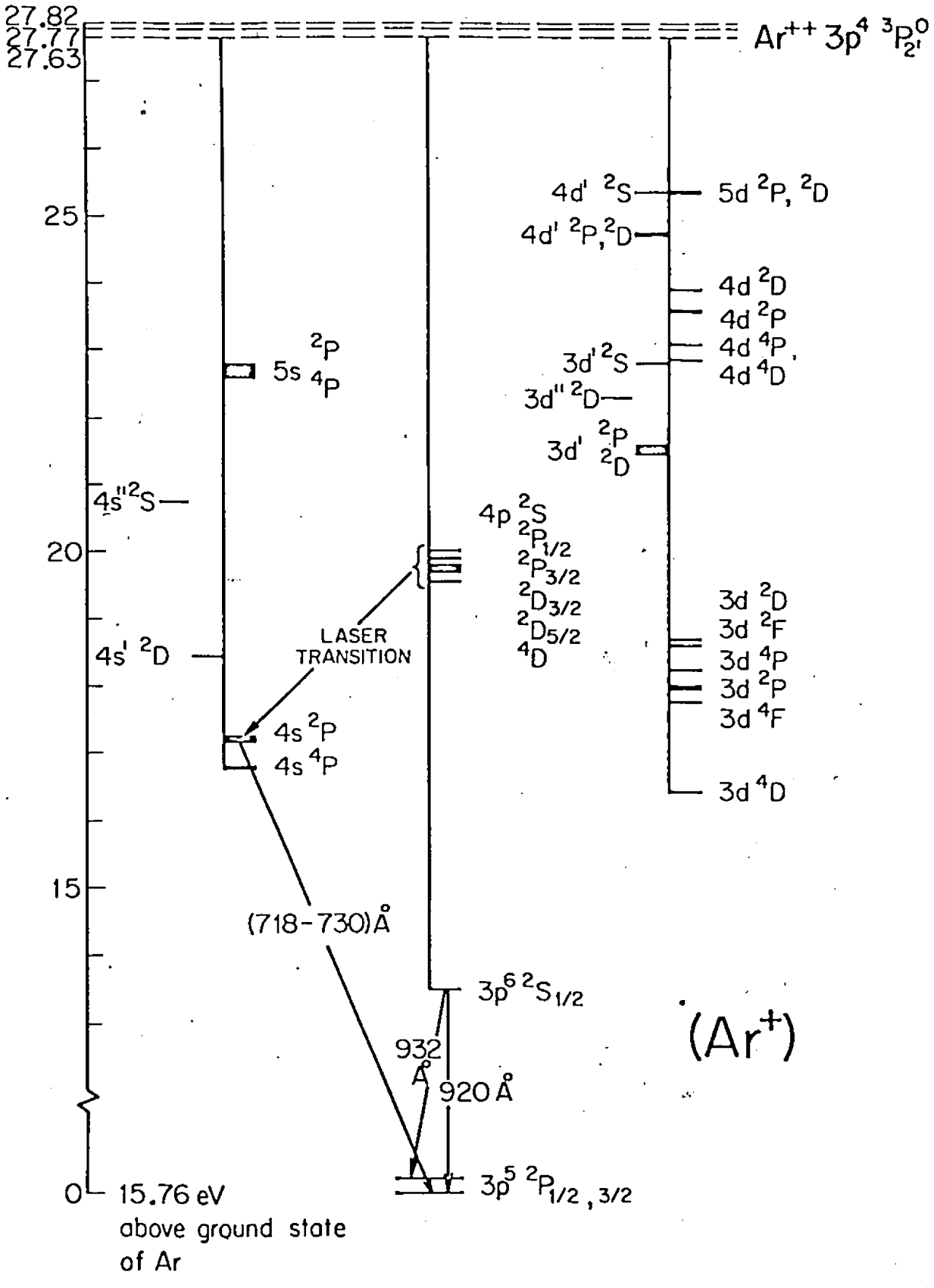

Fig.1.1 Simplified level diagram of Ar^+ illustrating some of the levels observed in the present work.

accessible due to their radiation in the visible and so a brief review of such measurements, and associated ones which help clarify cascade contributions, is given below.

(A) Excitation of the $3s^2\ 3p^4\ 4p$ Levels

Cross-section measurements on the excitation of the 4p level from the ground state of the atom have been done by Feltsan and Porch (1970) who measured all the relevant lines, by Latimer and St. John (1970) and Clout and Heddle (1971) who measured most of the laser transitions, and by Bennett et al (1966). Imre et al (1972) measured the excitation of the 4P levels by the direct collision of electrons with ground state argon ions, and show that the efficiency of excitation of the Ar II laser lines by slow electrons from the ground state of the ion is more than 15 times higher than the maximum efficiency of excitation of the same lines from the ground state of the neutral atom. There is considerable disagreement among the different groups regarding the absolute magnitudes of the cross-sections, but there is agreement on the shapes of the excitation functions and on the existence of a double maximum in many of them. The double peak appears in the excitation of the doublet but not the quartet levels, and the relative magnitudes of the two peaks vary considerably depending on the particular level being excited. For most lines having initial

^2P_J levels ($J=\frac{1}{2}, \frac{3}{2}$) the value of the second maximum is larger than the first maximum. For the remaining doublet lines, the second maxima are significantly weaker than the first ones. Theoretical estimates of the 4p level cross-sections have been made by Koozekanani using the sudden approximation. Serious discrepancy exist between the sudden approximation and the results obtained by Latimer and St. John (1970). For 4p ^2P_J ($J=\frac{1}{2}, \frac{3}{2}$) levels. Latimer and St. John showed that in the energy range 250 to 700 eV the cross-section varies approximately as E^{-1}. This is in disagreement with the sudden approximation which implies that the cross-section should fall off as $^{\ln E}/_{E}$ similar to the single-ionization cross-section. One would expect that the population of different J levels should be in accordance with their statistical weights. Koozekanani (1967) showed that for the $4p\,^2P_J$ levels with $J=\frac{1}{2}$ and $\frac{3}{2}$, the level cross-section divided by the degeneracy (2J+1) should be a constant, Latimer and St. John and Clout and Heddle's results bear out his prediction, and it is also true for the $4p\,^2D_J$ levels with $J=\frac{5}{2}$ and $\frac{3}{2}$.

(B) Previous Work on Branching Ratios:

In order to estimate cascading contributions and to calculate the cross-section of the level of interest, it is essential to know accurately the branching ratio of each of

the transitions. Branching ratios have been studied extensively by Rudko and Tang (1967) and Statz et al (1965) who calculated the transition probabilities of most of the lower configurations of Ar II using an intermediate coupling method. Most recently, Luyken (1972) using a multi-configuration model investigated the influence of configuration interaction, especially between members of the $3s^2\ 3p^4$ nd series, on the transition probabilities. Experimental measurements have been done by Bennett et al (1965) and Bakos et al (1966) who measured the life-times of the states. Line strengths measurements have been made by Olsen (1963) using the thermal arc plasma as a radiation source. Recently, Shumaker and Popenoe (1969) have measured in emission, the transition probabilities of the 4s-4p and 3d-4p transitions of Ar II.

The individual A coefficients calculated by Statz et al were not accurate, a few of the calculated branching ratios for the 4p → 4s transitions were off by a factor as large as 10 from the experimental measurements. Their calculated radiative lifetimes for the 4p states are reasonably good but the results did not include small contributions due to the 4P → 3d transitions. Rudko and Tang modified the calculation and included these corrections which for some of the quartet states, are not negligible. In the case of the 4p → 4s transitions, nearly all the calculated branching ratios are within 30% of

the measured values with the worst cases off by a factor of two. The greatest improvement of Rudko and Tang's calculations over earlier ones occurs in those cases involving weaker transitions. For the stronger transitions they obtained only slightly better agreement with the measured results. In the theoretical work of Rudko and Tang and of Statz et al, difficulties had been encountered with the 4p → 3d transitions, where large deviations from experimental values had been found. In most cases theoretical values were much higher (30-100%). The origin of this was understood by Luyken in terms of the large mixing between the $3p^4$ nd configurations. His results for the 4p → 3d transition are closer to the experimental values than any other theoretical values. However, the 4p → 4s transitions turned out to be not very sensitive to the improvements in the wave functions. He also overcame the large discrepancy between the measured and earlier calculated lifetime of the $3s3p^6\ ^2S_{\frac{1}{2}}$ state. This state is known to interact strongly with the $3s^2\ 3p^4$ nd $^2S_{\frac{1}{2}}$ states, in particular where n=3 and 4.

II. Configuration Interaction Effects.

Configuration interaction effects in the argon ion were first pointed out by Minnhagen (1963) in the course of a detailed investigation of ArII spectrum. Very strong

interaction was demonstrated to exist between the $3s3p^6\ ^2S_{\frac{1}{2}}$ and the $3s^2\ 3p^4\ nd'\ ^2S_{\frac{1}{2}}$ terms, in particular for n=3 and 4. It was tested later by Kjollerstrom, Moller and Svensson (1965) who carried out a theoretical investigation of the magnitudes of the electrostatic interaction integrals by means of wave functions derived from the Thomas - Fermi - Dirac statistical model of the atom. Their calculations showed that a very strong $3p^6\ ^2S - 3s^2 3p^4\ nd'\ ^2S$ interaction exists. Luyken (1972) in a study of the transition probabilities and radiative lifetimes for Ar II, analyzed this effect theoretically and showed that the wavefunction expansion of the $3s\ 3p^6\ ^2S_{\frac{1}{2}}$ state contained large contributions from $3s^2\ 3p^4\ 3d'\ ^2S_{\frac{1}{2}}$ and $3s^2\ 3p^4 4d'\ ^2S_{\frac{1}{2}}$ states, as well as small contributions from 10 other states. This mixing largely effects the lifetime of the $3s3p^6\ ^2S_{\frac{1}{2}}$ state. Therefore the $3s3p^6\ ^2S_{\frac{1}{2}}$ state does not uniquely correspond to the physical picture of a hole in the 3s shell. He has also demonstrated that the states of the $3s^2\ 3p^4\ 3d$ configuration mix strongly with states of higher $3s^2\ 3p^4$ nd configurations. This interaction induces a transfer of oscillator strength from the $3s^2\ 3p^4\ 3d$ to higher members of the same series. This effect can-not be neglected in any calculation of transition probabilities, where this configuration is involved. Luyken et al (1972) measured the cross-section for the excitation of $3s3p^6\ ^2S_{\frac{1}{2}}$ state by electron

impact in the energy range between the threshold and 20 keV by observing the radiative decay of the state in the vacuum U.V. They found that their results were consistent with Luyken's calculations and agree well with the theoretical values of the McGuire and Manson and Cooper namely that 40% of the oscillator strength is transferred to $3s^2\ 3p^6 - 3s^2\ 3p^4$ nd' transitions.

Weigold, Hood and Teubner (1973, 74) and Williams (1974) have observed the effect of configuration interaction in coincidence studies of the scattered and ejected electrons when argon is ionized by electron impact. The former group were unable to resolve the 3d' $^2S_{\frac{1}{2}}$ and the 4d' $^2S_{\frac{1}{2}}$ states. They found that the relative cross sections for the sum of 3d' and 4d' states and $3s3p^6$ state are 0.42 ± 0.04 and 0.58 ± 0.04 respectively. J. Williams (1974) has succeeded in resolving the 3d' and 4d' states in an e, 2e experiment similar to that of Weigold et al. He finds the contributions from the two states to be of comparable intensity and also observes some excitation of $3s^2\ 3p^4\ 4s'\ ^2S_{\frac{1}{2}}$ indicating configuration mixing with this state also. His estimated relative cross-section for $3s3p^6$, $3s^2\ 3p^4\ 3d'$ and $3s^2\ 3p^4\ 4d'$ are in the ratio 1.0: 0.4: 0.4 in rather good agreement with Weigold et al (1974).

Recently, Spears, Fischbeck and Carlson (1974) have

studied the photoionization of argon by using X-rays. They found that in addition to the main photoelectron peaks there appears satellite structure at slightly lower energy due to the same configuration interaction effects. Their measurements suggest that only 20% of the strength of 3s hole state was due to configuration mixing with 3d' and 4d' higher states. Luyken's calculations predicted 38%, Weigold et al found 42% and William's results give 43%. The discrepancies between theory and experimental data of different workers are significant. Spears et al found that the cross-sections of the 3d' and 4d' states depended slightly on X-ray energy. From Luyken's calculations the relative cross-sections for $3s\,3p^6$, $3p^4\,3d'$ and $3p^4\,4d'$ are 1.00: 0.50: 0.11. The small 4d' cross-section suggest that the mixing with the 4d' level is rather small. More refined calculations of the mixing of the states is essential, and hopefully more refined experimental methods such as the one discussed in this thesis will be able to reduce the current experimental uncertainties.

CHAPTER II

THEORY

2-1. Bethe - Born Approximation:

Theoretically the inelastic collisions of charged particles with atoms may be conveniently classified into two kinds; the fast collisions and the slow collisions. "Fast" or "Slow" collisions means that the particle velocity is "fast" or "slow" relative to a mean orbital velocity of the atomic electrons in the shell that pertains to the inelastic process under consideration. For sufficiently fast collisions, the influence of the incident particle upon an atom or molecule may be regarded as a sudden and small external perturbation. The incoming and outgoing particles are represented by plane waves, and no coupling involving intermediate states is considered (basis of the Born approximation).

Following the treatments of Inokuti (1971) and Donaldson (1972), the integrated cross-section Q_n for excitation to a specified state n at energy E_n, discrete or continuum, regardless of the angle of scattering of an incident electron, is obtained by integrating the differential cross-section dQ_n (equation 2.14 of Inokuti 1971) over all kinematically possible values of the momentum transfer $\hbar\underline{K}$ ($\underline{K} = \underline{k} - \underline{k}'$)

$$Q_n = \frac{4\pi a_o^2}{E/R} \int_{(Ka_o)^2_{min}}^{(Ka_o)^2_{max}} \frac{f_n(K)}{E_n/R} \frac{d(Ka_o)^2}{(Ka_o)^2} \quad \text{--- (1.1)}$$

where $(Ka_o)^2_{min}$ and $(Ka_o)^2_{max}$ are given by equation (2.17) and (2.18) of Inokuti (1971), E is the incident electron energy, R is the Rydberg constant, a_o is the Bohr radius and $f_n(K)$ is the generalized oscillator strength. It is related to the optical oscillator strength f_n as

$$\lim_{K \to 0} f_n(K) = f_n \quad \text{-----} \quad (1.2)$$

where f_n is defined by

$$f_n = (E_n/R)M_n^2 \quad \text{-----} \quad (1.3)$$

where M_n is the dipole matrix element.

Since the basic theoretical framework for dQ_n assumes sufficiently large E, Bethe (1930) recognized that it is advantageous to express Q_n in terms of an asymptotic expansion in inverse powers of $E = \frac{1}{2} mv^2$. The resulting expression then contains coefficients that are determined uniquely from the generalized oscillator strength $f_n(K)$. Hence for an optically allowed transition, the excitation cross-section of the state n is

$$Q_n = \frac{4\pi a_o^2}{E/R}\left[M_n^2 \ln\left(\frac{4C_n E}{R}\right) + \frac{\gamma_n}{E/R} + O\left(\frac{E_n^2}{E^2}\right)\right] \quad ---(1.4)$$

The leading term is known as the Bethe asymptotic cross-section. ln Cn is a property of the transition to state n and depends upon E_n. The second term signifies the difference between the Born cross-section and the Bethe asymptotic cross-section. For electron-atom collisions γ_n depends on the optical oscillator strength f_n. The sign of γ_n is also negative in the case of optically forbidden transitions for which the cross-section is

$$Q_n = \frac{4\pi a_o^2}{E/R}\left[b_n + \frac{\gamma_n}{E/R} + O\left(\frac{E_n^2}{E^2}\right)\right] \quad ----- \quad (1.5)$$

where

$$b_n = \int_{-\infty}^{\infty} \frac{f_n(K)}{E_{n/R}} d\ln(Ka_o)^2 \quad ----- \quad (1.6)$$

Fano (1954) pointed out that a plot of $Q_n \cdot E$ versus lnE for sufficiently large velocities (where Bethe Theory is applicable) will become a straight line, with a positive

slope proportional to M_n and hence to f_n. If the transition is optically forbidden, then the plot will have zero or negative slope. Hence by using the accepted values of the optical oscillator strength f_n, it is possible to normalize the relative cross-section measurements and put them on an absolute scale. The intercept with the horizontal axis yields a value of C_n which is independent of any normalization procedure. Thus direct comparison between theory and experiment is possible simply by comparing the respective values of C_n.

2-2. The Excitation Cross-Section:

Consider the schematic energy level diagram of Fig. 1.2. The volume rate of production of atoms in state j by electron impact is given by $N_g N_e v Q_j$, where N_g and N_e are the

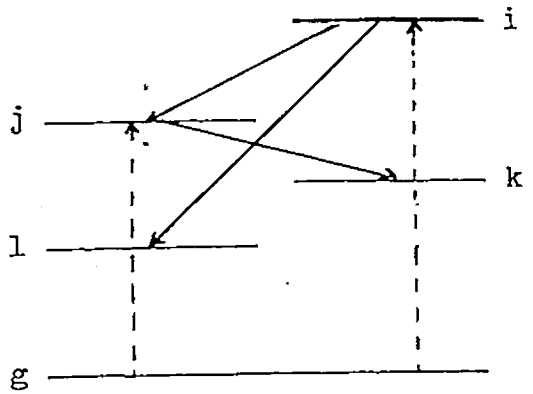

Figure 1.2. Schematic energy level diagram.

concentrations of atoms in the ground state and of electrons, respectively, v is the relative velocity of the electron and atom i.e. essentially the electron velocity and Q_j is the cross-section for excitation of the j^{th} level.

The volume rate of radiative depopulation is $N_j A_j$ where $A_j = \sum_{j>k} A_{jk}$ and A_{jk} is the Einstein transition probability for a spontaneous transition from state j to a lower state k. Cascade transitions populate the state j at a rate $\sum_{i>j} A_{ij} N_i$ where A_{ij} is the radiative transition probability from state i to state j.

We can neglect or eliminate the secondary processes such as collisional population and depopulation and resonance trapping if the following conditions are met. First, the electron beam current strength must be small so that collisions between excited atoms and a beam electron may be neglected (single collision conditions predominate). Secondly, the gas pressure must be so low that collisions between excited and normal atoms, which might lead to transfer of excitation, as well as effects due to imprisonment of resonance radiation, may also be ignored. Therefore it is essential in the experiment that a linear relationship between signal intensity and electron beam current and between signal intensity and gas pressure must be demonstrated in order to indicate that the secondary processes can be neglected.

We then have the rate of production of j-state excited atoms

$$\frac{dN_j}{dt} = N_g Q_j v N_e + \sum_{i>j} A_{ij} N_i - A_j N_j \quad \text{-----} \quad (1.7)$$

In equilibrium $dN_j/dt = 0$, we then have

$$N_g Q_j v N_e + \sum_{i>j} A_{ij} N_i - A_j N_j = 0 \qquad \text{-----} \quad (1.8)$$

In general, radiation corresponding to a particular transition will be observed. If J_{jk} is the rate of emission of photons per unit length of the electron beam corresponding to the transition from state j to state k, then

$$J_{jk} = A_{jk} N_j S \qquad \text{-----} \quad (1.9)$$

where S is the cross sectional area of the electron beam. Combined equations (1.8) and (1.9) and using expression for beam current $I = N_e veS$, we obtained,

$$Q_j = \left[\frac{J_{ik}}{B_{jk}} - \sum_{i>j} J_{ij} \right] / N_g \left(\frac{I}{e} \right) \qquad \text{---} \quad (1.10)$$

where $B_{jk} = A_{jk}/A_j$ is the branching ratio for the observed j-k transition, which can be obtained either from theory or experiment.

Thus by measuring the absolute intensities of the radiation emitted in transitions both to and from the j^{th} state of the atom, the direct excitation cross-section Q_j may be derived.

The cascade contribution to the population of state j can be estimated if the J_{ij} are measured. If the J_{ij} are not known and if the J_{il} are measured, then one can calculate the

J_{ij} by the relationship $J_{ij}=(A_{ij}/A_{il})J_{il}$. Then equation (1.10) transforms to

$$Q_j = \left[\frac{J_{jk}}{B_{jk}} - \sum_{i>j} J_{il}\frac{A_{ij}}{A_{il}}\right]\left[N_g\left(\frac{I}{e}\right)\right]^{-1} \quad ---(1.11)$$

Equation (1.10) may be written as

$$Q_j = Q_{jk}/B_{jk} - \sum_{i>j} Q_{ij} \quad ----- \quad (1.12)$$

where Q_{jk}, is the line cross-section for the j-k transition as defined by $Q_{jk} = J_{jk}/N_g(\frac{I}{e})$ --- (1.13)

If cascade is neglected, then

$$Q_j = Q_{jk}/B_{jk} \quad ----- \quad (1.14)$$

This equation indicates that the intensity of one line only need be determined absolutely to obtain Q_j, provided the branching ratio is known.

Equation (1.12) can also be written as

$$Q_j B_{jk} = Q_{jk}\left[1 - \frac{\sum_{i>j} J_{ij}}{\sum_{j>k} J_{jk}}\right] \quad ----- \quad (1.15)$$

with the assistance of the equations $Q_{ij}/Q_{jk} = J_{ij}/J_{jk}$ and $A_{jk}/A_j = J_{jk}/\sum_{j>k} J_{jk}$. Again Q_j can be deduced if the ratio of the quantities J_{ij}, J_{jk} are obtainable and the transition probabilities are known.

In optical experiments, one usually measures the relative

variation of signal intensity with the electron energy (the excitation function) of the particular line concerned. After the measured cross-section is put on an absolute scale, one obtains the "apparent" cross-section, which must then be corrected for the cascade contribution to give the true cross-section for the line being observed.

2.3. Elimination of Polarization Effects.

A detecting system, such as a monochromator, has different sensitivities to light polarized with its electric vector parallel and perpendicular to its entrance slit. Hence the monochromator can exert a polarizing effect on the light being transmitted such that the observed light intensity is no longer proportional to the cross-section for the transition. The effects of instrumental polarization may be eliminated from optical excitation functions measured perpendicular to the electron beam in the way described by Woolsey and Mc Conkey (1968), or Clout and Heddle (1969).

The polarization of the radiation is defined as

$$P = \frac{I(\parallel) - I(\perp)}{I(\parallel) + I(\perp)} \qquad \text{-----} \quad (1.16)$$

where $I(\parallel)$ and $I(\perp)$ are the photon fluxes per unit solid angle (observed at right angles to the electron beam) with electric vectors parallel and perpendicular to the electron

beam, respectively. The photon flux emitted into unit solid angle in a direction making an angle ϕ with the electron beam direction, for the j-k transition $J_{jk}(\phi)$ is given by.

$$J_{jk}(\phi) = I_{jk}(\parallel)\mathrm{Sin}^2\phi + I_{jk}(\perp)\mathrm{Cos}^2\phi + I_{jk}(\perp) \quad ---(1.17)$$

The total photon flux is then found by summing over all directions.

$$J_{jk} = \int J_{jk}(\phi)\,dW \quad --- \quad (1.18)$$

$$J_{jk} = \left(\frac{8\pi}{3}\right)\left[I_{jk}(\parallel) + 2I_{jk}(\perp)\right] \quad --- \quad (1.19)$$

Therefore the line cross-section Q_{jk} is written as

$$Q_{jk} = \frac{e}{N_g I}\cdot\frac{8\pi}{3}\left[I_{jk}(\parallel) + 2I_{jk}(\perp)\right] \quad --- \quad (1.20)$$

solve equations (1.16), (1.17) and (1.19), we obtained

$$J_{jk}(\phi) = \frac{J_{jk}}{4\pi}\ \frac{1-P\mathrm{Cos}^2\phi}{1-P/3} \quad ----- \quad (1.21)$$

from which it appears that, the effect of polarization of the light can be eliminated if observation is made at a certain angle such that $\mathrm{Cos}^2\phi = 1/3$ i.e., $\phi = 54^\circ\ 44'$. The observed signal is then proportional to $I_{jk}(\parallel)+2I_{jk}(\perp)$ ie to the total emitted intensity.

Following the treatments of Clout and Heddle (1969) we define $k_{\parallel}$ and $k_{\perp}$ to be the sensitivities of the detection system to light polarized with its electric vector parallel and perpendicular to the entrance slit of the monochromator. If the observations are made at an angle ϕ to the electron

beam and if the electron beam is in a plane oriented at an angle ψ to the entrance slit, as shown in Fig. (1.3), then the signal obtained will be

$$S(\phi,\psi)=(I(\parallel)\sin^2\phi+I(\perp)\cos^2\phi)\left[k_{\parallel}\cos^2\psi+k_{\perp}\sin^2\psi\right] + I(\perp)\left[k_{\parallel}\sin^2\psi+k_{\perp}\cos^2\psi\right] \quad \text{-----} \quad (1.22)$$

This leads to

$$S(\phi,\psi)=I(\parallel)\left[k_{\parallel}\cos^2\psi\sin^2\phi+k_{\perp}\sin^2\psi\sin^2\phi\right]+I(\perp)\left[k_{\parallel}(\sin^2\psi+\cos^2\psi\cos^2\phi)+k_{\perp}(\cos^2\psi+\sin^2\psi\cos^2\phi)\right] \quad \text{---(1.23)}$$

In order for the signal measured to be proportional to $I(\parallel)+2I(\perp)$, we require the two terms in the square brackets to be in the ratio of 1:2. For $\phi = 54^{\circ}\ 44'$, this leads to $\sin^2\psi = \frac{1}{2}$, i.e., $\psi = 45^{\circ}$, independent of $k_{\parallel}$ and $k_{\perp}$. Thus by suitable orientation of the electron beam with respect to the monochromator, a signal can be obtained which is proportional to Q_{jk}, free from the effects of the detecting equipment and regardless of the state of polarization of the light.

The apparatus discussed in the present experiment was the first to incorporate a specially oriented exciting beam in this way.

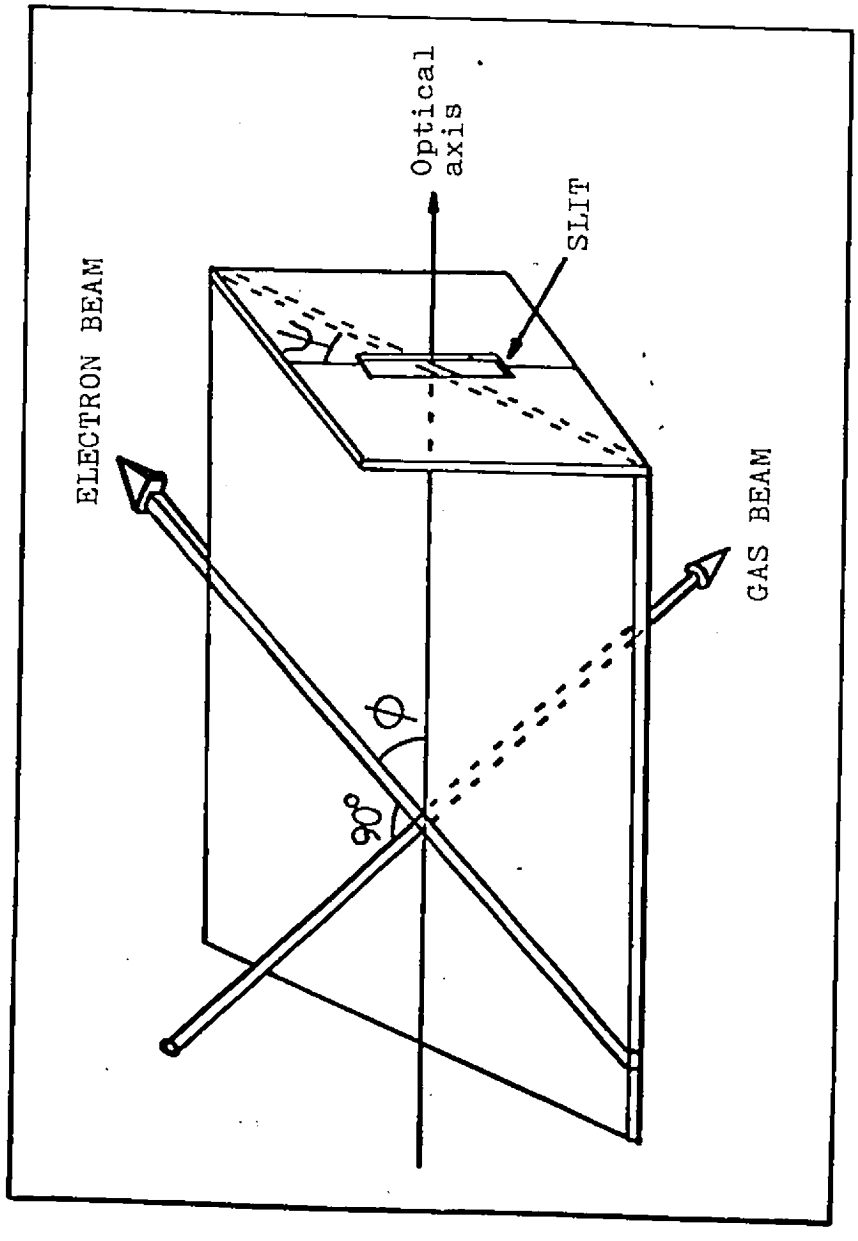

Fig. 1.3. The arrangement of electron beam, gas beam and the monochromator. For polarization free measurement, $\psi = 45^{\circ}$, and $\phi = 54^{\circ}44'$.

CHAPTER III

APPARATUS

The block diagram, figure 1.4, gives a schematic description of the experimental apparatus. The experimental method consists of crossing an atomic beam with a monoenergetic beam of electrons and observing the resulting photons. A cross beam method was chosen to allow a relatively high local number density within the gas beam while maintaining a low background pressure, in order to minimize any radiation trapping by the background gas. Low background pressure was maintained by directing the gas beam under study downwards into the mouth of a high speed oil diffusion pump through a rectangular stainless steel nozzle 5 mm X 1mm and 20 mm long. Polarization free measurements were obtained by suitable orientation of the electron beam with respect to the spectrometer as discussed earlier. A detailed description of the apparatus has been given by Donaldson et al (1972). In this chapter, the major parts of the apparatus will be described briefly in turn.

Vacuum Chamber:

The vacuum chamber was made from non-magnetic stainless

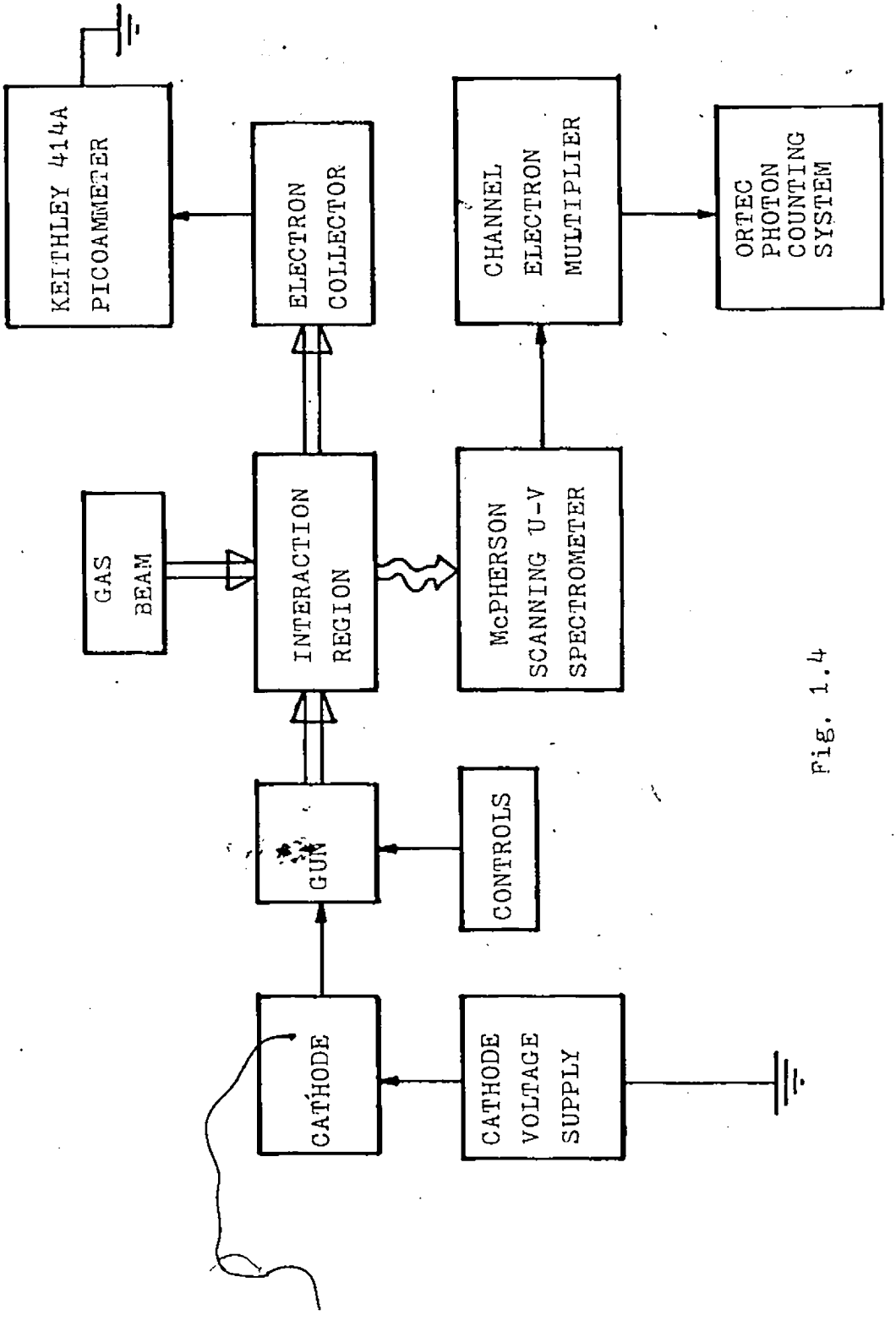

Fig. 1.4

steel. An outline of the design of the chamber is given in figure 1.5. The electron gun was located at port A, and port A' housed the collector, thus ensuring the angular configuration to give polarization free measurements.

The system was pumped by a standard Edwards four inch pumping system. The pressure in the main chamber was monitored by an ionization gauge and kept between 2×10^{-7} torr and 1×10^{-6} torr during operation.

Gas Beams:

High purity (99.999%) gases obtained from commercial cylinders were used. A flexible copper tube of length 20 cm connected the needle valve and the gas nozzle. The electron beam crossed the gas beam at right angles as shown in figure 1.6. The pressure at the input head was monitored continuously by an Edwards pirani gauge or a MKS baratron capacitance monometer gauge when needed. During the run the head pressure fluctuations were less than 1%.

Figure 1.7 shows a graph of photon intensity versus pressure for Ar 1048 Å line. Also shown is a similar plot for 543 - 547 Å lines of Ar^+ where no resonance trapping is expected. Clearly it is essential to work with a head pressure less than 5×10^{-3} torr if working with the neutral resonance lines. In the case of the ion lines no such

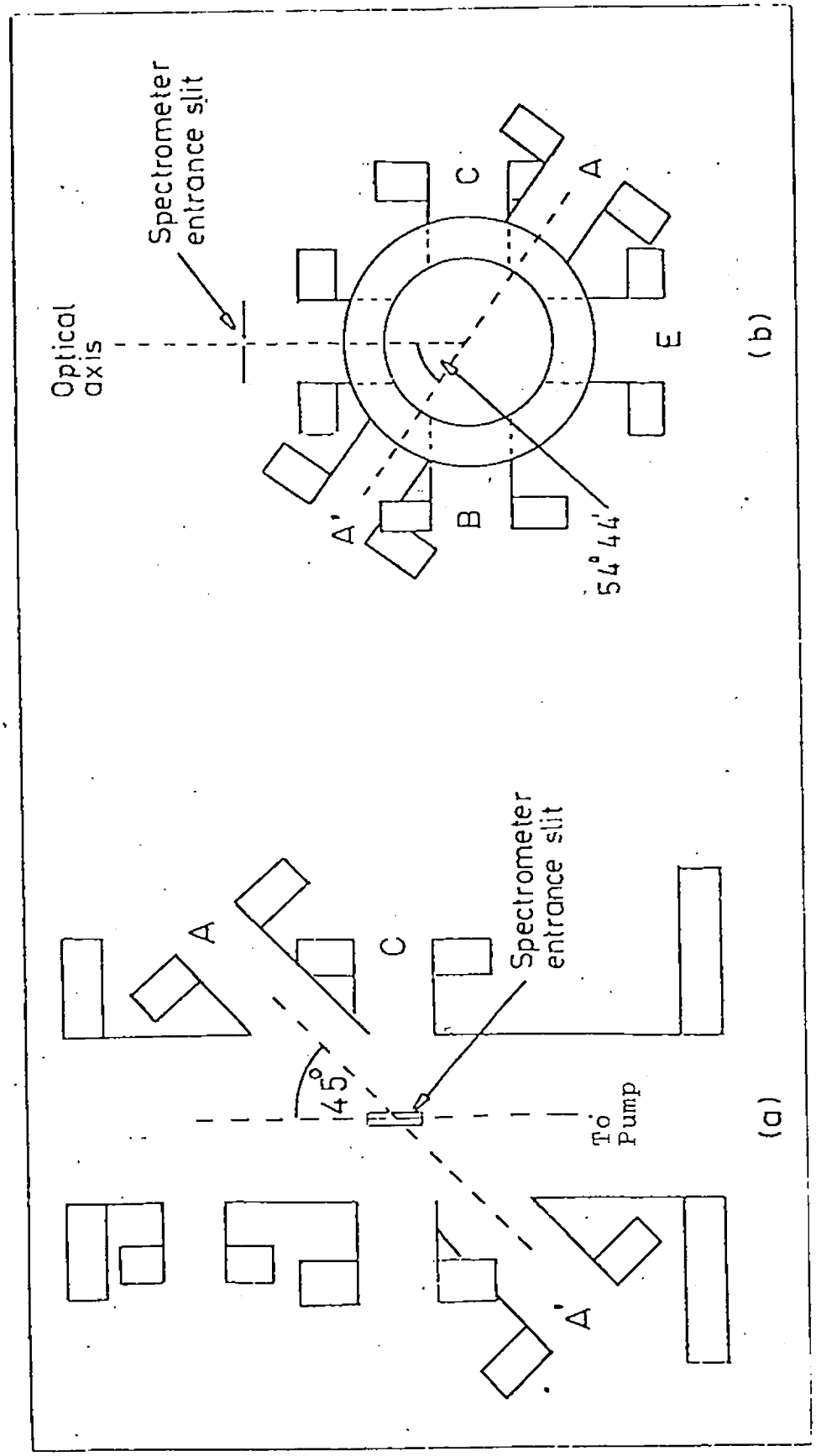

Fig. 1.5.

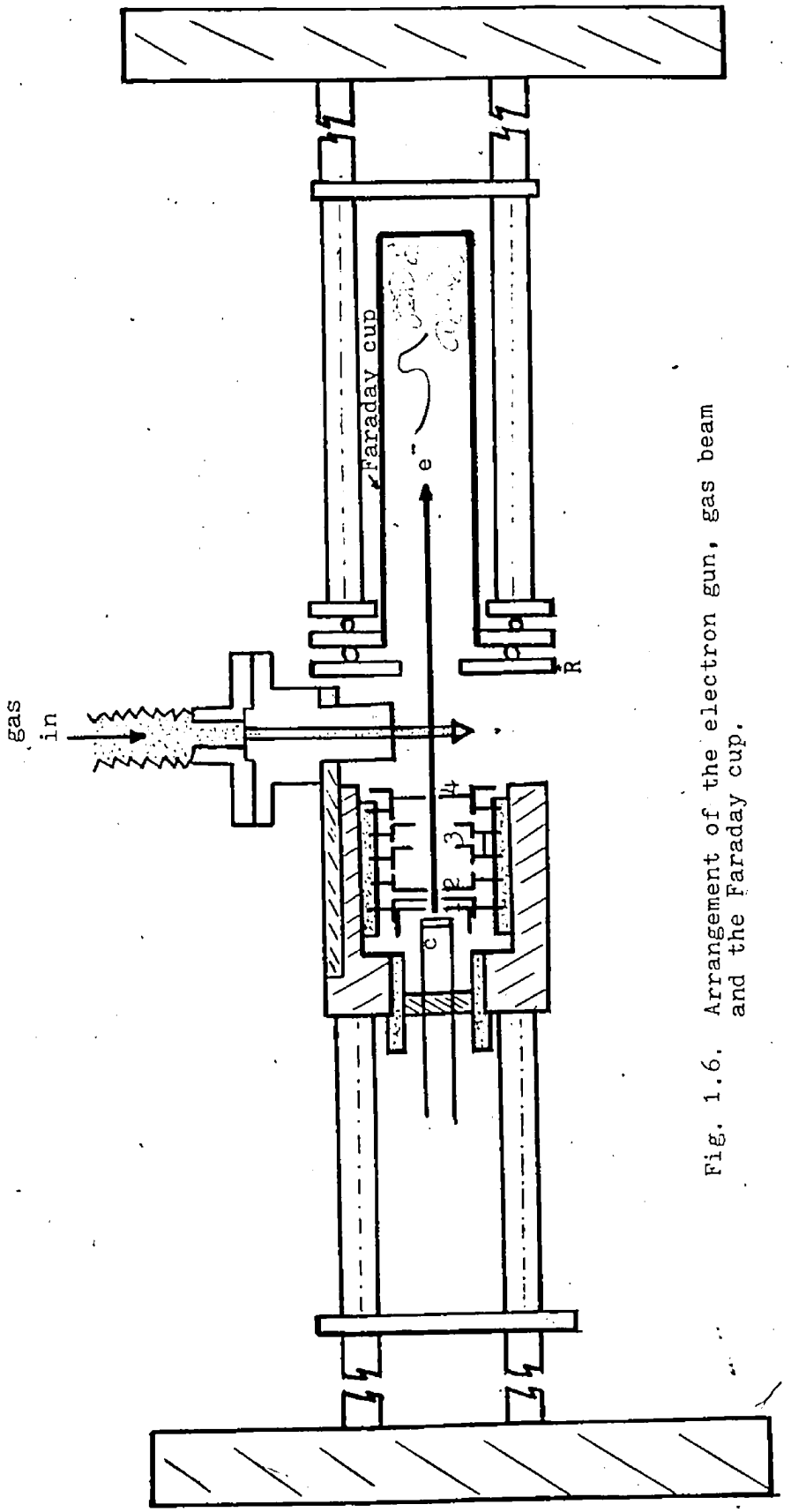

Fig. 1.6. Arrangement of the electron gun, gas beam and the Faraday cup.

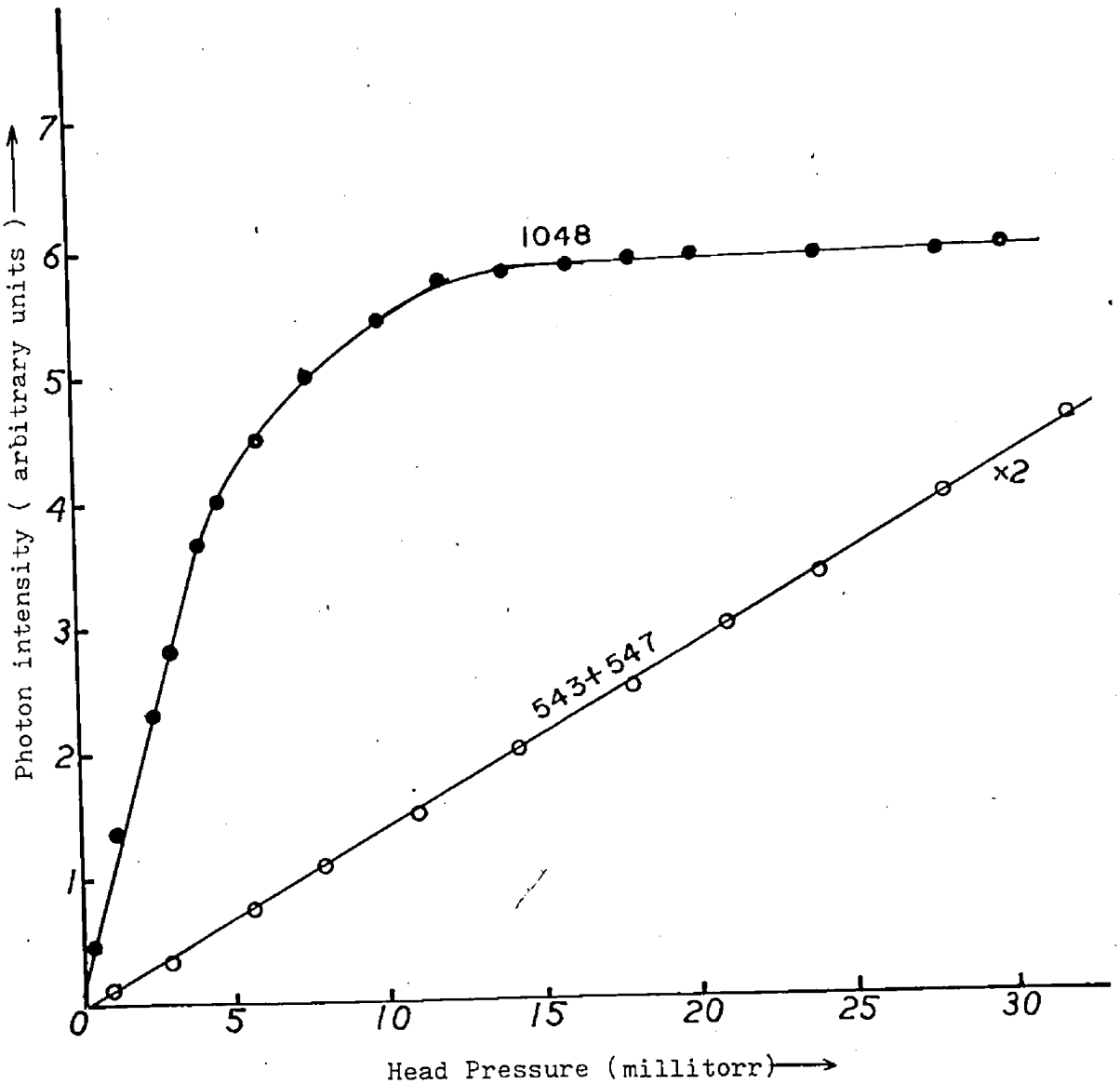

Fig. 1.7. A plot of photon signal intensity versus Head pressure of 1048A(●) for ArI and 543-547A (o) for ArII.

limitation is necessary.

Electron Gun and Collector:

The arrangement of the electron gun, electron collector, atomic beam and the interaction region is illustrated in figure 1.6. The electron gun is a modified version of the Amperex DH 3-91, employs aperture lenses throughout, and uses a planar oxide coated cathode. The aperture in the first electrode was enlarged to 1.5 mm diameter to increase available current through the gun. And the final electrode aperture was widened to 2 mm diameter to reduce the number of secondary electrons produced at that point. The optimum condition was judged to be that when the minimum possible current was collected on the final electrode A_4 and on the guard plate R which were both connected to ground through electrometers. The primary electron beam emerging from the final aperture crossed the atomic gas beam and was collected by a special designed stainless steel Faraday Cup. In order to prohibit the ejection of secondary electron into the interaction region. The Faraday Cup was positively biased with respect to the plate R and the interior was packed with nickel gauze and heavily sooted. The cup length is several times greater than its diameter.

All surfaces visible to the electrons, were sooted with

Acetylene soot in order to reduce electron reflection and secondary electron emission. The electron gun and the cathode were electrostatically shielded by a cylindrical gun holder. Holes were drilled through it to increase pumping speed. A special cathode mount was made to enable rapid replacement of oxide coated cathodes.

Studies of the threshold behaviour of the Ar 1048 Å line as shown in figure 1.8, indicated that the electron beam had an energy spread whose full width at half maximum was approximately 0.6 eV with a beam current of 130 μA. Figure 1.8 also shows how the contact potential for the gun was determined. The contact potential of the gun was approximately 4eV. It was taken as the difference between the energy at which the linear extrapolation cuts the energy axis and the known value of the onset for the transition. Frequent checks were made on the value of this contact potential over the time period during which the measurements was carried out.

As indicated in the previous section, it is essential that the signal intensity has a linear variation with the electron current, and this was observed to be so for all energies and electron beam currents up to 300 μA. Thus single collision conditions prevail.

Monochromator

The McPherson model 235 is a half-meter vacuum uv scanning monochromator. The optical system employed is the Seya-Namioka mounting of a concave grating. Two gratings were used in this work, one grating with 600 grooves/mm and reciprocal dispersion of 34 Å/mm and another grating with 1200 grooves/mm and reciprocal dispersion of 17 Å/mm. The grating with a reciprocal dispersion 17 Å/mm was coated with platinum and blazed for 700 Å. The other grating with reciprocal dispersion of 34 Å/mm was coated with aluminium, and a very thin coating of magnesium fluoride to protect the Al from oxidation and was blazed for 1500 Å .

In order to prevent oil vapour contamination of the grating the system was heavily trapped with both a thermo electric baffle and a liquid nitrogen cold trap. In addition a foreline absorption trap prevented back streaming of backing pump oil. A system of valves isolating the spectrometer chamber were opened only when readings were being taken.

It is important that only radiation from the required transition is being detected and also that the full spectral line is detected. In order to ensure this, a wavelength scan, plotting the signal against the wavelength, was obtained using narrow entrance and exit slits. After the wavelength setting on the monochromator was found then for various entrance slit widths a plot of the signal intensity versus the exit slit width was made. The conditions sought were those giving the

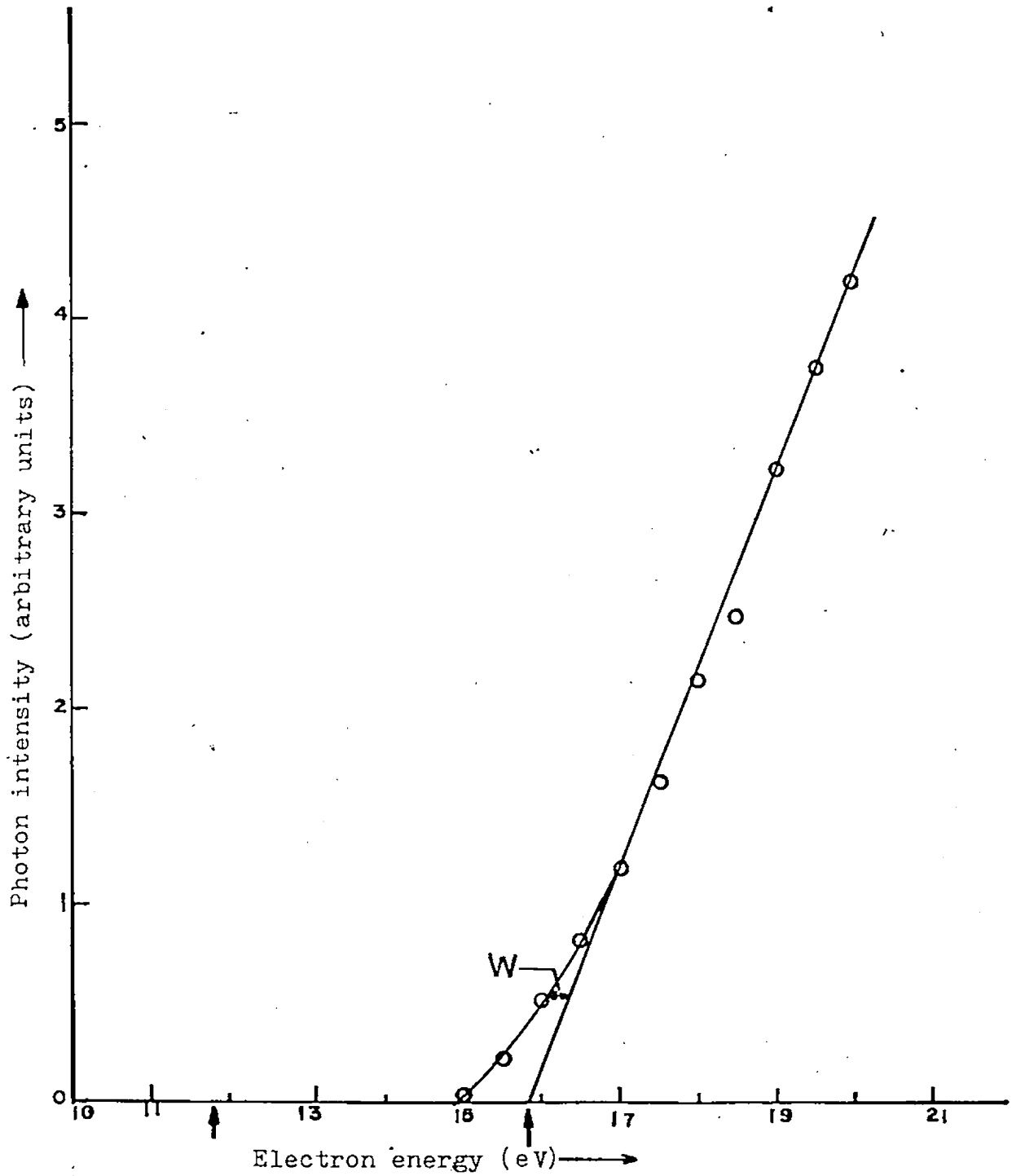

Fig. 1.8. The threshold behaviour for the 1048A line of ArI. W=0.3eV, is one half the value of the full width at half maximum of the energy spread. The contact potential of the gun is about 4eV (the difference between the energy at which the linear extrapolation cuts the energy axis and the known value of the onset for the transition).

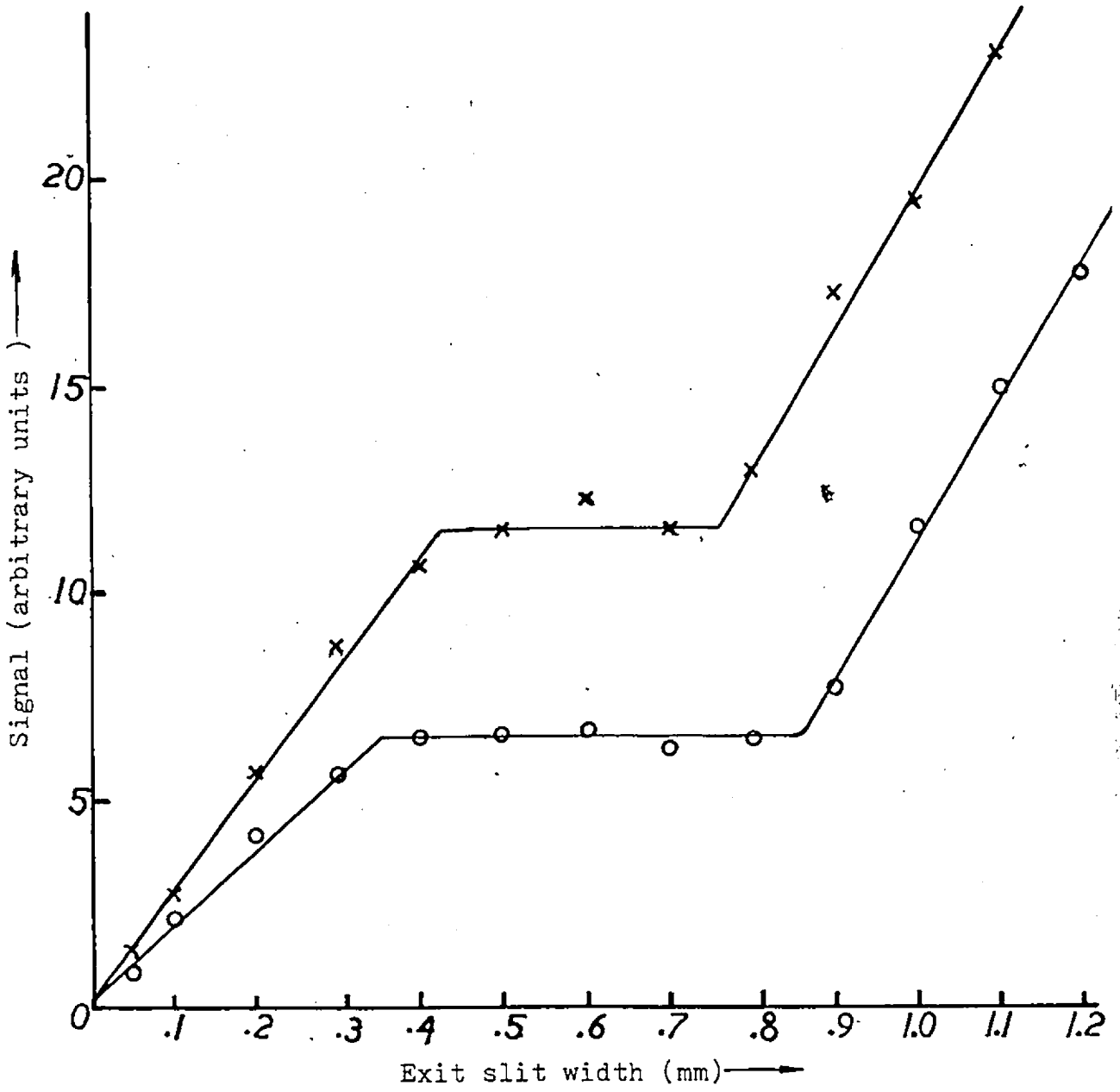

Fig. 1.9. Variation of detector signal with monochromator exit slit width for the 1067A line. The graphs correspond to entrance slit width of 0.4mm(X), and 0.3mm(o).

widest possible entrance slit which could be used with saturation of the signal at the exit slit, but without any contribution from neighbouring lines. These conditions gave the maximum signal while ensuring complete resolution of the transition under studied. Figure 1.9 shows the signal intensity versus the exit slit width plots for the 1067 Å line for two different entrance slit widths. It is seen that for an exit slit width of 0.6 mm, the resolution is adequate as indicated by a good plateau for both entrance slit widths of 0.4 mm and 0.3 mm. This procedure was repeated for every transition observed.

Detector:

The photons emitted were detected by a channel electron multiplier (CEM). A Bendix model no. 4028 was used, which has an entrance cone of 8 mm diameter. The end of the spiral was closed off for pulse counting purposes.

The operating voltage for 1×10^8 gain is 2800 V. The CEM can detect photons from 500 Å up to 1500 Å. The detection efficiency at 1500 Å is only 1% of the efficiency at 1000 Å. The signal to noise ratio is higher than the more traditional sodium salicylate-coated photomultiplier.

Photon Counting System:

Pulses from the channeltron were amplified and fed into a conventional Ortec photon counting system consisting of an amplifier, discriminator and scaler. Wavelength scans were carried out either manually point by point or by connecting the output of the ratemeter to an Y - T recorder.

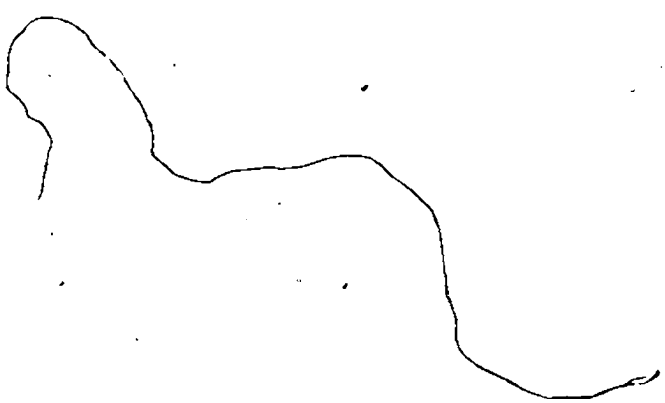

CHAPTER IV

CALIBRATION PROCEDURES

In the study of excitation processes by means of the emitted radiation the calibration of the optical equipment to determine absolute intensities is a major problem especially when the intensity measurements are performed in the vacuum U-V region.

It is known (McConkey and Latimer 1965), that, in a gas beaming system, such as the one currently being used, provided conditions of molecular flow prevail, the number density in the beam is independent of the nature of the gas, and depends only on the head pressure. Hence provided the same head pressures and electron beam currents are used in each case, the intensities of two lines or groups of lines can be directly compared.

The best established cross-sections in the vacuum U-V are those of the resonance lines of the rare gases, especially helium and neon. This is because of the accurately known optical oscillator strengths for these transitions. In this work we have used the 584, 537, 522 $\mathring{A}$ (2, 3, $4\,^1P - 1\,^1S$) He lines and the 736 $\mathring{A}$ ($2P^5\ 3S - 2P^6$) resonance line of Ne as

basic standards together with the Bethe normalization procedure. Using these lines the quantum efficiency of the detection system was established at these particular wavelengths. Little variation in quantum efficiency was found over the range 522 - 584 Å as shown in figure 1.10. and for this reason, the quantum efficiency at 490 Å was assumed to be the same as at 522 Å. This should introduce very little additional error in the measurements at this wavelength.

The actual comparison between two lines or groups of lines was through comparison of the slopes of intensity-pressure plots. Negligible error is introduced in the slope comparison and so the error in the measured cross-section is determined mainly by the error in the cross-section of the standard line. For the helium lines this should not exceed 15 % where as for the Ne line it is somewhat larger, (20-25) %. Additional errors were introduced when the lines under consideration were not very close in wavelength to the standard line, e.g., the lines around 660 Å, when overlap of adjacent lines occurred and when low signal strengths led to appreciable statistical uncertainties. It is believed that the values for the integrated cross-section of a group of lines, are accurate to ± 10% in addition to the possible error in the standard lines. The values given for the cross-sections

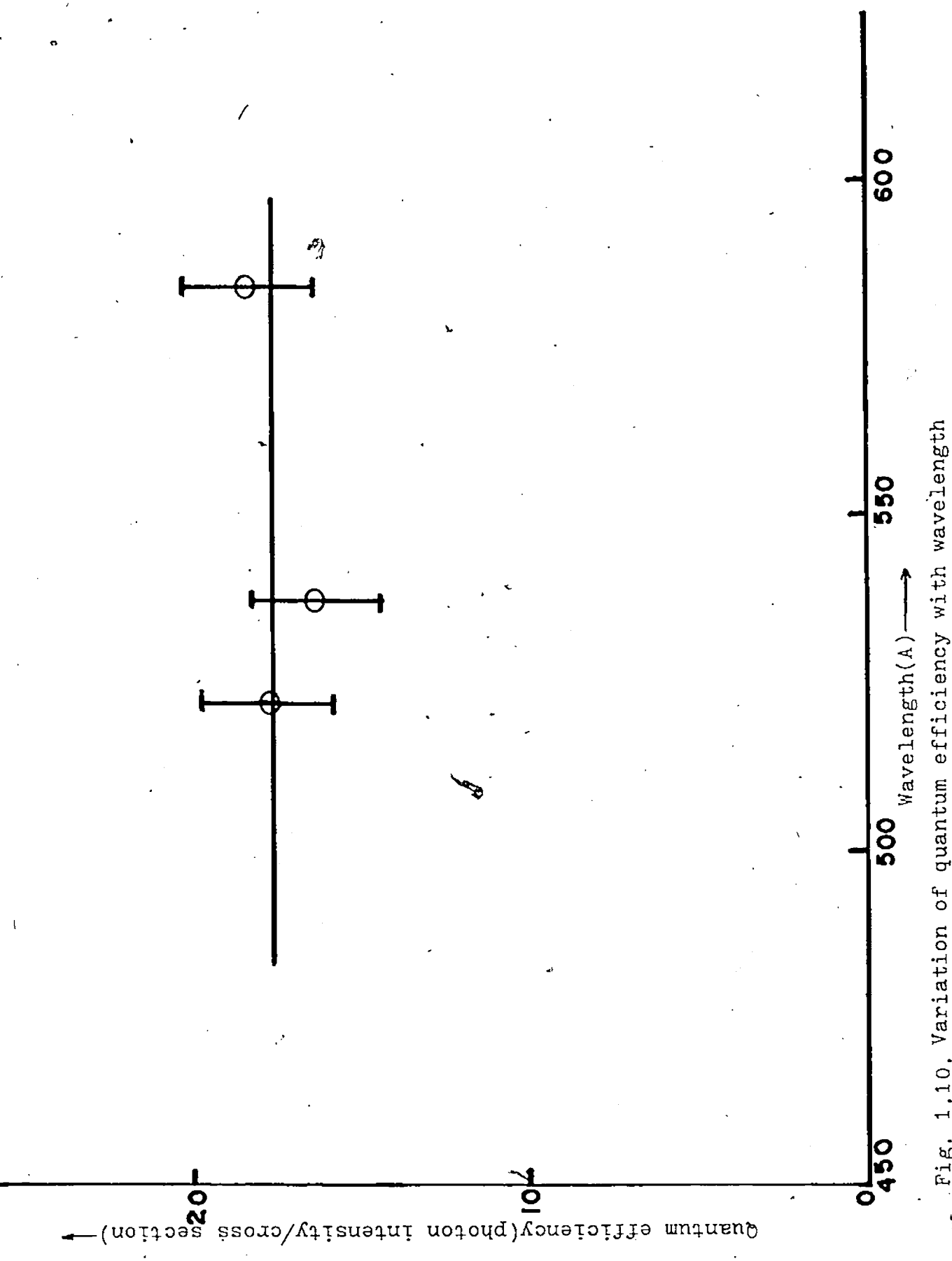

Fig. 1.10. Variation of quantum efficiency with wavelength

of individual lines within a group have been obtained from wavelength scans. This introduces an additional error which does not exceed 10% except where the lines were very closely spaced.

In general, cascade gives a rather important contribution to the population of resonance levels. Normally cascade is not simple to estimate but it is convenient to analyze a particular case, namely the case of a cascade contribution which varies inversely as the electron energy at high energy (optical forbidden character where $Q_{cascade} \propto E^{-1}$) (This problem has also been discussed by Van Raan (1973).

Assume that we are observing emission from a state which is dipole allowed from the atomic ground state, i.e. the cross-section varies according to

$$Q_n = \frac{4\pi a_o^2}{E/R} \frac{f_n}{E_n/R} \ln \frac{4C_n E}{R} \qquad \text{-----} \quad (1.24)$$

and that the significant cascade contribution to the observed radiation arises from higher levels which are inaccessible by dipole transitions from the ground state. Therefore the observed cross-section at high energy consists of sum of two components which may be written, after simplifying, as

$$\begin{aligned} Q_{total} &= Q_{direct} + Q_{cascade} \\ &= (Af/E)\ln CE + B/E \end{aligned} \qquad \text{-----} \quad (1.25)$$

where A and B are constants and f is the oscillator strength of the direct transition. This may be written as

$$Q_{total} = (Af/E)\ln C'E \qquad \text{-----} \quad (1.26)$$

where $C' = C \exp(B/Af)$

Hence, provided the cascade component has the proper variation with electron energy in the high energy region, it is not necessary to know the magnitude of this component, and therefore the calibration procedure can be carried out to obtain the absolute apparent cross-section as if no cascade was occurring.

This is an important effect in practice, for example, the cascade contribution to the n^1P states of helium comes from n^1S and n^1D states all of which are optically forbidden from the ground state of helium and all of which posses cross-sections which vary inversely as the energy at high energies (Van Raan et al 1971). The major cascade contributor to the upper level of the 736 Å Ne line is the $2p_1 - 1s_2$ (5852) transition. De Jough (1971) has shown that a plot of QE vs lnE of this radiation becomes constant above electron energies of about 500 eV, which is expected since $2p_n$ levels are optically forbidden from the neon ground state. Hence, it seems justifiable to assume that cascade will simply provide a constant background on a Bethe plot at high energies. Assuming this to be the case, one can ignore the magnitude

of the cascade contribution as discussed previously and establish the magnitude of the apparent cross section using the measured value of C' and the known value of f.

This calibration method has many advantages. Geometrical factors cancel out and many serious sources of error such as using different parts of the grating or the detector are avoided.

CHAPTER V

RESULTS AND DISCUSSION

Figure 1.1 is a simplified term diagram of Ar^+. Configurations investigated in the present work were $3s^2 3p^4 nS$ with n = 4 and 5, $3s^2 3p^4 nd$ with n=3, 4 and 5, $3s^2 3p^4 4s'$, $3s^2 3p^4 nd'$ with n = 3 and 4. The unprimed terms are based on the $3s^2 3p^4 (^3P)$ State of Ar^{++} and the primed terms are based on $3s^2 3p^4 (^1D)$ of Ar^{++}. All of these configuration combine optically with the $3s^2 3p^5$ ground state of Ar^+ yielding radiation in the vacuum ultraviolet spectral region below 1000 Å.

Because of the large number of levels involved and the consequent large number of often closely spaced lines, it was normally not possible to make cross-section measurements on individual lines. The procedure which was adopted to obtain the cross sections listed in Table 1.1 was to measure the integrated cross section of a group of lines and then obtain the relative cross sections of the different lines within the group by making a careful wavelength intensity scan using much narrower entry and exit slits on the monochromator. This was sometimes a difficult procedure as illustrated in Fig. 1.11 which shows an intensity wavelength scan in the

TABLE 1.1

Apparent cross section of Ar^+ lines measured at 100 eV incident electron energy.

Wavelength (Å)	Transition	Cross section (10^{-19} cm^2)	Integrated cross section
487.23	$3p^4 4d'\,^2S_{\frac{1}{2}} - 3p^5\,^2P_{3/2}$	4.2	
487.28	$3p^4 5d\,^2P_{3/2} - 3p^5\,^2P_{3/2}$		
488.75	$5d\,^2D_{5/2} - {}^2P_{3/2}$	5.6	15.1
488.99	$5d\,^2P_{\frac{1}{2}} - {}^2P_{3/2}$		
489.20	$5d\,^2D_{3/2} - {}^2P_{3/2}$		
490.65	$4d'\,^2S_{\frac{1}{2}} - {}^2P_{\frac{1}{2}}$	4.8	
490.70	$5d\,^2P_{3/2} - {}^2P_{\frac{1}{2}}$		
492.42	$5d\,^2P_{\frac{1}{2}} - {}^2P_{\frac{1}{2}}$	0.5	
518.91	$4d\,^2D_{3/2} - {}^2P_{3/2}$	9.1	
519.33	$4d\,^2D_{5/2} - {}^2P_{3/2}$		
522.79	$4d\,^2D_{3/2} - {}^2P_{\frac{1}{2}}$	4.9	
524.68	$4d\,^2P_{3/2} - {}^2P_{3/2}$	4.4	21.1
526.50	$4d\,^2P_{\frac{1}{2}} - {}^2P_{3/2}$	0.9	
530.49	$4d\,^2P_{\frac{1}{2}} - {}^2P_{\frac{1}{2}}$	1.8	
542.91	$4d\,^4D_{\frac{1}{2}} - {}^2P_{3/2}$	4.3	
543.21	$3d'\,^2S_{\frac{1}{2}} - {}^2P_{3/2}$	7.1	
543.73	$5s\,^2P_{\frac{1}{2}} - {}^2P_{3/2}$	2.5	

546.18	$5s\ ^2P_{3/2} - {}^2P_{3/2}$	1.7	25.0
547.17	$4d\ ^4D_{\frac{1}{2}} - {}^2P_{\frac{1}{2}}$	2.3	
547.46	$3d'\ ^2S_{\frac{1}{2}} - {}^2P_{\frac{1}{2}}$	4.9	
547.99	$5s\ ^2P_{\frac{1}{2}} - {}^2P_{\frac{1}{2}}$	1.6	
548.78	$5s\ ^4P_{3/2} - {}^2P_{3/2}$	0.6	
550.48	$5s\ ^2P_{3/2} - {}^2P_{\frac{1}{2}}$	0.3	
550.896	$5s\ ^4P_{\frac{1}{2}} - {}^2P_{\frac{1}{2}}$	0.2	
572.01	$3d'\ ^2P_{\frac{1}{2}} - {}^2P_{3/2}$	2.7	
573.36	$3d'\ ^2P_{3/2} - {}^2P_{3/2}$	12.4	
576.74	$3d'\ ^2P_{\frac{1}{2}} - {}^2P_{\frac{1}{2}}$	5.2	46.6
578.11	$3d'\ ^2P_{3/2} - {}^2P_{\frac{1}{2}}$	6.9	
578.60	$3d'\ ^2D_{3/2} - {}^2P_{3/2}$		
580.26	$3d'\ ^2D_{5/2} - {}^2P_{3/2}$	13.3	
583.44	$3d'\ ^2D_{3/2} - {}^2P_{\frac{1}{2}}$	6.1	
597.70	$4s''\ ^2S_{\frac{1}{2}} - {}^2P_{3/2}$	5.3	7.8
602.86	$4s''\ ^2S_{\frac{1}{2}} - {}^2P_{\frac{1}{2}}$	2.5	
612.37	$3d'\ ^2F_{5/2} - {}^2P_{3/2}$	2.5	
661.87(broad)	$3d\ ^2D_{5/2} - {}^2P_{3/2}$	8.5	
664.56	$3d\ ^2D_{3/2} - {}^2P_{3/2}$	1.2	

660.01	$3d\ ^2F_{5/2} - ^2P_{3/2}$	3.1	
670.95	$3d\ ^2D_{3/2} - ^2P_{\frac{1}{2}}$	5.9	
671.85	$4s'\ ^2D_{5/2} - ^2P_{3/2}$	14.4	
672.86	$4s'\ ^2D_{3/2} - ^2P_{3/2}$	0.6	
676.24	$3d\ ^4P_{5/2} - ^2P_{3/2}$	1.3	
677.95	$3d\ ^4P_{3/2} - ^2P_{3/2}$	1.1	
679.22	$3d\ ^4P_{\frac{1}{2}} - ^2P_{3/2}$	9.0	
679.40	$4s'\ ^2D_{3/2} - ^2P_{\frac{1}{2}}$		
686.49	$3d\ ^2P_{3/2} - ^2P_{3/2}$	1.1	
690.17 ArIII	$3d\ ^5D - 3p^4\ ^3P$	0.9	
691.04(broad)	$3d\ ^2P_{\frac{1}{2}} - ^2P_{3/2}$	0.8	
693.30	$3d\ ^2P_{3/2} - ^2P_{\frac{1}{2}}$	1.5	
697.49	$3d\ ^4F_{3/2} - ^2P_{3/2}$	0.5	
697.94	$3d\ ^2P_{\frac{1}{2}} - ^2P_{\frac{1}{2}}$	0.8	
698.77	$3d\ ^4F_{5/2} - ^2P_{3/2}$	1.6	
704.523	$3d\ ^4F_{3/2} - ^2P_{\frac{1}{2}}$	1.1	
718.09	$4s\ ^2P_{\frac{1}{2}} - ^2P_{3/2}$	3.8	
723.36	$4s\ ^2P_{3/2} - ^2P_{3/2}$	18.0	32
725.55	$4s\ ^2P_{\frac{1}{2}} - ^2P_{\frac{1}{2}}$	7.5	
730.93	$4s\ ^2P_{3/2} - ^2P_{\frac{1}{2}}$	2.7	
754.82	$3d\ ^4D_{5/2} - ^2P_{3/2}$	1.0	
762.20	$3d\ ^4D_{3/2} - ^2P_{\frac{1}{2}}$	0.5	

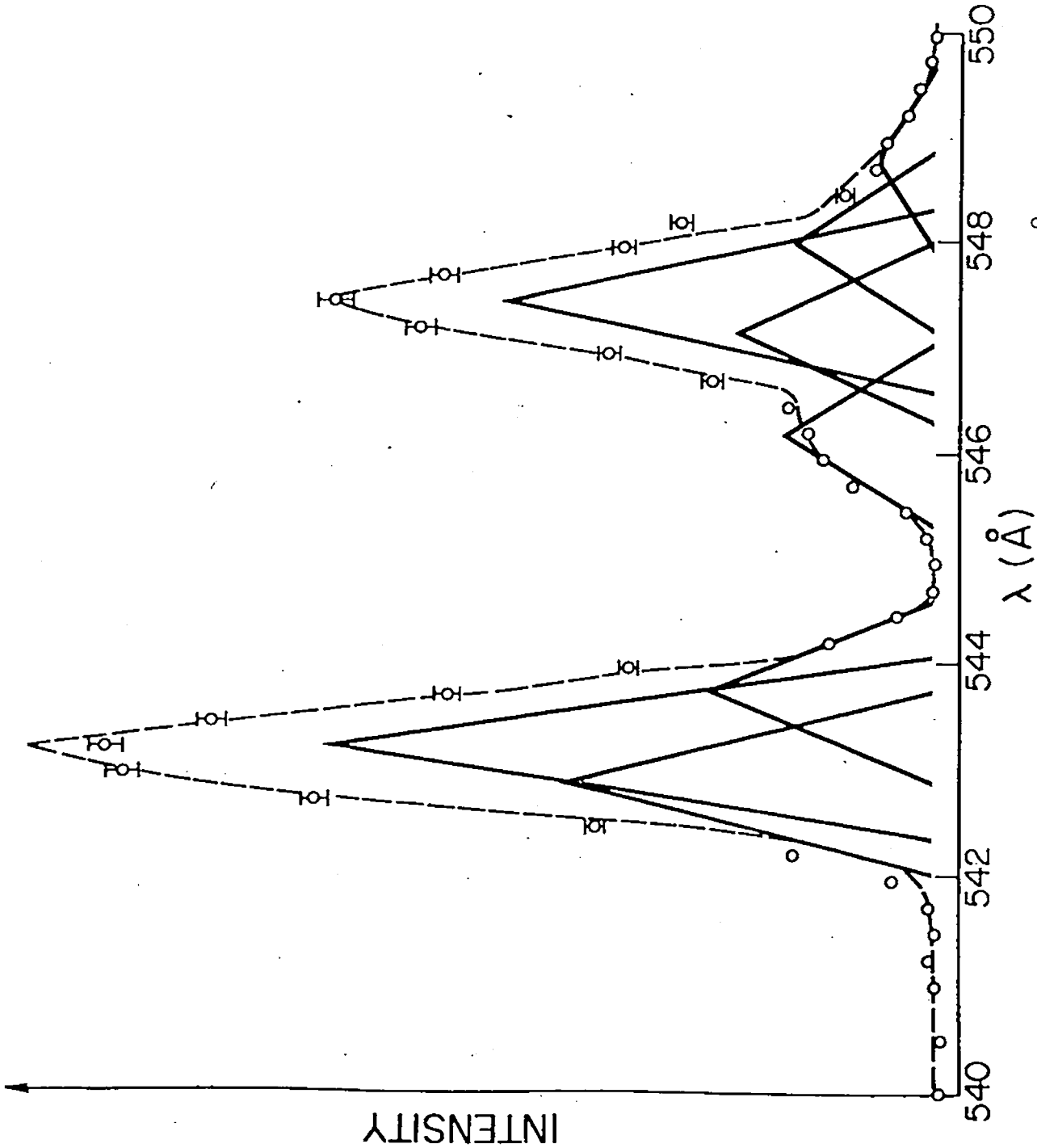

Fig.1.11. Intensity-wavelength scan in the 542-550Å region. The dashed line, drawn through the experimental points, is the sum of the solid curves which indicate the contributions of the individual spectral features.

540-550 Å region together with the deconvolution to obtain the individual line profiles knowing the slit function of the monochromator. Because of the difficulties involved in such process, the quoted cross section for closely spaced lines must be considered as only an approximation. Where it was possible to measure cross sections for individual lines or pairs of lines it was found that the values obtained from the wavelength scan and the values measured directly were in close agreement. For example, the apparent cross section for excitation of the 583.4 Å ($3d'\ ^2D_{3/2} - {}^2P_{\frac{1}{2}}$) line at 100 ev incident electron energy, obtained from a measurement of the integrated cross section of the 572 - 584 Å group of lines and the associated wavelength scan, was 6.4×10^{-19} cm^2 while the value obtained directly was 6.1×10^{-19} cm^2, the difference of 5% is well within the error bars in the measurements.

Before going into the individual configurations, a number of points should be made in connection with the figures shown in figure 1.12 to figure 1.18. It can be seen that in all cases with the exception of the features at 543 - 547 Å and 486 - 492 Å, the Bethe plots have a negative slope at high energy. This is in agreement with theoretical predictions and is due to the two electron nature of the transitions involved. The figures clearly indicate that a distinctly different excitation process is involved in the excitation of

the $3d'\ ^2S_{\frac{1}{2}}$ and $4d'\ ^2S_{\frac{1}{2}}$ states at high energies.

In most cases, the excitation functions exhibit a secondary peak or shoulder at about 55 eV in addition to the main peak which occurs at around 90 eV. This double peaked structure is often a feature of the simultaneous ionization and excitation in Ar and might be associated with autoionization effects which would diminish as the excitation energy of the state becomes larger in agreement with the observation.

It should be noted that the cross sections given in Table 1.1 and in connection with the figures have not been corrected for cascade effects. Further discussion of cascade effects is given in connection with the individual configurations.

Possible interference effects which might be occuring from Ar III lines was carefully checked using the Tables of Striganov and Sventitskii (1968). The only line which could be positively identified was the 690.17 Å, $3p^4\ ^3P - 3d\ ^5D$ line. Possible Ar III contributions were therefore assumed negligible and neglected.

Individual Configurations

1) The 736 Å Ne line:

This neon resonance line was used to calibrate the four lines 718 - 730 Å of Ar^+. There are due to decay from the lower level involved in the argon ion laser. Therefore, the

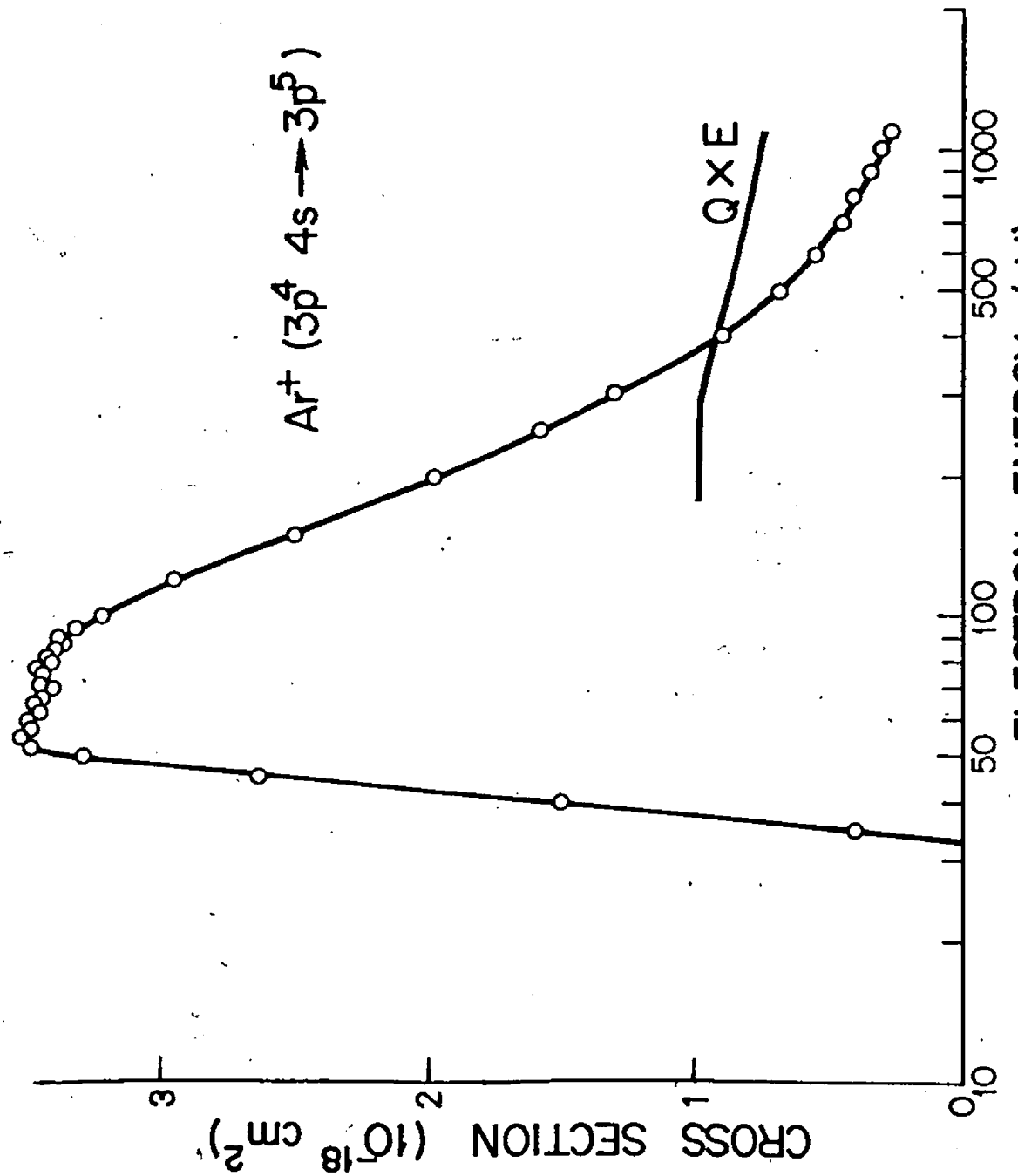

Fig.1.12. Apparent excitation function of the 718-731 Å group of lines of ArII. A plot of the cross section times energy is also shown.

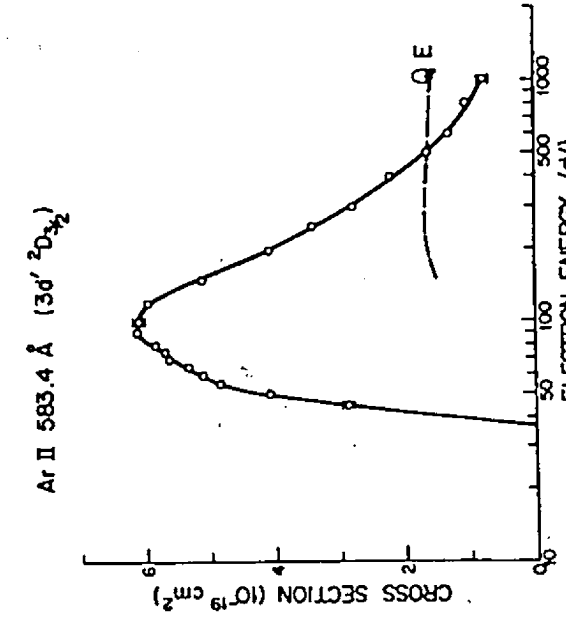

Fig.1.14. Apparent excitation function of the 583.4 Å Ar II line. A Bethe plot is also shown.

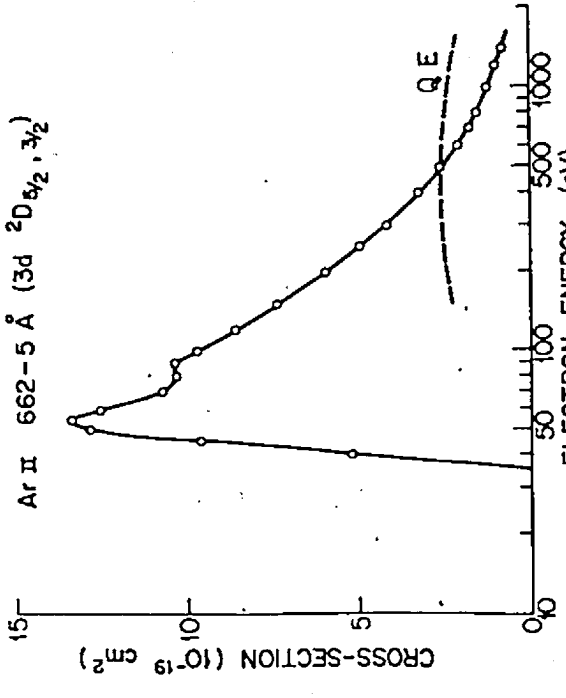

Fig. 1.13. Apparent excitation function of the 662-5 Å Ar II line. A Bethe plot is also shown.

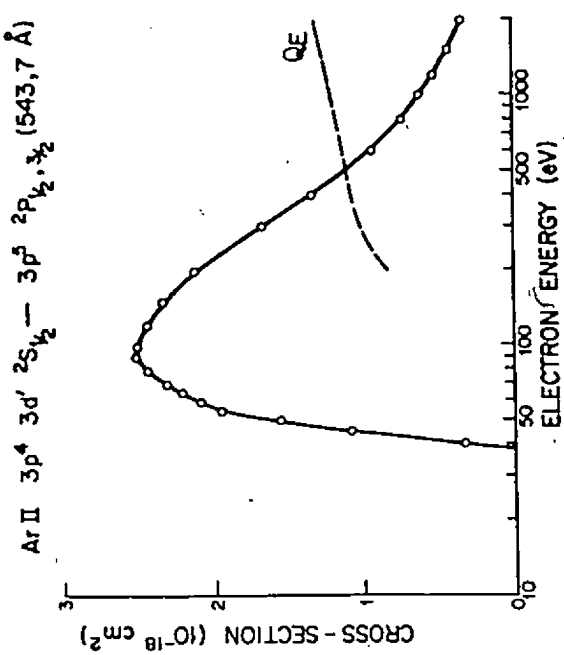

Fig.1.15. Apparent excitation function of the 572-3 Å ArII line. A Bethe plot is also shown.

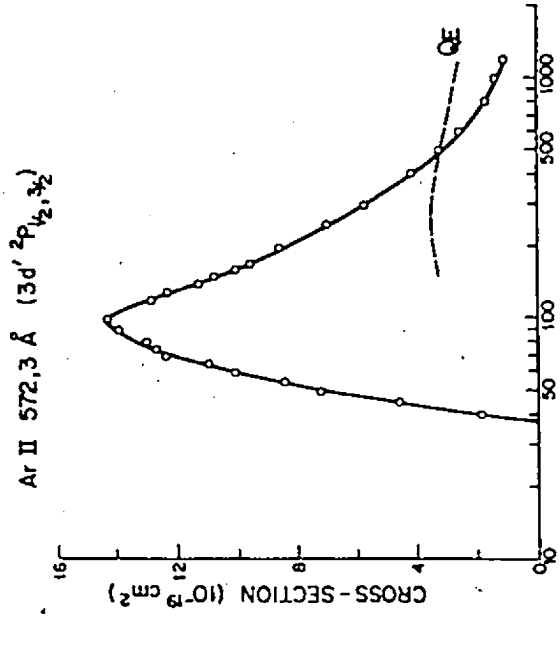

Fig.1.16. Apparent excitation function of the 543,7 Å Ar II line. A Bethe plot is also shown.

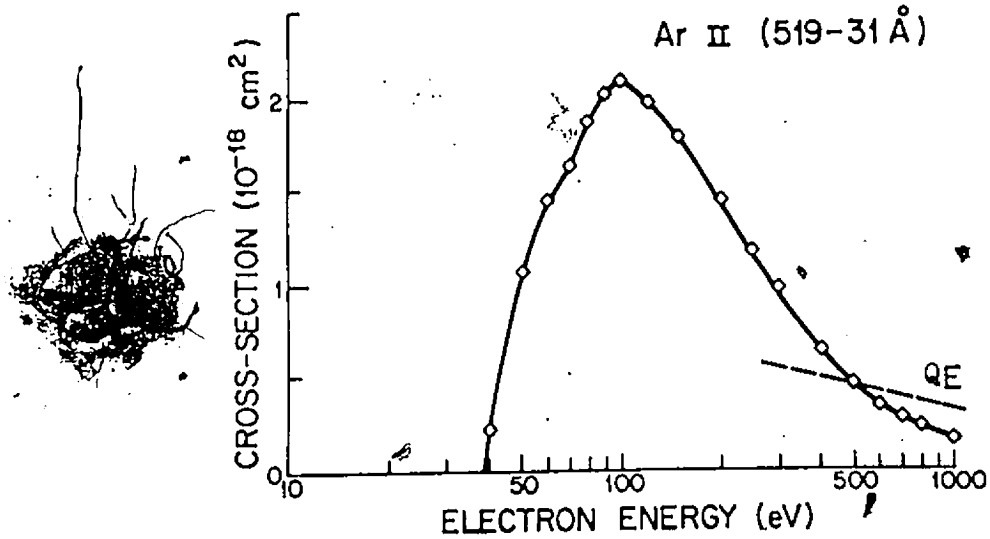

Fig.1.17. Apparent excitation function of the 519-31 Å ArII line. A Bethe plot is also shown.

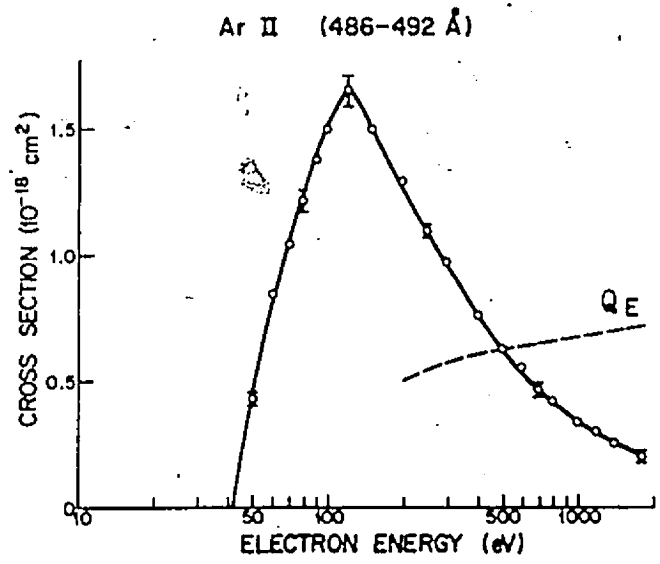

Fig.1.18. Apparent excitation function of the 486-492 Å ArII line. A Bethe plot is also shown.

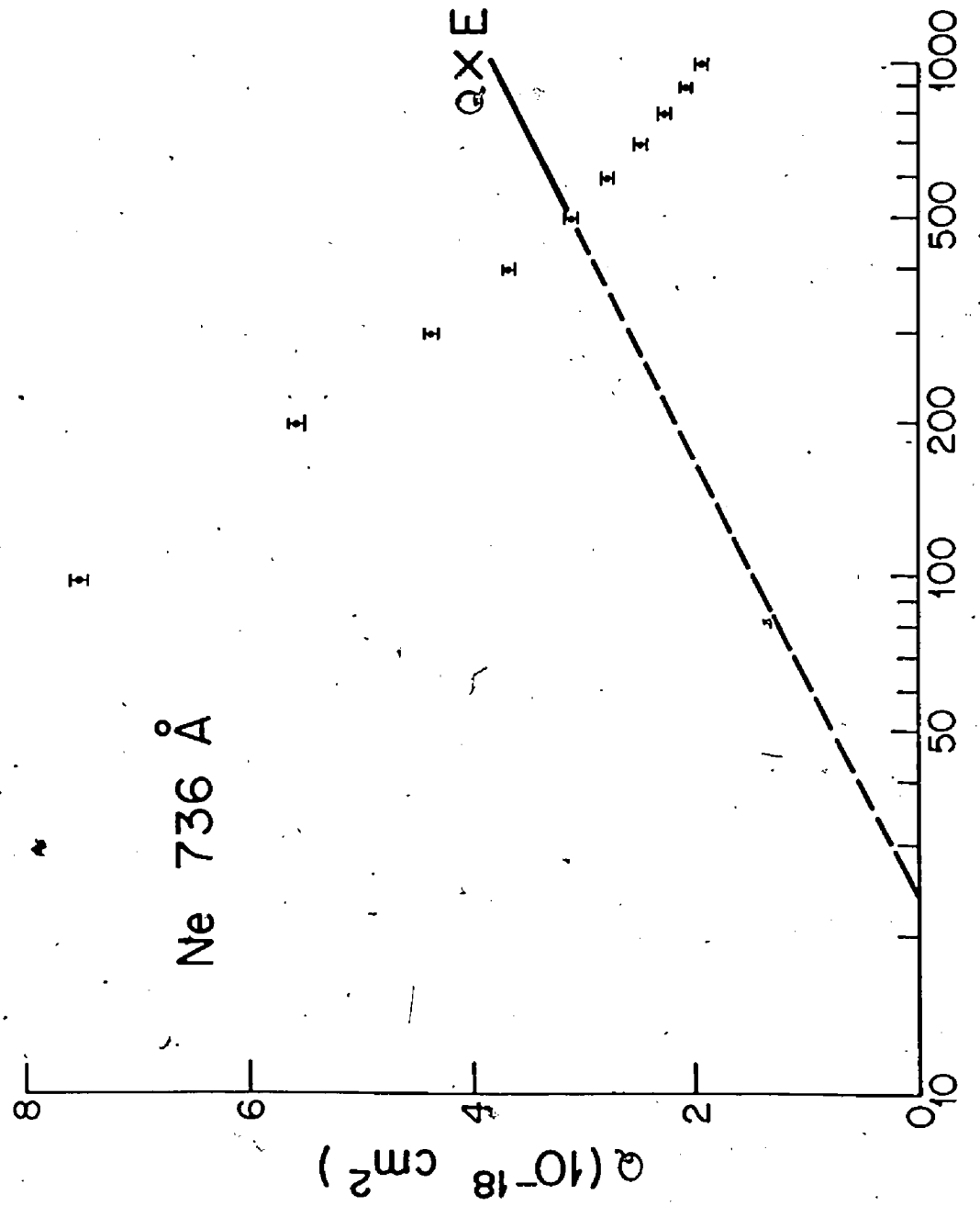

Fig.1.19. Variation of apparent cross section of the 736 Å neon resonance line with incident electron energy. A Bethe plot is also shown.

intensity of the 736 Å neon line was first put on an absolute scale using the Bethe - Born relationship (1.16) and (1.18). A careful plot was made of the line intensity vs. impact electron energy, Figure 1.19, and the straight line relationship between QE and ln E was found to hold above 400 eV. Using a least squares fitting procedure, the intercept with the energy axis was found to occur at 24.2 $\pm$ 4.0 eV yielding a value of C' of 0.04 $\pm$ 0.007. This may be compared with the value of 0.0515 obtained by Van Raan (1973). For the oscillator strength of the line, we chose a value of 0.132 which was the mean of two recent determinations of this parameter by de Jongh and Van Eck (1971) and by Lawrence (1968, 1969). This enabled the measured line intensities to be put on the absolute basis indicated in Figure 1.19. The accuracy of this calibration is limited by the accuracy in the oscillator strength (10% or better as quoted by both groups given above) and by possible systematic errors in C', due to statistical fluctuations in the count rates, (17.5%). The error introduced into the cross section evaluated at 1 kev is only 5% due to fact that C' comes in in the logarithmic factor.

It is important to establish that the high energy shape of the excitation function is not being affected by instrumental factors such as the existence of low energy secondary electrons in the electron beam. This effect would tend to increase the

observed cross section at high energies which in turn would lead to a decrease in the measured value of C'. To ensure that this does not happen we checked in the present instance by measuring C' for the $2^1P - 1^1S$ He transition where accurate experimental and theoretical values of C' are available for comparison.

As discussed previously the major cascade contributor to the 736 Å line has a cross section which varies inversely with energy at high energy. Hence the cascade will simply provide a constant background on a Bethe plot.

2) $3s^2\ 3p^4\ 4s$ Configuration

As shown in Figure 1.1, these are the lower levels involved in the argon ion laser transitions. Excitation of these levels from the atomic ground state involves a two electron transition; one 3p electron is ejected and simultaneously another one is excited to a 4s orbit. The decay leads to the emission of four lines in the wavelength range 718 - 731 Å, Figure 1.20. The highly resolved wavelength scan was taken with narrow slits at 100 eV electron energy. With these narrow slits, excessively long counting times had to be used to get reasonable statistics, so it was not judged feasible to measure the excitation functions of the four lines individually.

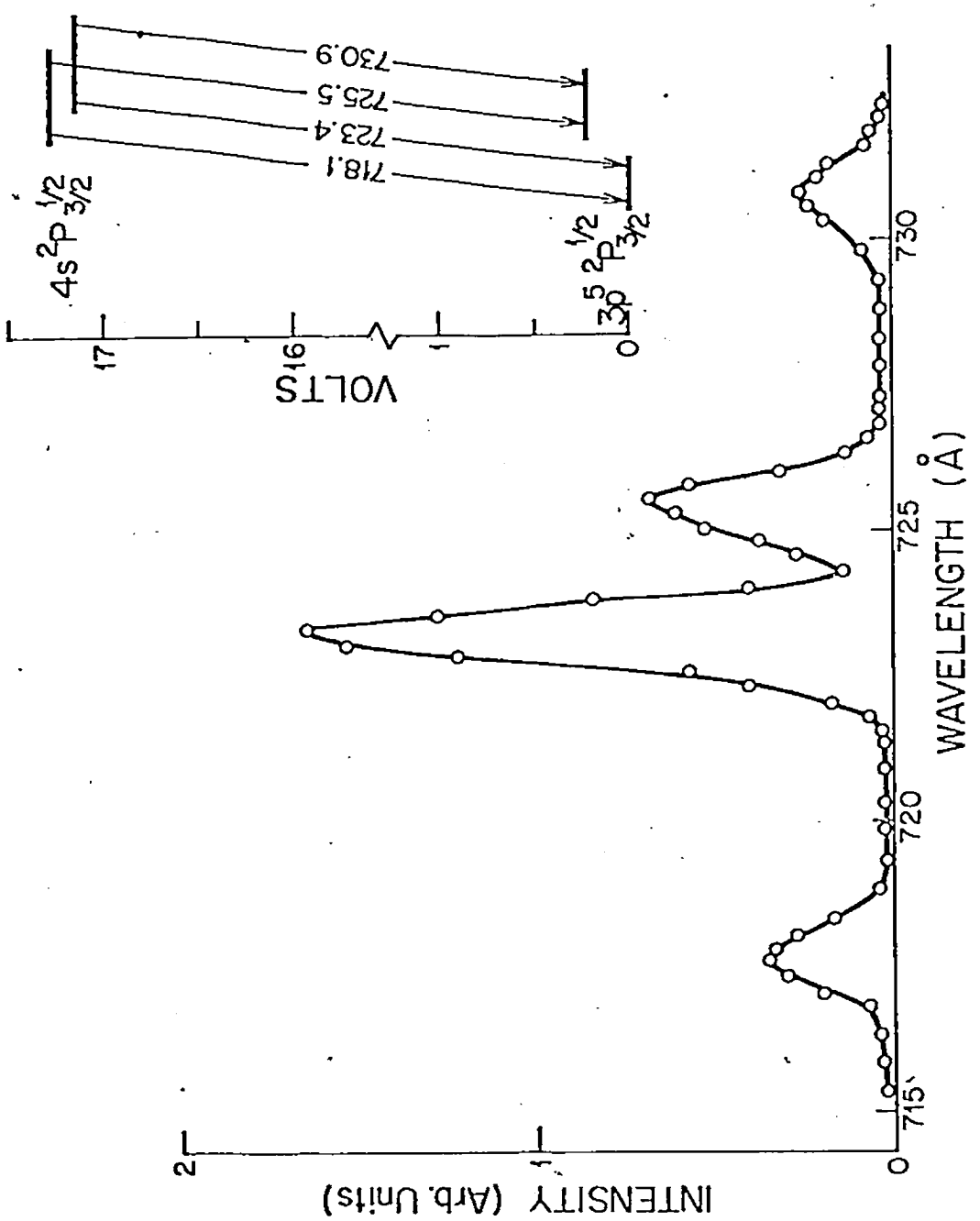

Fig.1.20. Intensity Wavelength scan showing the relative intensities of the four lines shown in the insert.

The excitation function of the combined lines is shown in figure 1.12. It has not been corrected for cascade, and it was made absolute by comparison with the 736 Å Ne line as discussed previously. Any changes in detector sensitivity over this small spectral range were assumed to be negligible. The intensities comparison of the 736 Å Ne line and the 718 - 731 Å Ar lines is shown in figure 1.21, which gives intensity - pressure plots of the two lines at 100 eV electron energy. The head pressure was measured directly using a Baratron capacitance manometer and the electron beam currents were kept the same for both plots. The combined cross section of the four lines at 100 eV was found to have a value of 3.2 x 10^{-18} cm^2. As the error introduced in the comparison is negligible, the error in this cross section will be determined by the error in the Ne line at 100 eV (approximately 25%).

As shown in figure 1.12, a double maximum in the curve is seen to occur at about 55 eV and 80 eV, although the structure is not so pronounced as for the 932 and 920 Å lines (See Tan, Donaldson and McConkey 1974). The presence of these maxima might be due to the existence of similar features in the cascading radiation from the $3s^2$ $3p^4$ 4p group (See Chapter I). Figure 1.12 also gives a plot of cross section times energy vs. log energy. This can be seen to run flat, ie. E^{-1} behavior, and then fall off with negative slope at high energy.

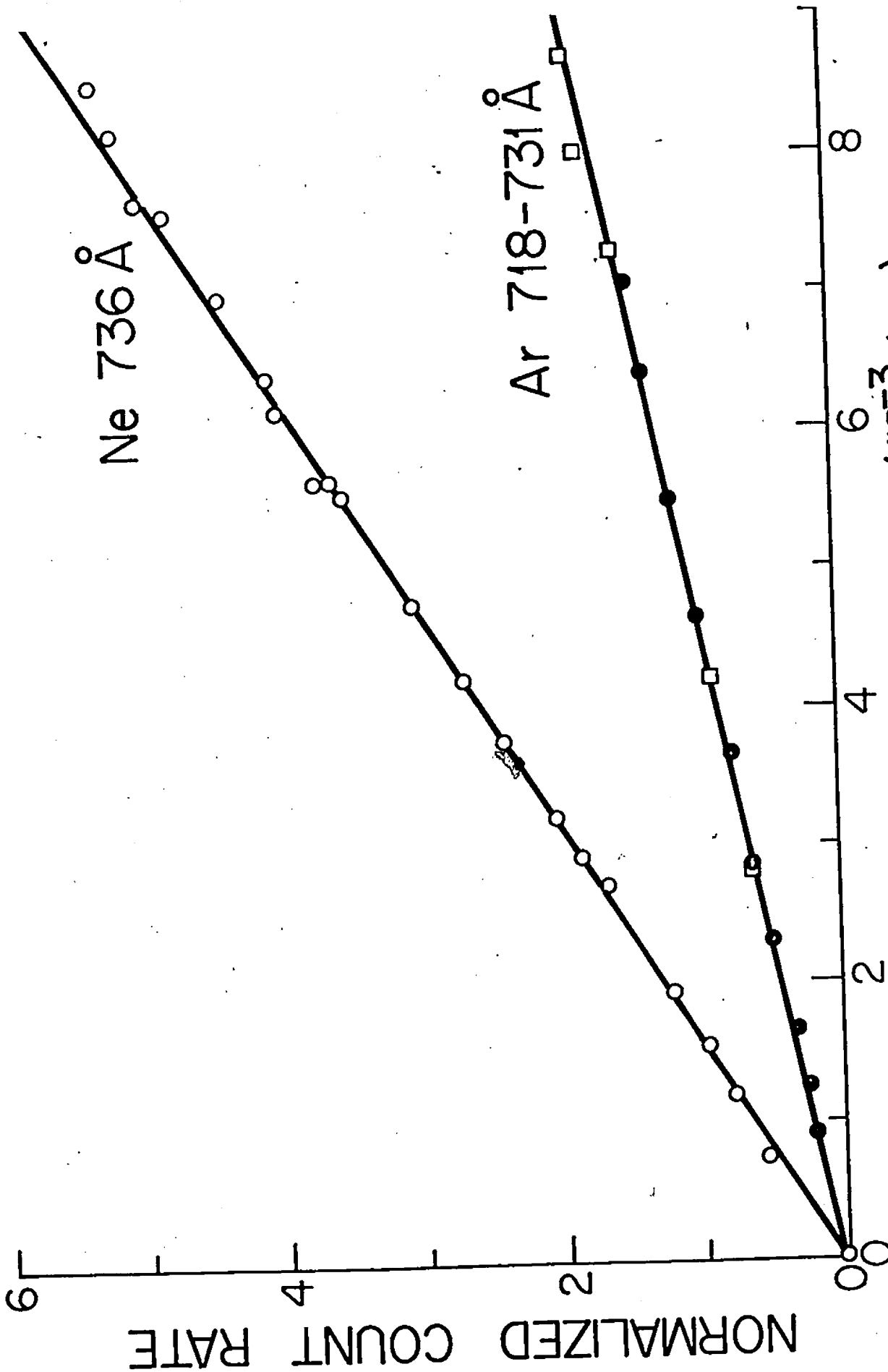

Fig.1.21. Comparison of the 736A Ne and the 718-731A Ar^+ line intensities.

The levels cascading into the $3s^2\ 3p^4\ 4s$ levels are mainly from the $3s^2\ 3p^4\ 4p$ group. The maximum cross sections for these cascade transitions observed by different groups are shown in Table 1.2. From the results obtained by these three groups and because the 4s level can only decay to the ionic ground state, it is possible to account for a maximum of about 67% and a minimum of about 39% of the observed intensity of the 718 - 731 Å emission in terms of cascade.

The relative intensities of the four lines obtained from the wavelength scan are given in Table 1.3 together with the theoretical transition probabilities of Lugken (1972), and the earlier calculations of Statz et al (1965) and Koster et al (1968), where configuration interaction was not considered. For lines originating from the same upper level, the intensity ratio should give the transition probability ratio directly. Our value for 726/718 ratio is 2.0, which can be compared with a value of 1.77 by Luyken and 2.0 by Statz and co-workers. For the 723/731 ratio, we get a value of 6.65 compared to the theoretical values of 6.92 (Luyken) and 5.12 (Statz). As Luyken's estimated uncertainty in the transition probabilities is 30%, the agreement between experiment and theory is quite satisfactory. An estimate of the relative level cross sections for the two 4s $^2P_{\frac{1}{2},\ \frac{3}{2}}$ levels can be obtained using the relative intensities in Table 1.3. We get a value for the $(J=\frac{3}{2})/(J=\frac{1}{2})$

TABLE 1.2.

Maximum cross sections for cascading transitions into 4s levels. The energies at which the maxima occur are given in brackets. Intercombination lines involving the quartet levels are not considered.

Transition	Wavelength (Å)	Cross section (10^{-20} cm^2) Clout and Heddle (1971)	Latimer and St. John (1970)	Feltsan and Povch (1970)
$4p\ ^2S_{\frac{1}{2}} - 4s\ ^2P_{\frac{1}{2}}$	4579	11.5(51)	18(54)	6.0(60)
$4p\ ^2P_{\frac{1}{2}} - 4s\ ^2P_{\frac{1}{2}}$	4889			4.3(93-97)
$4p\ ^2P_{3/2} - 4s\ ^2P_{\frac{1}{2}}$	4765	34.3(85)	52(90)	33(97-105)
$4p\ ^2D_{3/2} - 4s\ ^2P_{\frac{1}{2}}$	4965	13.8(55)	17(54)	12.1(60)
$4p\ ^2P_{\frac{1}{2}} - 4s\ ^2P_{3/2}$	4658	19.5(80)	40(90)	14.8(97-102)
$4p\ ^2P_{3/2} - 4s\ ^2P_{3/2}$	4545			12.3(97-105)
$4p\ ^2D_{3/2} - 4s\ ^2P_{3/2}$	4727			13.1(60)
$4p\ ^2D_{5/2} - 4s\ ^2P_{3/2}$	4880	44.9(52)	59(54)	30.5(60)

TABLE 1.3.

Transition probabilities and observed relative intensities of the 718-731 Å lines.

Transition	Wavelength (Å)	Transition probability (10^8 s^{-1}) Luyken	Statz et al	Relative intensity (present work)
$3p^5\ ^2P_{\frac{3}{2}} - 4s\ ^2P_{\frac{1}{2}}$	718.1	8.25	9.5	1.4
$^2P_{\frac{3}{2}} - 4s\ ^2P_{3/2}$	723.4	19.3	23	6.65
$3p^5\ ^2P_{\frac{1}{2}} - 4s\ ^2P_{\frac{1}{2}}$	725.6	14.6	19	2.8
$^2P_{\frac{1}{2}} - 4s\ ^2P_{3/2}$	730.9	3.15	4.5	1.0

ratio of 1.82. In the absence of cascade, one might expect the ratio to be given by the ratio of the statistical weights, namely 2.

3) $3s^2\ 3p^4\ 3d$ configuration:

As the states of this configuration can only decay to the ground $3s^2\ 3p^5\ ^2P_{\frac{1}{2}, \frac{3}{2}}$ states, the cross sections are obtained directly from the measured cross sections. The results have been tabulated in the second column of Table 1.4.

The most significant cascade into the 3d levels will be from the 4p levels. It is possible to estimate the magnitude of some of these cascade transition by using the measurements of Feltsan pouch (1970) for 4p - 4s and 4p - 3d transition together with the known branching ratio for the 4p levels given by Luyken (1972). The uncertainty in this procedure is about 40%. The cascade corrected values have been tabulated in the third column of Table 1.4. It can be seen that cascade is especially significant for the ^4D levels, and also probably for the ^4P levels though no measurements are available to check this. The significant cascade for the ^4P levels may be seen in column 5 of Table 1.4, where the measured level cross sections were divided by the transition probability and the statistical weight. These values should be constant within a given multiplet if direct excitation is occurring. As shown in the table, this rule is closely observed except for the ^4P

TABLE 1.4.

Data for $3p^4$ 3d configuration.

State	Measured level cross section at 100 eV ($10^{-19}cm^2$)	Corrected for cascade	Transition probability[a] ($10^8 sec^{-1}$)	$Q/(A(2J+1))$[b] ($10^{-27}cm^2 sec$)
$^4F_{5/2}$	1.6	1.46	0.014	17.4
$^4F_{3/2}$	1.6	1.58	0.024	16.5
$^4D_{5/2}$	1.0	0.33	0.0017	32.4
$^4D_{3/2}$	0.5	0.10	0.00076	32.9
$^4P_{5/2}$	1.3		0.045	4.8
$^4P_{3/2}$	1.1		0.037	7.4
$^4P_{1/2}$	0.5		0.045	5.6
$^2F_{5/2}$	3.1		1.41	0.37
$^2D_{5/2}$	8.5		16.7	0.08
$^2D_{3/2}$	7.1		17.22	0.10
$^2P_{3/2}$	2.6	2.17	0.348	1.55
$^2P_{1/2}$	1.6	1.24	0.386	1.60

[a] Luyken, 1972.

[b] When possible, Q is the cascade corrected cross section. Otherwise the measured cross section was used.

multiplets, which is almost certainly due to the effect of cascade.

When a detailed comparison is made between the experimentally measured relative transition probabilities for transitions to the two ground states from a common upper state, the agreement with the theoretical calculations is not so good in all cases. For example, in the case of the $^2D_{3/2}$ upper state the relative transition probability to the $^2P_{3/2}$ and $^2P_{1/2}$ ground states is 0.2 compared with the Luyken's theoretical value of 0.18. For the $^2P_{3/2}$ and $^2P_{1/2}$ upper states the experimental ratios are 0.73 and 1.0 respectively, compared to theoretical values of 2.6 and 0.33.

It is noted that, the excitation function for a pair of 3d levels, figure 1.13, has a much more pronounced low energy peak around 55 eV when compared with other excitation functions. In general, the higher the excitation energy of the state the less pronounced this peak becomes supporting the conclusion that it is caused by autoionization effects whose significance will decrease as one goes to states of higher energy. Figure 1-13 also shows the expected negative slope of the Bethe plot at high electron energies.

4) $3s^2\ 3p^4\ 4s'$ configuration:

The total cross section for the $4s'$ levels at 100 eV was

observed to be 23.5 x 10^{-18} cm^2 compared with a value of 32 x 10^{-19} cm^2 for the 4s levels at the same energy. No cascade corrections were made because no measurements have been reported for the 4p' $^2D_{5/2,\ 3/2}$ - 4s' $^2D_{5/2,\ 3/2}$ cascading transitions which are expected to be strong. Feltsan and Povch (1970) have measured some of the 4p' - 4s' transitions and the theoretical calculation of these transition probabilities has been done by Luyken (1972). Luyken did not consider the possibility of decay from 4s' $^2D_{3/2}$ to the $^2P_{1/2}$ ground state, though as shown in Table 1.1, this transition is very strong, about 14 times stronger than the transition to the $^2P_{3/2}$ ground state (some uncertainty arises here because of blending with the 3d $^4P_{1/2}$ - $^2P_{3/2}$ transition, but this is likely to be the same order of magnitude as the transitions from the other ^4P levels and therefore weak). The 4s' ^2D levels may be affected by configuration interaction with the 3d ^2D levels as discussed later.

5) $3s^2\ 3p^4\ 3d'$ Configuration:

Figures 1.14 - 1.16 illustrate the excitation functions obtained for states of different orbital angular momentum. The low energy behavior (up to 100 eV) of the function is similar to the other lines discussed but high energy behavior, as demonstrated by the Bethe plots, is distinctly different for

the $^2S_{\frac{1}{2}}$ levels due to the effects of configuration interaction as discussed later.

Numerical data for the individual transitions is given in Table 1.1 while these apparent level cross sections listed in the second column of Table 1.5. Cascade contributions from higher states (for example 5p' state) are likely to be small at 100 eV because of the small cross sections for excitation of these states. Justification for the unimportance of cascade comes from column 4 of Table 1.5 where the apparent cross sections have been divided by the transition probabilities and statistical weights. Within a given multiplet this figure is approximately constant as one would expect if direct excitation is dominant.

Comparison of the experimental and theoretical branching ratios to the two ground states are shown in the final two columns in Table 1.5. The agreement is seen to be good considering the possible error in the cross sections of the closely spaced lines.

6) $3s^2\ 3p^4\ 4d$ Configurations.

Excitation functions for the 4d states are illustrated in figure 1.17. The Bethe plot has the expected negative slope at high energy. In common with all the other functions it has a maximum around 100 ev with some structure at about 60 eV.

TABLE 1.5.

Data for the $3p^4 3d'$ configuration.

State	Measured cross-section at 100eV ($10^{-19}cm^2$)	A coefficient[a] (10^8 sec^{-1})	$\frac{Q \times 10^{-29}}{A(2J+1)}$	Branching ratio to ground states	
				Measured	Calculated[a]
$^2D_{5/2}$	13.3	159	1.39		
$^2D_{3/2}$	9.55	148.3	1.61	0.57	0.43
$^2P_{3/2}$	15.85	210.8	1.88	3.59	3.32
$^2P_{\frac{1}{2}}$	7.9	208.6	1.89	0.52	0.58
$^2S_{\frac{1}{2}}$	12.0	244.6	2.45	1.45	1.79

[a] Luyken, 1972.

TABLE 1.6.

Data for $3d^4 4d$ configuration.

State	Total measured line cross section from state at 100 eV. ($10^{-19}cm^2$)	Branching ratio[a]	Apparent Level cross-section($10^{-19}cm^2$)
$^4D_{\frac{1}{2}}$	6.6	0.26	25.5
$^2D_{5/2}$	4.55	0.27	16.9
$^2D_{3/2}$	9.45	0.06	157.5
$^2P_{3/2}$	4.4	0.056	78.6
$^2P_{\frac{1}{2}}$	2.7	0.136	19.9

[a] Rudko and Tang, 1967.

The total measured line cross sections for transitions to the ground states are listed in the second column of Table 1.6. Using the branching ratios of Rudko and Tang listed in the third column of Table 1.6, the total apparent level cross sections so obtained were listed in the final column of Table 1.6. These cross sections are anomalously high. It is evident that the measured line cross sections are considerably higher than those of the corresponding 3d states. This is anomalous as one normally considers an n^{-3} dependence of cross section with principal quantum number. It is unlikely that these levels are strongly populated by cascade from higher levels. Any such cascade will be predominantly from the higher np states with $n \geq 6$. The cross sections for excitation of these states should be well down on those of the 4P states and measurements of these states by Feltsan and Povch (1970), Latimer and St. John (1970) and Clout and Heddle (1971) have shown that these cross-sections be of the order of 10^{-19} cm^2 or less. In addition, if significant population of higher np states were occurring, then this would show up as anomalously high cascade excitation of other states, for example 4S, 5S or 3d. This is not observed to be the case.

This leads to the conclusion that the large excitation of the 4d levels must be caused by configuration interaction effects probably with the 3d configuration leading to a transfer

of excitation from these levels. Minnhagen (1963, 1959) has pointed out that $3d\,^2P$ and $3d'\,^2P$ interact strongly as do $3d\,^2D$, $3d'\,^2D$, $3d''\,^2D$, $4S'\,^2D$ and $4d\,^2D$. Luyken (1972) has examined the situation more quantitatively and has demonstrated that the states of $3p^4\ 3d$ configuration mix strongly with states of higher $3s^2\ 3p^4$ nd configurations, which results in a transfer of oscillator strength from the $3p^4\ 3d$ to $3p^4\ 4d$. Because of the computational difficulties involved Luyken was unable to take proper account of these interactions in his transition probability calculation of the 3d states and hence the calculated values for the 3d states are subject to large errors.

7). $3s^2\ 3p^4$, 5s configuration.

The data concerning this configuration is summarized in Table 1.7. The branching ratio to the ground state was obtained by using the theoretical values of lifetimes and transition probabilities calculated by Rudko and Tang (1967, 1968). Using the calculated branching ratio gives a total apparent $5s\ ^2P$ level cross section of 7.8×10^{-19} cm^2 at 100 ev. From the non-constancy of final column of Table 1.7, it is evident that cascade must be responsible for a large fraction of the excitation. If a 30% cascade component is assumed for this $5s^2P$ level then the level cross-section is

approximately half the cascade corrected level cross-section of the 4s ^2P levels which was measured by Tan et al (1974). This is what would be expected assuming an n^{-3} dependence of cross section with principal quantum number.

From Table 1.1, the relative transitions probabilities to the two ground states from the 5s $^2P_{3/2}$ and 5s $^2P_{1/2}$ states are 5.7 and 1.6 respectively. Theoretical calculation of these transition probabilities are not available.

8) $3s^2\ 3p^4\ 4d'$ and $3s^2\ 3p^4\ 5d$ configuration.

Due to the extreme overlap between the $3p^4\ 4d'$ and $3p^4$ 5d configurations and within the $3p^4$ 5d configuration itself it is only possible to put estimates on the cross-sections for the different levels. These are given in Table 1.8. As in the case of $3p^4$ 3d and $3p^4$ 4d excitation of the $3p^4$ 5d ^2D terms predominates over the ^2P and other terms. The large cross-section of $4d'\ ^2S_{1/2}$ is due to configuration mixing with $3s\ 3p^6\ ^2S_{1/2}$ as discussed later.

The excitation function for the 486 - 492 Å group of lines which includes contributions from both 4d' and 5d states is illustrated in figure 1.18. At high energies it will be dominated by $4d'\ ^2S_{1/2}$ state, and the positive slope of the Bethe plots is evidence for this. (See below).

TABLE 1.7.

Data for $3p^4 5s$ configuration.

State	Total measured line cross section at 100 eV ($10^{-19}cm^2$)	Branching ratio[a]	Level cross section ($10^{-19}cm^2$)	$\frac{Q}{A(2J+1)}$ ($10^{-27}cm^2sec$)
$^2P_{3/2}$	2.0	0.72	2.8	0.091
$^2P_{\frac{1}{2}}$	4.1	0.82	5.0	0.275

[a]Rudko and Tang, 1968.

TABLE 1.8.

Data for 4d' and 5d configuration.

State	Measured apparent cross section at 100 eV. (10^{-19} cm^2)
4d' $^2S_{\frac{1}{2}}$	8.6
5d $^2P_{3/2}$	0.5
5d $^2P_{\frac{1}{2}}$	1.5
5d $^2D_{5/2,3/2}$	4.6

Configuration Interaction Among the $^2S_{\frac{1}{2}}$ States.

Configuration interaction has been demonstrated to exist between the states of the 3d, 3d', 4d, and 4s' configurations, but this is outshadowed by the interaction between the 3s $3p^6$ $^2S_{\frac{1}{2}}$ and the $3s^2$ $3p^4$ 3d' $^2S_{\frac{1}{2}}$ and $3s^2$ $3p^4$ 4d' $^2S_{\frac{1}{2}}$ states. Luyken investigated this effect theoretically and showed that the wave function expansion of the 3s $3p^6$ $^2S_{\frac{1}{2}}$ state contained large contributions from the $3s^2$ $3p^4$ 3d' $^2S_{\frac{1}{2}}$ and $3s^2$ $3p^4$ 4d' $^2S_{\frac{1}{2}}$ states. Hence: -

$$\psi(3s\ 3p^6\ ^2S_{\frac{1}{2}}) = 0.78764\ |3s\ 3p^6\ ^2S_{\frac{1}{2}}\rangle - 0.55573\ |3p^4\ 3d'\ ^2S_{\frac{1}{2}}\rangle$$
$$- 0.26416\ |3p^4\ 4d'\ ^2S_{\frac{1}{2}}\rangle + 0.02091\ |3p^4\ 4s''\ ^2S_{\frac{1}{2}}\rangle$$
$$+ \text{small components from some other states.}$$

He has demonstrated that about 40% of the oscillator strength for the transition $3s^2$ $3p^6$ - 3s $3p^6$ was transferred to $3s^2$ $3p^6$ - $3s^2$ $3p^4$ nd' transition.

Quantitative information on this interaction obtained in the present work is shown in figure 1.22 and Table 1.9. This information is compared with Luyken's calculations and with other data obtained by different experimental techniques.

It is clearly seen from figure 1.16 and figure 1.18 that the high energy behavior of the $^2S_{\frac{1}{2}}$ excitation functions are distinctly different from others because of the strong interaction with the 3s p^6 $^2S_{\frac{1}{2}}$ state. Since the $^2S_{\frac{1}{2}}$ levels are

not complicated by significant cascade, the level cross sections can be obtained unambiguously.

For $3d'\ ^2S_{\frac{1}{2}}$, Luyken's calculations indicate that the only depopulating transitions which need be considered are those to the ground states. Cascade into this state should not be a problem because of the small cross sections of the states which would be involved. Further, any cascade contribution will fall off rapidly with energy because of the two electron nature of the initial excitation. Hence the $3d'\ ^2S_{\frac{1}{2}}$ level cross-section is represented by the sum of the cross-sections for 543 and 547 Å. A complicating feature which must be accounted for is the possible contribution to the measured cross-section from the nearby lines. Again this effect will decrease towards high electron energy. Quartet states show an especially rapid decrease in cross-section with energy (Feltsan and Povch 1970) and so it is assumed that contribution from these states may be neglected at high energies. To correct for contributions from 5s levels, it was assumed that the 5s excitation function was similar in shape to the 4s excitation function. Background contributions were thus calculated to vary from 10% at 1 keV to 7% at 2 keV.

Transitions from the $4d'$ state to states other than $^2P_{\frac{1}{2},\frac{3}{2}}$ ground states are also probably insignificant. Only three were recorded by Minnhagen and these with low intensities.

We assumed that the sum of the line cross-sections for 487 and 491 Å gives the total $4d'\ ^2S_{\frac{1}{2}}$ level cross-section. Table 1.1 indicates that overlap with adjacent lines is a serious problem at 100 eV. The significance will decrease as the electron energy increases for the reasons discussed previously. As a first approximation to this background contribution at higher energies, the 5d excitation function was assumed to have the same shape as the 4d one. This enabled background corrections of 15% at 1 Kev and 10% at 1800 eV to be estimated.

For $3s\ 3p^6\ ^2S_{\frac{1}{2}}$ the only possible transitions are to the ground states and the only possibly significant cascade into this level is from the $4p'\ ^2P$ states via the 1575 and 1560 Å lines. This was investigated by Luyken et al (1972) and found to be negligible. Hence, no corrections for cascade need be applied and the $3s\ 3p^6\ ^2S_{\frac{1}{2}}$ level cross-section is simply the sum of the cross-sections for 920 and 932 Å.

It is shown in figure 1.22 that the ratio of the $3s\ 3p^6\ ^2S_{\frac{1}{2}}$ and $3d'\ ^2S_{\frac{1}{2}}$ cross-sections was foumd to reach a constant value of 4.15 above 1 keV, and the ratio of the $3s\ 3p^6\ ^2S_{\frac{1}{2}}$ and $4d'\ ^2S_{\frac{1}{2}}$ cross-sections reached a constant value of 7.9 at energies exceeding 1 keV. The constancy of the cross-section ratio at high energy plus the fact that the Bethe plots all have a positive slope is conclusive supporting evidence for the existance of configuration interaction linking the three levels.

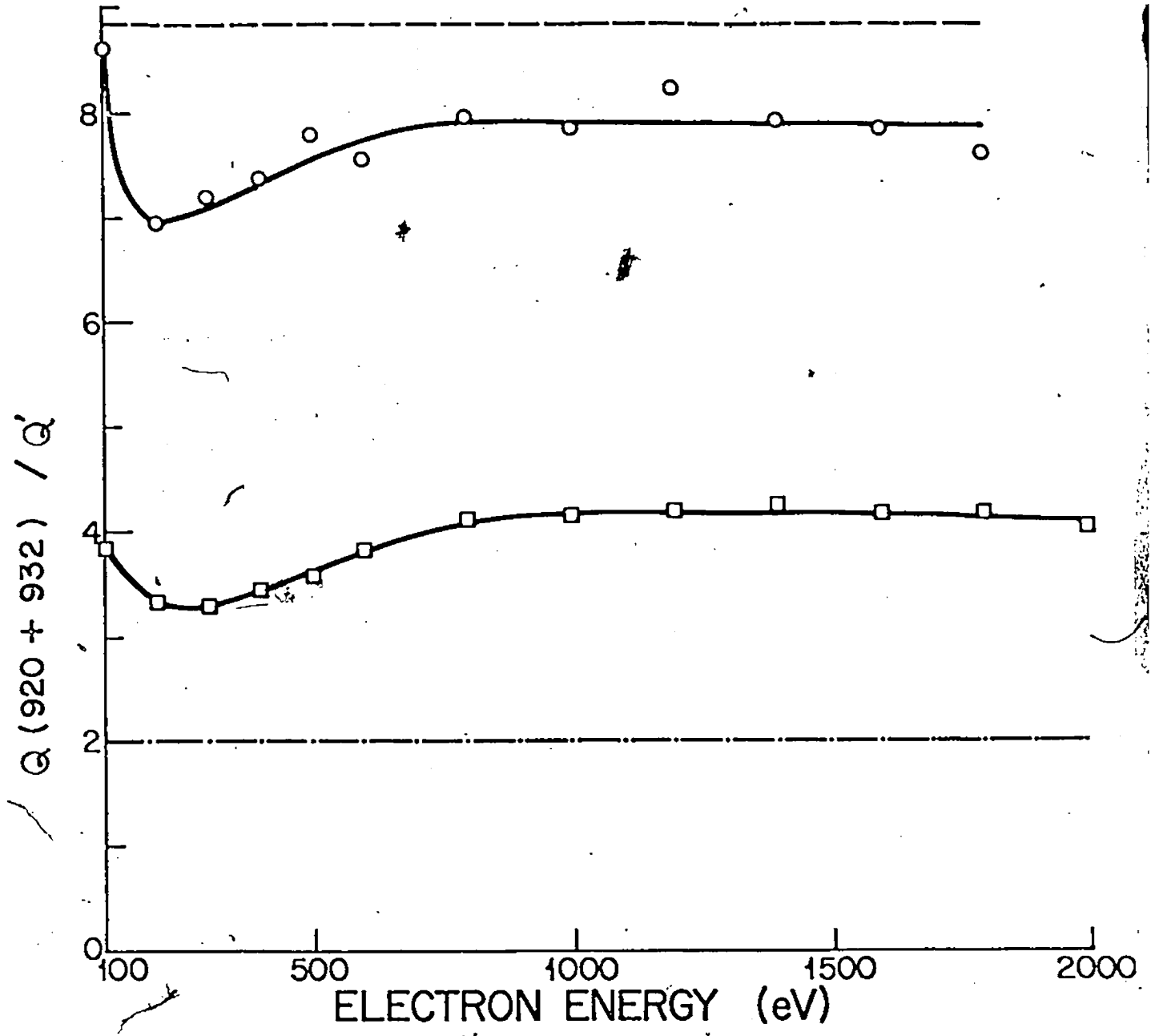

Fig.1.22. Ratio of $3s3p^6\ ^2S_{\frac{1}{2}}$ cross section Q'(920+932) to the $3s^2 3p^4 nd'\ ^2S_{\frac{1}{2}}$ cross section Q' as a function of electron energy. Dashed line(----), n=4, Luyken(theory); (-o-o-), n=4, present work; dash-dot line(-·-·-), n=3, Luyken(theory); (-□-□-), n=3, present work.

TABLE 1.9.

Relative cross sections of $^2S_{\frac{1}{2}}$ states.

State	Present work[a] (electron impact)	Luyken[b] (theory)	Spears et al. (X-ray input)	Weigold et al. (e-2e experiment)	J.Williams[c] (e-2e experiment)
$3s3p^6$	100	100	100	100	100
$3p^4 3d'$	24^{+13}_{-9}	50	$(15\text{-}19)\pm 2^d$	72 ± 12^e	40 ± 5
$3p^4 4d'$	12.7^{+7}_{-4}	11	$(6\text{-}8)\pm 3^d$		40 ± 5
$3p^4 4s''$	$10.6\pm 3.2^*$	1.4			5 ± 2

[a] Errors given in the present work are based on assumed errors of ±20% in the cross-section values.

[b] Luyken, 1972.

[c] Private communication, 1974.

[d] Spears et al. found that their values depend slightly on X-ray energy.

[e] Weigold et al. were unable to resolve the 3d' and 4d' states.

* Cross section measured at 100 eV.

The relative corss-section of the $4s''\ ^2S_{\frac{1}{2}}$ state was only measured at 100 eV. The value obtained is given in Table 1.9. It is obvious that this measurement, as well as the value obtained by J. Williams is much higher than Luyken's predictions. Cascade contributions are likely from the 4p'', 5p and 4d states. The only available measurement is by Feltsan and Povch (1970) for the $5p^4\ D_{\frac{1}{2}} - 4s''\ ^2S_{\frac{1}{2}}$ transition. Thus cascade into this state may be quite significant but unfortunately we have no way of quantitatively determining its magnitude. Even if direct excitation accounts for only 20% of the observed signal, we still get disagreement with the theoretical predictions.

A number of additional points are evident from figure 1.22 and also from Table 1.9. The drop offs in the ratios towards lower energy are consistant with interference from cascade and neighbouring lines. Our data suggests that the mixing of the $3s\ 3p^6\ ^2S_{\frac{1}{2}}$ state with the 3d' state is smaller than Luyken's calculations whereas mixing with the 4d' state and 4s'' state seems to be rather stronger. Our error bars are unfortunately two large to be definite about this discrepancy. Weigold et al (1973) and J. Williams (private communication 1974) find a much larger contribution from the combined d'states than do Spears et al (1974) (see Table 1.9) or the present work. J. Williams has succeeded in resolving

the 3d' and 4d' states and found that they are of equal intensity.

CHAPTER VI

CONCLUSION

We have presented polarization free measurements of the cross-sections for the 4s, 4 s', 5s, 3d, 4d, 5d, 3d' and 4d' configurations of Ar^+ using electron impact.

A double peaked structure has been demonstrated to be a common feature of the Ar^+ excitation functions.

The measured cross-sections were made absolute by using the well known resonance lines of He (522, 537, 584 Å) and Ne (736 Å) as basic standards. The actual comparison between two lines or groups of lines was through comparison of the slopes of intensity-pressure plots.

Except where configuration interaction with the 3s $3p^6$ $^2S_{\frac{1}{2}}$ state is occurring, the high energy dependence of the cross-section is shown to be consistant with the dipole-forbidden, two electron nature of the exciting transitions from the Ar ground state. Cascade is shown to be an important excitation process for the 4s levels. Where cascade could be properly taken into account, it was demonstrated that states of given orbital angular momentum and multiplicity were populated according to their statistical weights. In some cases significant discrepancies were observed between

experimental relative transition probabilities and theoretical calculations.

Considerable evidence was uncovered for configuration interaction effects. Those caused considerable enhancement of the $3d'$, $4d'$ and 4d level cross sections. Quantitive measurements of the mixing between $3s\ 3p^6\ ^2S_{\frac{1}{2}}$ and $3s^2\ 3p^4\ 3d'$ and $4d'\ ^2S_{\frac{1}{2}}$ were made and discrepancies with theory and other experimental work were demonstrated.

This work has formed the basis of three publications, Tan et al (1974), Tan and McConkey (1975a, 1975b).

PART II

Electron-Photon Angular Correlations in Electron Helium And Electron-Argon Collisions

CHAPTER VII

REVIEW OF PREVIOUS WORK

In recent years, coincidence techniques have been used to measure the parameters of electron-atom collisions. The first electron-photon coincidence experiment was done by Imhof and Read to measure the lifetime of the three helium states: $3\,^3D$, $4\,^3S$ and $4\,^1S$ (1969, 1971). King et al (1972) measured the "threshold" polarization of helium $1\,^1S - 3\,^1P - 2\,^1P$ process by measuring in coincidence inelastically forward scattered electrons and the photons observed at 90° to the incident beam direction and polarized parallel and perpendicular to this direction. In 1971 Macek and Jaceks developed a theory relating electron-photon coincidence rates to collision parameters such as inelastic scattering amplitudes, partial sub-level cross-sections and phase angles of scattering amplitudes. Since then considerable progress has been made in such studies, particularly in connection with experimental investigations of inelastic electron-photon angular correlations. Recently, Fano and Macek (1973) have related the electron-photon angular correlation to target orientation and alignment parameters. Blum and Kleinpoppen (1975) formulated the theory of coincidence experiments in

terms of polarization density matrices, or, equivalently, the Stokes parameters. The progress both on the experimental and theoretical side namely the extraction of collision amplitudes and the detailed analysis of target parameters has brought us to a much deeper understanding of the electron-atom excitation process.

In 1974 Eminyan et al had studied extensively the electron-photon angular correlations measured by delayed coincidences between electrons scattered inelastically from helium and 584 A photons emitted in the decay of the $2\,^1P$ state. From the angular correlation they deduced the ratio of the differential cross-sections for exciting the degenerate magnetic sublevels of the 2^1P state $\left(\lambda=\frac{\sigma_0}{\sigma_0+2\sigma_1}\right)$ and the relative phase of the corresponding excitation amplitudes, $|\chi|$, for electron scattering angles between 16^o and 40^o and for incident electron energies in the range 40 to 200 ev. Their measurements demonstrated the inadequacy of the Born approximation which predicted that the transition $2^1P - 1^1S$ should be completely polarized parallel to the momentum transfer direction, which means that no photon emission would occur in that direction. This is contradicted by experiment. The data also showed that electron-helium collisions produced considerable atomic orientation, which indicates the degree to which orbital angular momentum is transfered to the atom

during the collision. Further the alignment of the atomic dipole radiation pattern can depart significantly from the direction of linear momentum transfer at larger scattering angles. Their results showed satisfactory agreement with the recent distorted wave calculation of Madison and Shelton (1973). Large discrepancy was observed at large scattering angles between the measurements of Eminyan et al (1974) and the ten-channel eikonal treatment of Flannery and McCann and the many body approach of Thomas et al (1974). Significantly, these theories give very good agreement with experiment if comparison is made with total or with differential cross-sections. This is because most of the scattering occurs in the forward angles.

Arriola, Teubner, Ughabe and Weigold (1975) recently reported electron-photon angular correlations from the excitation of the J=1 levels in argon at 11.62 and 11.83 V and the 1067 and 1048 Å photons which result from the decay of these levels to the $^1S_0$ ground state. The excited J=1 levels are $^3P_1$ and $^1P_1$ states in the L-S coupling scheme. Due to insufficient energy resolution, the electron photon angular correlations from the excitation/deexcitation of the $^1P_1$ and $^3P_1$ could not be separated from each other. They attempted to extract λ and χ parameters from the measured angular correlations by estimating the relative cross-

sections for the excitation of the triplet state from theory and the corresponding ratio in Neon. They assumed a value of approximately 0.2 at the energy and angles employed in the experiment. For this ratio they claimed their results were, within the experimental error, consistant with $\lambda_1 = \lambda_3$ and $\chi_1 = \chi_3$.

However, it is questionable whether their procedure was justified and separate measurements of the singlet and triplet angular correlations are needed to resolve the issue.

In 1975 Kleinpoppen, Blum and Standage reported the theoretical and experimental analysis of polarization and coherence of coincident photon radiation. The electron-photon coincidences was based on the assumption of coherent excitation of the magnetic sub-levels. Based upon this assumption, they extracted the parameters λ and χ from the angular correlation measurements for the helium 2^1P-1^1S and 3^1P - 1^1S transitions together with the 3^1P-2^1S transition at 80ev. In comparison with theoretical predictions, their measurements when compared with the distorted wave approximation of Madison and Shelton, were in remarkably good agreement in λ whereas the agreement with the phase parameter χ is only qualitatively satisfactory.

In order to prove the previous model of coherent excitation it is necessary to observe the photons and study their

polarization perpendicular to the scattering plane. (See theoretical section). Standage and Kleinpoppen (1975) first investigated the He 3^1P - 2^1S (5016A) transition at an incident electron energy of 80eV. They were able to demonstrate the coherence of the photon beam and hence of the excitation process by measuring the Stokes parameters involved and demonstrating that the degree of polarization of the photon beam (Born & Wolf 1959)was unity. They also concluded that for helium 3^1P, λ and χ data obtained from the angular correlation measurements in the scattering plane were consistent with the polarization data measured perpendicular to the scattering plane.

These measurements are significant for several reasons. Previous experimental work in electron-atom collisions has usually involved averages over significant parameters in the scattering. Differential cross-section measurements do not distinguish the excitations to degenerate magnetic sublevels. Measurements of line polarization in excitation function experiments do separate the contributions of magnetic sublevels but obtain only integral cross-sections. Furthermore the relative phases of the excitation amplitudes for degenerate magnetic sublevels can be deduced in an electron photon coincidence experiment .

CHAPTER VIII

THEORY

The theory of measurements in which photons are detected in delayed coincidence with scattered electrons has been developed in a form which relates the coincidence rates for electron-photon angular correlations to the collision parameters (Macek and Jaceks 1971) or to the orientation and alignment parameters (Fano and Macek 1973) or to the Stokes parameters (Blum and Kleinpoppen).

The basic physics underlying electron-photon correlations is most easily demonstrated by the inelastic excitation of the 1^1S_o-2^1P_1 , transition and the subsequent emission of radiation when spin-spin and spin-orbit effects are negligible.

A 2^1P state of He excited from the ground state 1^1S_o in a field free region by electron impact in which the electron is scattered in a particular direction (θ_e, ϕ_e) measured relative to the electron beam axis, can be described as a coherent superposition of degenerate magnetic sublevels as follows.

$$\psi(^1P) = a_o|10> + a_1|11> + a_{-1}|1-1> \quad ---(2.1)$$

with a_o, a_1 and a_{-1} as excitation amplitudes for the transition under the selection rules $\Delta M_L = 0$ and $\Delta M_L = \pm 1$. The excitation amplitudes $a_{M_L}(E_o, \theta_e, \phi_e)$ describe the

excitation to particular magnetic sublevels $|L,M_L\rangle$ by electrons of incident energy E_o scattered through an angle θ_e and ϕ_e. Mirror symmetry of the scattering process with respect to the scattering plane (the incoming electron beam and the inelastically scattered electron direction define a scattering plane) requires that $a_1 = -a_{-1}$. The above wave function can be normalized so that the amplitudes a_o and a_1 are related to the differential cross-sections for exciting the magnetic sub-levels as follow.

$$\left.\begin{aligned} |a_1|^2 &= \sigma_1 \\ |a_o|^2 &= \sigma_o \\ 2|a_1|^2 + |a_o|^2 &= \sigma \end{aligned}\right\} \qquad \text{------(2.2)}$$

Here σ is the total differential excitation cross-section.

The amplitudes a_{M_L} are in general complex numbers defined only up to an overall phase factor. If a_o is assumed real and positive, the relative phase χ between a_1 and a_o is then defined by:

$$a_1 = |a_1| \exp.i\chi \qquad \text{------(2.3)}$$

Therefore ψ is described completely for given E_o, θ_e and ϕ_e by parameters σ, λ and χ. Thus a measurement of σ, λ and χ constitutes a complete determination of the scattering. σ is a measure of the probability of electron scattering in different directions, while λ and χ describe the state of the atom after the collision. The parameters λ and χ are more sensitive tests of the approximations involved in the theory

than are differential cross-sections.

The general formulation of Macek and Jaceks which relates the coincidence rate to the collision parameters λ, σ and χ without measurement of polarization is

$$\frac{dN_c}{d\Omega_\nu d\Omega_e} = C\left\{A_{oo} + A_{11} + (A_{11} - A_{oo})\cos^2\theta_\nu + \sqrt{2}\,\mathrm{Re}A_{o1}\sin 2\theta_\nu \cos(\phi_e - \phi_\nu) + A_{1-1}\sin^2\theta_\nu \cos 2(\phi_e - \phi_\nu)\right\} \quad \text{-----(2.4)}$$

where C is a constant depending on particle density of the incoming beam, the velocity of the beam and the target atom density. A_{jk} are quantities which are determined by the structural features of the atom affecting the coupling schemes, effects due to the width and separation of energy levels and the excitation amplitudes to be measured. The schematic collision geometry is shown in Fig. 2.1. The incoming beam axis is taken to be the Z axis. The angular coordinates of the electron detector are denoted by θ_e and ϕ_e and the coordinates of the photon detector by θ_ν and ϕ_ν. The incoming beam axis and the inelastically scattered electron direction define a scattering plane, so that the geometry possesses only reflection symmetry.

For the excitation de-excitation process of helium $1^1S_o - 2^1P_1 - 1^1S_o$ we have for A_{jk} (see Macek and Jaceks) :—

$$\left.\begin{aligned} A_{oo} &= \sigma_0/\gamma, \quad A_{11} = -A_{1-1} = \sigma_1/\gamma \\ A_{o1} &= \mathrm{Re}\langle a_o a_1^* \rangle/\gamma = (\sigma_o\sigma_1)^{\frac{1}{2}}\cos\chi/\gamma \end{aligned}\right\} \text{------(2.5)}$$

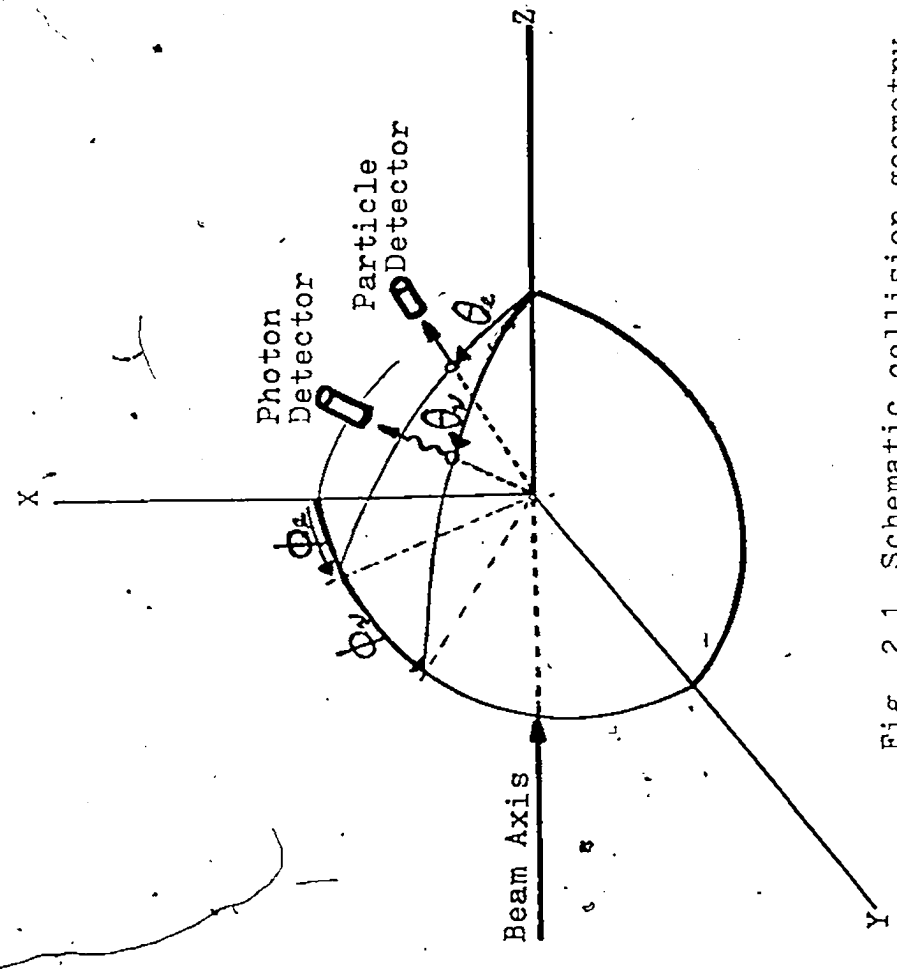

Fig. 2.1. Schematic collision geometry.

where $1/\gamma$ is the mean life of the excited atom.

Equation (2.5) then takes the form

$$\frac{dN_c}{d\Omega_e d\Omega_\nu} = N_c \infty \sigma \left\{ \lambda \sin^2\theta_\nu + (1-\lambda)\left[1 - \sin^2\theta_\nu \cos^2(\phi_e - \phi_\nu)\right] + \left[\lambda(1-\lambda)\right]^{\frac{1}{2}} \cos\chi \sin 2\theta_\nu \cos(\phi_e - \phi_\nu) \right\} \quad ---(2.6)$$

When the experimental arrangement is such that the photons are detected in the scattering plane on the opposite side of the electron beam ie. $\phi_e - \phi_\nu = \pi$ (Coplanar geometry) equation (2.6) reduced to the following form.

$$N_c \infty \sigma \left\{ \lambda \sin^2\theta_\nu + (1-\lambda)\cos^2\theta_\nu - \left[\lambda(1-\lambda)\right]^{\frac{1}{2}} \cos\chi \sin 2\theta_\nu \right\} \quad ----(2.7)$$

where N_c is a positive sinusoidal function of θ_ν whose mean value is 1/2 and whose period is π. It varies between 0 and 1 as a function of λ, $|\chi|$ and θ_ν.

In the present experiment, the electron beam is incident in the z direction on the target located at the origin of coordinates. Inelastically scattered electrons are scattered, at fixed angle of 42°. Photons are detected perpendicular to the incident beam direction that is $\theta_\nu = \pi/2$. equation 2.7 is then reduced to a simple form as follows:

$$N_c \infty \sigma \left[\lambda + (1-\lambda)\sin^2(\phi_e - \phi_\nu) \right] \quad -----(2.8)$$

The coincidence rate depends only on λ and the relative angle between the electron detector and the photon detector. Therefore λ can be obtained directly by the ratio of the number of coincidence counts at $\phi_e - \phi_\nu = 0$ or π to that at $\phi_e - \phi_\nu = \pi/2$, that

is $$\lambda = \frac{N_c(0)}{N_c(\pi/2)} \qquad \text{-----(2.9)}$$

This arrangement greatly simplified the determination of the parameter λ at the cost of losing all the information about χ.

The coincidence rate N_c given above was derived on the assumption that the states involved in the observed process can be described in terms of L-S coupling and that the excitation of the sublevels with $\Delta M_L = 0$ and $\Delta M_L = \pm 1$ is coherent. In the case of argon this assumption is questionable. And in our experiment a lack of energy resolution allows only the observation of an overall coincidence rate involving two processes namely the excitation of both $^1S_o - ^1P_1$ and $^1S_o - ^3P_1$ transitions and the subsequent decay of 1048 Å and 1067 Å photons. The $^1S_o - ^3P_{o,2}$ process yields metastable states and does not contribute to the genuine coincidence rate. Since the separation of the excited states is much larger than their level widths, the two relevant processes can be considered to be incoherently mixed. Therefore, if the validity of L-S coupling is postulated, the observed coincidence rate is given by:

$$N_c \propto \sigma^{(s)} \left[(1-\lambda^{(s)})\sin^2(\phi_e - \phi_\nu) + \lambda^{(s)}\right] + \sigma^{(t)}\left[(1-\lambda^{(t)})\cdot \sin^2(\phi_e - \phi_\nu) + \lambda^{(t)}\right] \qquad \text{-----(2.10)}$$

where the superscripts (s) and (t) refer to the singlet and

the triplet channel respectively. Let

$$k=\sigma^{(t)}/\sigma^{(s)} \quad \text{-----(2.11)}$$

equation (2.11) gives

$$\frac{N_c(0)}{N_c(\pi/2)} = (1+k)^{-1}\,\lambda^{(s)} + (1+k^{-1})^{-1}\,\lambda^{(t)} \quad \text{-----(2.12)}$$

Thus the experiment does not yield values for the two channels separately (unless $\lambda^{(s)}=\lambda^{(t)}$), but only a relationship between them. This relationship is illustrated in Fg. (2.2). For the sake of argument, assume that $k<(1+k^{-1})N_c(0)/N_c(90^o)<1$. As by definition, $\lambda<1$ for both channels the permitted range of λ valves are limited. If, on some other ground, one of the two parameters can be assigned a value then the other becomes fully determined.

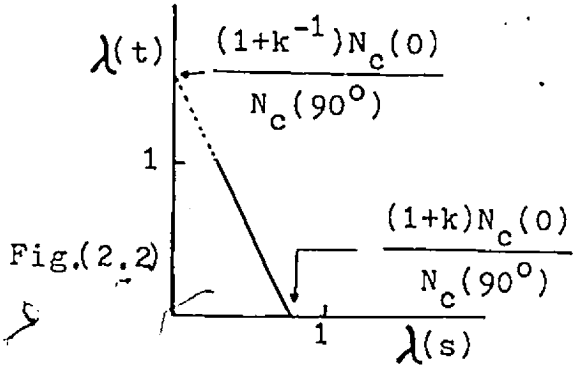

Fig.(2.2)

It goes without saying that the value of k must be derived from some independent evidence and the smaller k the narrower the allowed range of $\lambda^{(s)}$ but $\lambda^{(t)}$ becomes increasingly indeterminate.

Polarization Correlation:

In order to be able to measure the relative phase of the excitation amplitudes χ using our system, an alternative approach which includes the polarization of the de-excitation radiation in equation (2.4) can be used. When the photon

polarization is considered the general equation which relate the coincidence rate to the collision parameters is as follows (see Masek and Jaceks 1971, equation 15).

$$N'_c(\beta) \propto \{A_{oo}\cos^2\beta + A_{11}\sin^2\beta + (A_{11}-A_{oo})\cos^2\beta\cos^2\theta_\nu + \sqrt{2}\,\mathrm{Re}A_{o1}[\sin 2\theta_\nu\cos^2\beta\cos(\phi_e-\phi_\nu) + \sin 2\beta\sin\theta_\nu\sin(\phi_e-\phi_\nu)] - \mathrm{Re}A_{1-1}[(\cos^2\beta\cos^2\theta_\nu - \sin^2\beta\cos 2(\phi_e-\phi_\nu) + \sin 2\beta\cos\theta_\nu\sin 2(\phi_e-\phi_\nu)]\} \quad ----(2.13)$$

where β is the angle of the analyser axis relative to the incident electron beam direction: When the photon is observed perpendicular to the scattering plane, ie. $\theta_\nu=\pi/2$ and $\phi_e-\phi_\nu=\pi/2$ and if we take $\mathrm{Re}A_{1-1} \equiv A_{1-1}$, we obtain:

$$N'_c(\beta) \propto \left\{A_{oo}\cos^2\beta + (A_{11}-A_{1-1})\sin^2\beta + \sqrt{2}\,\mathrm{Re}A_{o1}\sin 2\beta\right\} \quad ---(1.14)$$

Let:

$$N_c(\beta) = A_{oo}\cos^2\beta + (A_{11}-A_{1-1})\sin^2\beta + \sqrt{2}\,\mathrm{Re}A_{o1}\sin 2\beta \quad ---(2.15)$$

By performing two coincidence measurements one at angle β and one at $\beta+\pi/2$ relative to the incident electron beam direction using a linear polarizer, we obtain a polarization ratio

$$P(\beta) = \frac{N_c(\beta) - N_c(\beta+\pi/2)}{N_c(\beta) + N_c(\beta+\pi/2)} \quad -----(2.16)$$

Substituting (2.15) into (2.16)

$$\therefore \quad P(\beta) = \frac{A_{oo}-(A_{11}-A_{1-1})}{A_{oo}+(A_{11}-A_{1-1})}\cos 2\beta + \frac{2\sqrt{2}\,\mathrm{Re}A_{o1}}{A_{oo}+(A_{11}-A_{1-1})}\sin 2\beta \quad ---(2.17)$$

The relationship between the quantities A_{jk} and the excitation amplitudes of interest depend on the atomic species under consideration. For $He: {}^1S\text{-}2^1P$ transition.

$$P(\beta) = (2\lambda-1)\cos 2\beta + 2\sqrt{\lambda(1-\lambda)}\cos\chi\sin 2\beta \quad -----(2.18)$$

P. S. Farago (private communication) has shown that we may

write $P(\beta)$ in a general form applicable to different atomic species as

$$P(\beta)=P_{th}\left\{\left[2\lambda-1\right]\cos 2\beta+2\sqrt{\lambda(1-\lambda)}\cos\chi\sin 2\beta\right\} \quad ---(2.19)$$

where P_{th} is the "threshold polarization". For helium 1^1S-2^1P transition $P_{th}=1$. For H transition $1^2S_{\frac{1}{2}}$-$2^2P_{\frac{1}{2},3/2}$, $P_{th}=3/7$ and for Na transition $3^2S_{\frac{1}{2}}$-$3^2P_{\frac{1}{2},3/2}$, $P_{th}=3r/1+r$ where $r=(1/6)-\Delta r$ with $0.13<\Delta r<0.73/6$

Equation (2.19) gives for He 1^1S-2^1P transition

$$P(0) = 2\lambda-1 \quad -----(2.20)$$

and

$$P(\pi/4) = 2\sqrt{\lambda(1-\lambda)}\cos\chi \quad -----(2.21)$$

Note that the orientation of the dipoles (equation 26 of Masek and Jaceks 1971) or the angle at which the minimum of the radiation pattern occurs is characterized by:

$$\tan 2\theta_{min} = \frac{2\sqrt{2}\,\mathrm{Re}(a_0 a_1^*)}{\sigma_0-2\sigma_1} = \frac{P(\pi/4)}{P(0)} = \frac{2\sqrt{\lambda(1-\lambda)}\cos\chi}{2\lambda-1} \quad ---(2.22)$$

Thus a measurement of $P(0)$ and $P(\pi/4)$ is equivalent to a scan of the angular correlation in coplanar observation. A knowledge of these two independent linear polarization values are sufficient for the determination of λ, $|\chi|$ and θ_{min}. In order to obtain the sign of χ a measure of the circular polarization of the photons is required as discussed later. We note that $P(0)$ and $P(\pi/4)$ are the first two Stokes parameters designated P_1 and P_2 by Kleinpoppen et al (1975).

Degree of Coherence of Photons and the Stokes Parameters

We have previously mentioned that, the co-planar angular correlation function (equation 2.7) was based upon the model of coherent excitation, disregarding photon polarization. Although this is expected to be correct for the transition, it cannot be unambiguously proved. This is because the angular correlation as observed in the scattering plane can also be fitted to an angular correlation which results from the incoherent superposition of two harmonic oscillators, oscillating incoherently parallel to the main axes of the polarization ellipse. Thus, to obtain more conclusive information, it is necessary to measure the degree of coherence of the photons emitted perpendicular to the scattering plane. (Note: partially polarized light can be regarded as the superposition of incoherent polarized components emitted by atoms in a particular state but with different values of the magnetic quantum number M_L. Fano 1949).

The properties of light are most conveniently considered in terms of four Stokes parameters S_0, S_1, S_2, S_3, which form the components of a four-vector in polarization space.

The monochromatic Stokes parameters are defined in terms of the electric vectors in two mutually orthogonal directions perpendicular to the direction of propagation. Assuming that the light wave is propagating in the Y direction

$$
\begin{aligned}
S_o &= a_z^2 + a_x^2 \\
S_1 &= a_z^2 - a_x^2 \\
S_2 &= 2\mathrm{Re}(a_z a_x^*) \\
S_3 &= 2\mathrm{Im}(a_z a_x^*)
\end{aligned}
\qquad \text{-----(2.23)}
$$

where a_z and a_x are the complex amplitudes of the two orthogonal electric vectors E_z and E_x. S_o is the intensity of the light; S_1 and S_2 are measurements of linear polarization and S_3 is a measure of circular polarization of the beam.

S_o, S_1, S_2, and S_3 are measurable quantities and the simplest and most common way to measure these Stokes parameters is to use a linear polarizer and a quarter wave plate. The Stokes parameters can be measured as follows:

$$
\begin{aligned}
S_o &= I(\alpha=0^\circ) + I(\alpha=90^\circ) \\
S_1 &= I(\alpha=0^\circ) - I(\alpha=90^\circ) \\
S_2 &= I(\alpha=45^\circ) - I(\alpha=135^\circ) \\
S_3 &= I(\mathrm{RHC}) - I(\mathrm{LHC})
\end{aligned}
\qquad \text{-----(2.24)}
$$

With regard to photons observed perpendicular to the scattering plane, $I(\alpha)$ is the linear polarized intensity component measured at a polarization angle, α, to the incident electron beam. RHC and LHC stand for right hand and left hand circular polarization.

S_1, S_2 and S_3 are related in a simple way to the angle

$\psi\left|0\leq\psi\leq\frac{\pi}{2}\right|$ (See figure 2.3) which specifies the orientation of the ellipse and the angle $\gamma\left|-\frac{\pi}{4}\leq\gamma\leq\frac{\pi}{4}\right|$ which characterizes the ellipticity and the sense of the ellipse is being described. By convention, right-hand polarization is identified by a positive value of γ and left-hand by a negative one. The following relations hold (Born and Wolf 1959):

$$\begin{aligned} S_1 &= S_o \mathrm{Cos}2\gamma\, \mathrm{Cos}2\psi \\ S_2 &= S_o \mathrm{Cos}2\gamma\, \mathrm{Sin}2\psi \\ S_3 &= S_o \mathrm{Sin}2\gamma \end{aligned} \qquad \text{-----(2.25)}$$

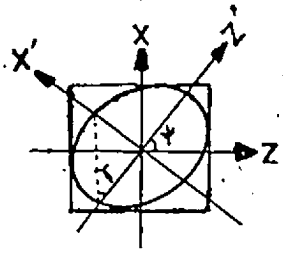

Figure 2.3

The degree of polarization is given by

$$P = (S_1^2+S_2^2+S_3^2)^{\frac{1}{2}}/S_o \qquad \text{-----(2.26)}$$

A light beam is completely coherent, if and only if the beam is completely polarized; that is P=1; partial polarization; P<1 , is a consequence and characteristic sympton of incomplete coherence. A completely incoherent beam of light is unpolarized; P=0.

An alternative treatment of polarization is to introduce the density matrix. According to quantum mechanics, the density matrix which represents the polarization state of a light beam is a 2 x 2 matrix, such as:

$$J = \begin{vmatrix} \langle E_z E_z^* \rangle & \langle E_z E_x^* \rangle \\ \langle E_x E_z^* \rangle & \langle E_x E_x^* \rangle \end{vmatrix} = \begin{vmatrix} \langle a_z^2 \rangle & \langle a_z a_x \exp.i\beta_{zx} \rangle \\ \langle a_x a_z \exp.-i\beta_{zx} \rangle & \langle a_x^2 \rangle \end{vmatrix} \text{---(2.27)}$$

where $E_z(t)=a_z(t)\exp.i(\beta_z-\omega t)$ and $E_x(t)=a_x(t)\exp.i(\beta_x-\omega t)$

represent two mutually orthogonal electric vectors. This matrix equally well characterizes the polarization of the radiation in as much as its diagonal elements yield the total intensity; $\mathrm{Tr}\, J = J_{zz}+J_{xx}=\langle E_z E_z^* + E_x E_x^* \rangle$. The off diagonal elements are complex but they are conjugates of each other; such as $J_{zx}=J_{xz}^*$. These four matrix elements are related to the Stokes parameters as follows:

$$\begin{aligned} S_o &= J_{zz} + J_{xx} \\ S_1 &= J_{zz} - J_{xx} \\ S_2 &= J_{zx} + J_{xz} \\ S_3 &= i(J_{xz} - J_{zx}) \end{aligned} \qquad \text{-----(2.28)}$$

The characteristic criterion for completely polarized radiation, $S_o^2 = S_1^2 + S_2^2 + S_3^2$ is equivalent to the condition $\det J = 0$ which follows immediately from (2.28).

Additional quantities which characterize the degree of coherence of the emitted light can be determined from measurements of Stokes parameters. Following Born and Wolf (1959), the 'correlation factor' for partially coherent quasi-monochromatic light is as follows:

$$\mu_{zx} = |\mu_{zx}| \exp.i\beta_{zx} = \frac{J_{zx}}{\sqrt{J_{zz} \cdot J_{xx}}} = \frac{S_2 + iS_3}{(S_o^2 - S_1^2)^{\frac{1}{2}}} \qquad \text{-----(2.29)}$$

μ_{zx} is a measure of the correlation between the x and z

components of the electric vector of the radiation, $|\mu_{zx}|$ is a measure of their "degree of coherence" and β_{xz} is a measure of their 'effective phase difference'.

Since $S_o^2 = S_1^2 + S_2^2 + S_3^2$ (Born and Wolf 1959), it can be shown that $|\mu_{zx}| \leq 1$; the equality sign holds if and only if the light is completely coherent.

Consider once again the $2^1P - 1^1S$ transitions in He excited by electrons. The collision prepares the atom in the State $\psi(^1P) = a_o\psi_o + a_1\psi_1 + a_{-1}\psi_{-1}$ (equation 2.1). ψ is invariant to reflections in the scattering plane and therefore $a_1 = -a_{-1}$, with the Condon - Shortly phase convention. Thus,

$$\begin{aligned}\psi &= a_o\psi_o + a_1(\psi_1 - \psi_{-1}) \\ &= a_o\psi_z - a_1\sqrt{2}\psi_x \qquad \text{-----(2.30)}\end{aligned}$$

where the z and x subscripts denote the angular part of the wave functions, and a_o and $a_1\sqrt{2}$ are the complex amplitudes of the two radiating oscillators respectively.

Classically ψ_z and ψ_x may represent perpendicular unit polarization vectors and ψ, the resultant polarization vector for a beam with complex amplitudes a_o and $a_1\sqrt{2}$. This means that $|a_o|^2$ and $2|a_1|^2$ yield the intensities one would measure after passing this beam through an analyzer oriented in the direction of ψ_z and ψ_x, respectively. In the quantum description, ψ_z and ψ_x represent orthogonal polarization states

for a photon, and $|a_0|^2$ and $2|a_1|^2$ yield the relative probabilities for a single photon to pass through an analyzer which admits only quanta in the state ψ_z and ψ_x, respectively. In both cases the state of polarization of the photon is completely determined by the two complex amplitudes a_0 and $a_1\sqrt{2}$. Therefore the Stokes parameters for the polarization of this state are:

$$\begin{aligned} S_0 &= |a_0|^2 + 2|a_1|^2 \\ S_1 &= |a_0|^2 - 2|a_1|^2 \\ S_2 &= 2\sqrt{2}\,\mathrm{Re}(a_0 a_1^*) \\ S_3 &= 2\sqrt{2}\,\mathrm{Im}(a_0 a_1^*) \end{aligned} \qquad \text{----- (2.31)}$$

And therefore we have

$$\frac{S_1}{S_0} = \frac{|a_0|^2-2|a_1|^2}{|a_0|^2+2|a_1|^2} = \frac{\sigma_0-2\sigma_1}{\sigma_0+2\sigma_1} = 2\lambda - 1 \qquad \text{--- (2.32)}$$

$$\frac{S_2}{S_0} = \frac{2\sqrt{2}\,\mathrm{Re}(a_0 a_1^*)}{|a_0|^2+2|a_1|^2} = 2[\lambda(1-\lambda)]^{\frac{1}{2}}\cos\chi \qquad \text{---(2.33)}$$

$$\frac{S_3}{S_0} = \frac{2\sqrt{2}\,\mathrm{Im}(a_0 a_1^*)}{|a_0|^2+2|a_1|^2} = 2[\lambda(1-\lambda)]^{\frac{1}{2}}\sin\chi \qquad \text{--- (2.34)}$$

where $\lambda=\frac{\sigma_0}{\sigma}$ and χ is the phase difference between a_0 and a_1. In general nonzero values for S_2 and S_3 depend upon non-random phase difference χ between the excitation amplitudes a_0 and a_1. In traditional electron atom excitation experiments, with axial symmetry, S_2 and S_3 are zero. It also follows from equations (2.38), (2.39) and (2.40) that P=1 is independent of the impact energy and the scattering angle. By comparing equations (2.20) and (2.32), equations (2.21) and

(2.33), we have:

$$S_1 = S_o P(0) \quad \text{---} \quad (2.35)$$

$$S_2 = S_o P(\pi/4) \quad \text{---} \quad (2.36)$$

also let $P(\text{circ}) = -S_3/S_o = -2[\lambda(1-\lambda)]^{\frac{1}{2}} \sin\chi$ ---(2.37)

Hence $I(0)+I(90^o) = I(45^o)+I(135^o) = S_o$ ---(2.38)

The angles characteristic of the orientation and ellipticity are related to the polarization components more elegantly than in equation (2.31) as follows:

$$\begin{aligned} P(0) &= \cos 2\gamma \cos 2\psi \\ P(\pi/4) &= \cos 2\gamma \sin 2\psi \\ P(\text{circ}) &= -\sin 2\gamma \end{aligned} \quad \text{---} \quad (2.39)$$

And $$\tan 2\psi = \frac{P(\pi/4)}{P(0)} \quad \text{-----} \quad (2.40)$$

follows immediately from equation (2.39).

In order to justify the assumption that the magnetic sublevels of the ^1P state of He are coherently excited, one has to measure: $P(0)$, $P(\pi/4)$ and $P(\text{circ})$ and show that

$$P^2(0) + P^2(\pi/4) + P^2(\text{circ}) = 1 \quad \text{---} \quad (2.41)$$

(Note that, from Kleinpoppen et al's experimental results, for the $3^1P - 2^1S$ (5016Å) He transition, the values χ extracted from angular correlation data are in reasonable agreement with the measured $|\beta_{zx}|$, the phase difference between the z and x components of the electric vector observed perpendicular to the scattering plane. (See earlier).

This semiclassical approach is justified when there are no fine or hyperfine structure depolarization, as for ^1P-^1S transition in He .

The linear polarization of the emission from the 2^1P-1^1S transition under consideration can be obtained as follows:

$$P_{zy}^{lin} = (I_z - I_y)/(I_z + I_y) = |a_d|^2/|a_o|^2 = 1 \qquad ---(2.42)$$

$$P_{zx}^{lin} = (I_z - I_x)/(I_z + I_x) = (|a_d|^2 - 2|a_1|^2)/(|a_d|^2 + 2|a_1|^2) = 2\lambda - 1 \qquad ---(2.43)$$

$$P_{xy}^{lin} = (I_x - I_y)/(I_x + I_y) = 2|a_1|^2/2|a_1|^2 = 1 \qquad ---(2.44)$$

where I_x, I_y, I_z are the intensity components polarized parallel to the x , y and z directions respectively; direction of emission is perpendicular to the polarization vectors of the polarized intensity components.

Elliptical polarized light, represented by equation (2.30), resulting from the two linear oscillators can be regarded as a superposition of right-hand circularly polarized light and left hand circularly polarized light with different amplitudes. Thus the circularly polarized light when viewing in +y direction is

$$P_{xz}(circ) = \frac{N^+ - N^-}{N^+ + N^-} = -2\sqrt{\lambda(1-\lambda)}\ \mathrm{Sin}\chi \qquad --- \quad (2.45)$$

where N^+ and N^- are the number of photons with spin parallel and antiparallel to the direction of propagation, in this case the +y direction.

No circular polarization occurs if the direction of observation of the photons is within the scattering plane (xz plane) which is equivalent to the fact that no "net" orbital angular momentum transfer takes place within the scattering plane (will be discussed later).

$$P_{xy}^{circ} = P_{yz}^{circ} = 0 \qquad \text{---} \quad (2.46)$$

The results also explain why $I_y=0$ in equation (2.42) and (2.44).

Target Parameters

Consider the collision Geometry as shown in fig.(2,4). The atom is the center of the scattering force in the scattering plane formed by incoming and outgoing electrons.

Figure 2.4

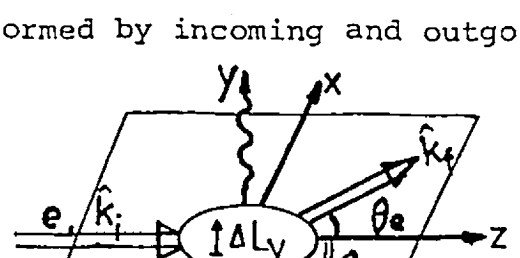

Parity invariance of atomic excitation processes require a zero pseudoscalar, this means in our case that $\Delta\hat{L}_i \cdot \hat{k}_f$ must vanish where $\hat{k}_f$ is the wave vector of the outgoing electron and $\hat{L}_i$ is the orbital angular momentum transfer with respect to the coordinate axis $i = x, y$ or z. Thus the only possible non zero component of the orbital angular momentum transfer is $\Delta\hat{L}_y$. And therefore the orientation of the atom in the excited state is only possible perpendicular to the scattering plane. For the transition $2^1P - 1^1S$ in He , the "target parameters," are the expectation values of angular momentum quantities $\langle L_i \rangle$ and $\langle L_i^2 \rangle$ ($i = x, y$ and z axes), which characterize the angular momentum state of the atom. These parameters can be connected with the collision parameters λ and χ (Kleinpoppen 1974) as follows:

$$\langle L_x \rangle = 0 \ , \quad \langle L_y \rangle = -2\left[\lambda(1-\lambda)\right]^{\frac{1}{2}} \sin\chi \ , \quad \langle L_z \rangle = 0 \ ,$$
$$\langle L_x^2 \rangle = \lambda \ , \quad \langle L_y^2 \rangle = 1 \ , \quad \langle L_z^2 \rangle = 1-\lambda \ . \qquad ---(2.47)$$

with $L^2 = L_x^2 + L_y^2 + L_z^2 = L(L+1) = 2$ for $L=1$.

The quantity $\langle L_y \rangle$ is equal to the circular polarization $P(\text{circ})$ of coincidence photons emitted perpendicular to the plane of scattering. The significance of χ can be seen from this quantity, i.e. the deviation of χ from zero measures the extent to which 2^1P He atoms are produced in an oriented state by scattering at a given energy and scattering angles.

The Stokes parameters can also be linked with the "target parameters" or the alignment and orientation parameters of the excited atom (Fano and Macek 1973).

When the photons are viewed in $+y$ direction, we have at the detector frame: (Berry et al 1974)

$$S_1/S_o = \langle L_x^2 - L_z^2 \rangle \ / \ \langle L_y^2 \rangle \qquad ---(2.48)$$
$$S_2/S_o = 2\mathrm{Re}\langle L_x L_z \rangle \ / \ \langle L_y^2 \rangle \qquad ---(2.49)$$
$$S_3/S_o = -\langle L_y \rangle / \langle L_y^2 \rangle \qquad ---(2.50)$$

S_1/S_o is related to the alignment along the beam axis, while S_2/S_o measures the correlation of L_x and L_z. There can

be no $< L_x L_y >$ or $< L_z L_y >$ correlation because of the reflection symmetry in the xz plane.

The Fano-Macek alignment tensor and orientation vector in the case of coherent excitation of the ^1P state of helium, when photons are viewed in +y direction is connected with λ and χ in the collision frame as follows:

$$A_o^{col} = \tfrac{1}{2} < 3L_z^2 - L^2 > = \tfrac{1}{2}(1-3\lambda) \quad ---(2.51)$$

$$A_{1+}^{col} = \tfrac{1}{2} < L_x L_z + L_z L_x > = \tfrac{1}{2}\left[\lambda(1-\lambda)\right]^{\frac{1}{2}} \cos\chi \quad ---(2.52)$$

$$A_{2+}^{col} = \tfrac{1}{2} < L_x^2 - L_y^2 > = \tfrac{1}{2}(\lambda - 1) \quad ---(2.53)$$

and $$O_{1-}^{col} = \tfrac{1}{2} < L_y > = -\left[\lambda(1-\lambda)\right]^{\frac{1}{2}} \sin\chi \quad ---(2.54)$$

It is just the occurence of the nonzero components A_{2+}^{col}, A_{1+}^{col} and O_{1-}^{col} which implies coherent superposition of states with different M_L values.

Fano and Macek's alignment and orientation parameters in the collision frame may also link with the Stokes parameters at the detector frame as follows:

$$A_o^{col} = -(S_o + 3S_1)/4S_o \quad ---(2.55)$$

$$A_{1+}^{col} = -S_2/2S_o \quad ---(2.56)$$

$$A_{2+}^{col} = (S_1 - S_o)/4S_o \quad ---(2.57)$$

and $$O_{1-}^{col} = -S_3/2S_o \quad ---(2.58)$$

Thus, based upon the model of coherent excitation of ^1P

state of helium, Fano and Macek's alignment and orientation parameters can be measured directly by measuring the Stokes parameters at the detector frame (linear and circular polarizations of the emitted photons.)

CHAPTER IX

APPARATUS

The apparatus consists of six main parts: an electron gun, a cylindrical mirror electrostatic energy analyser, photon detector, uv polarizer, atomic beam source and electron detector, all enclosed within a vacuum chamber. The block schematic diagram of the apparatus is shown in Fig. 2.5 Each part of the apparatus will be described in turn.

The experimental method consists of crossing an atomic beam with a monoenergetic beam of electrons and observing delay coincidences between the inelastically scattered electrons and the photons emitted in the decay of the excited atomic state.

Electrons having lost the appropriate excitation energy are scattered through 42^{o} from the incident beam direction through a ring aperture S_1, as shown in figure 2.6 The Electrons are then slowed down to the desired analysis energy by apertures S_2 and S_3 which are held at the same potential. The energy analyzed electrons are then detected by a channel electron multiplier (CEM) located beyond S_5; on the symmetry axis. The emitted photons are

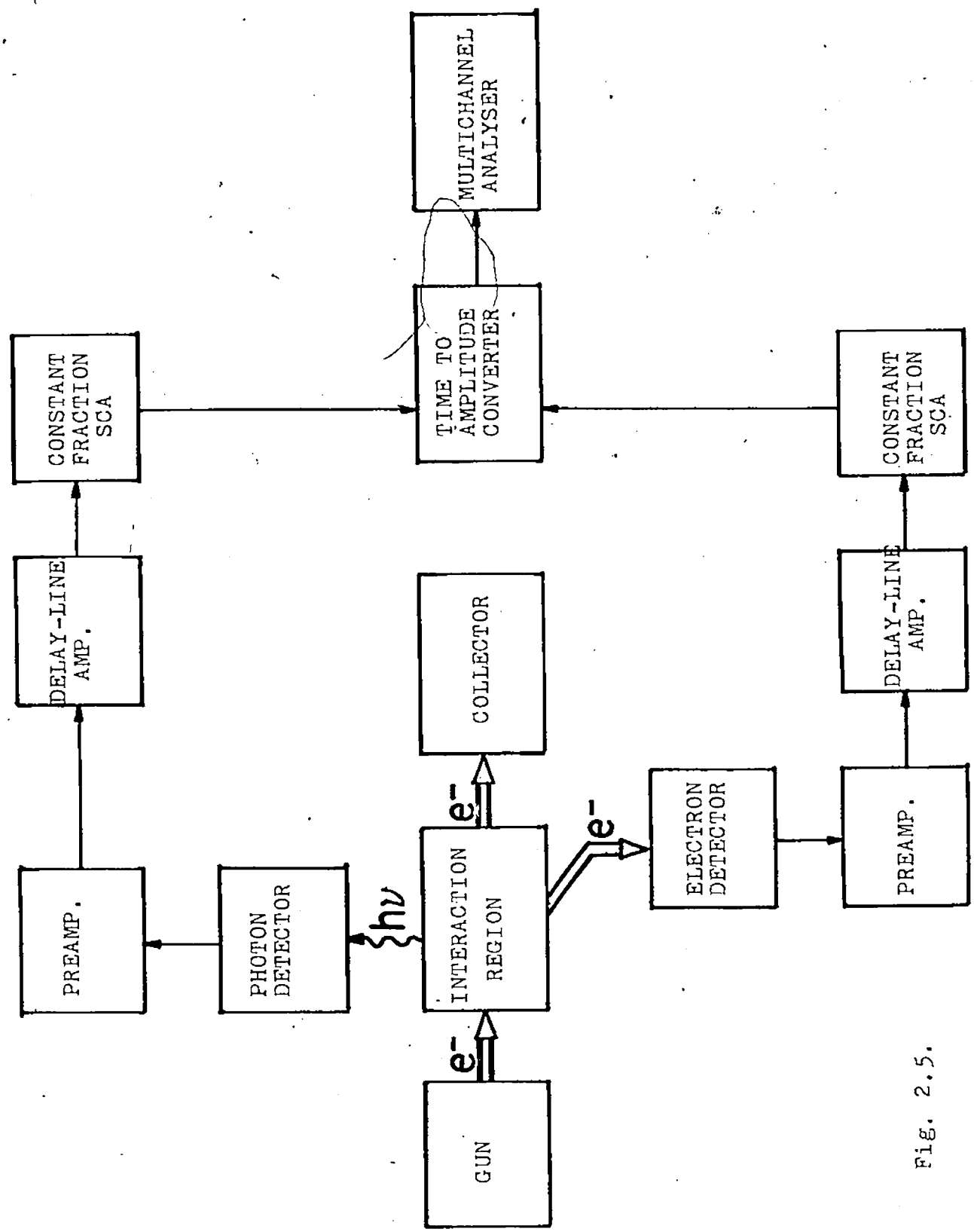

Fig. 2.5.

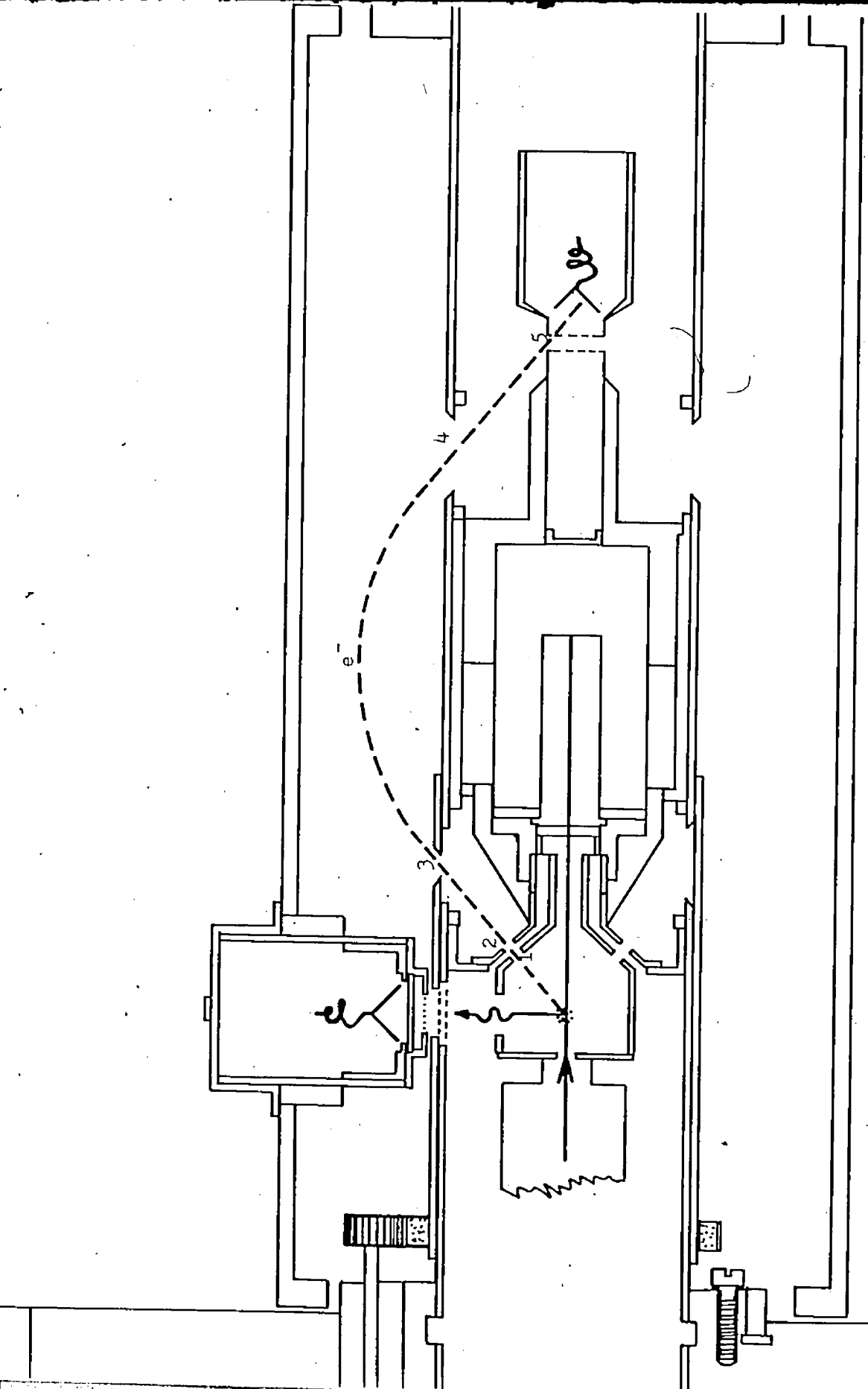

Fig. 2.6. A cross section view of the apparatus.

detected at right angles to the incident beam direction by another CEM detector. Both photon detector and electron detector are shielded to prevent leaking of the CEM field. A rotatable mask M as shown in figure 2.7 allows the angle between the photon and scattered electron directions to be varied between -20 and + 300 degrees.

During the run, the electron beam current, typically 400 nA-600nA, is continuously monitored by a Faraday cup located 40 mm beyond the interaction region, 5 mm from the exit of a 15 mm long 5 mm diameter tunnel. The last lens of the electron gun and the interaction chamber fit together so that the parallel electron beam emerging from the gun travels along the symmetry axis. The relatively high electron beam current is needed to increase the rate of events to compensate for the low counting rates obtained at the large value of θ_e (the electron scattering angle). During any run, the pressure fluctuation was less than $\pm 1\%$ and the current fluctuation was less than $\pm 5\%$.

It is essential to work under conditions where a linear plot is obtained for signal intensity against head pressure P_H and against electron beam current I . This is demonstrated in figure 2.8 and figure 2.9 The linear relationship between the signal intensity and the Head pressure ensured that no imprisonment of resonance radiation occurred. A photon,

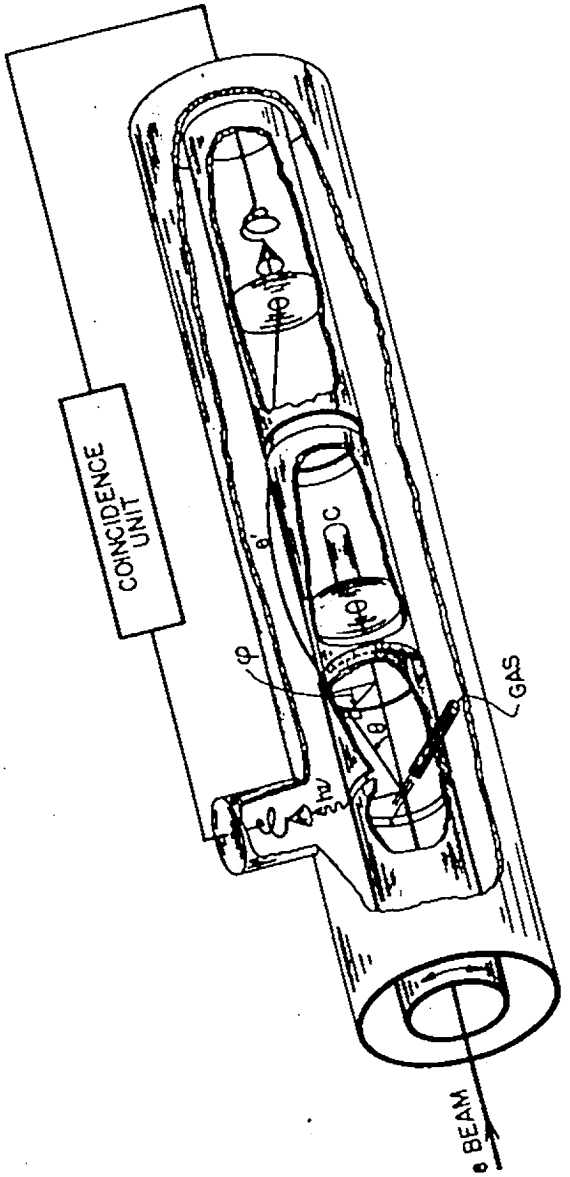

Fig. 2.7. Schematic diagram of apparatus.

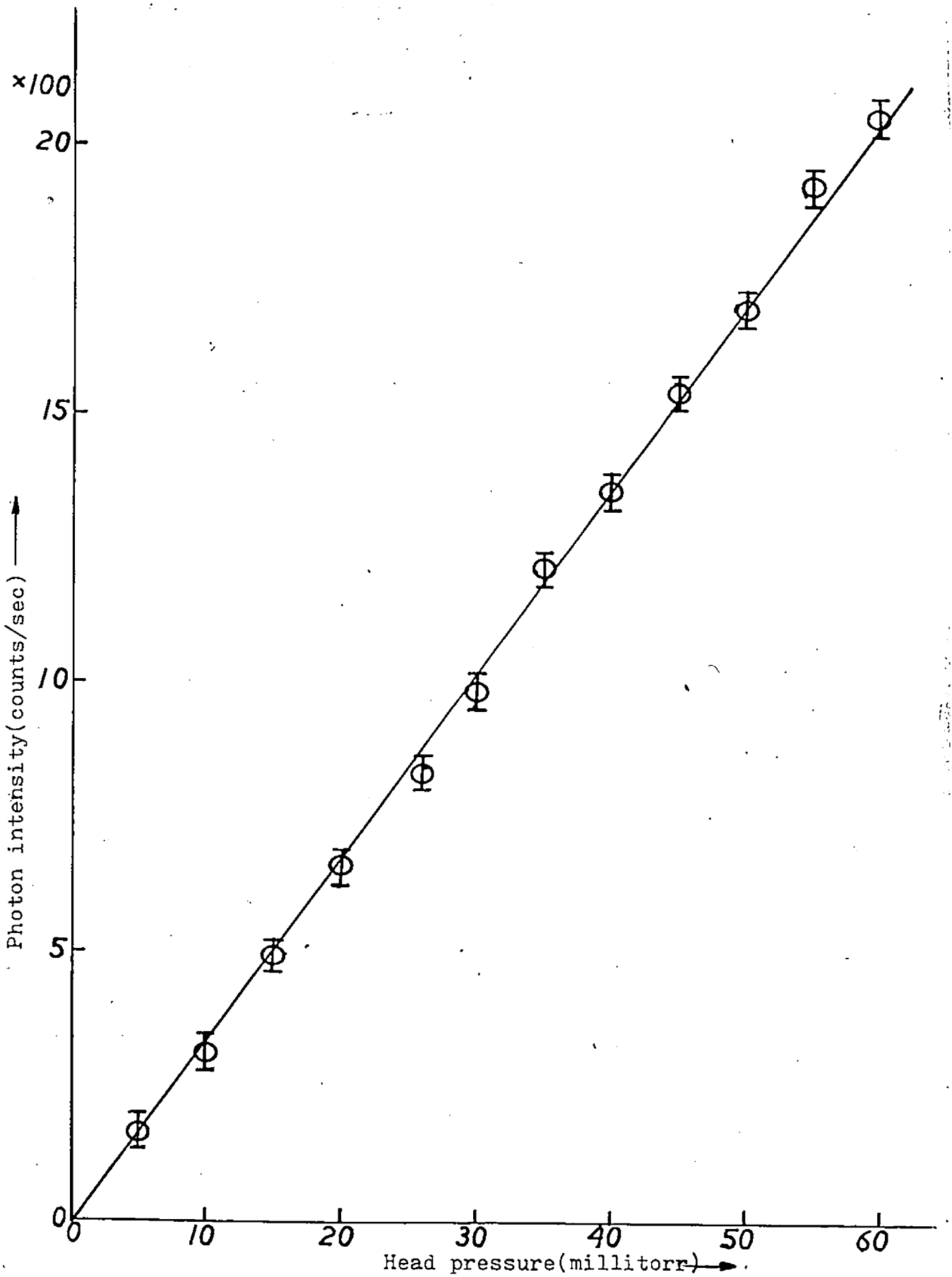

Fig. 2.8. A plot of photon signal intensity versus head pressure for He 584A line at 40eV.

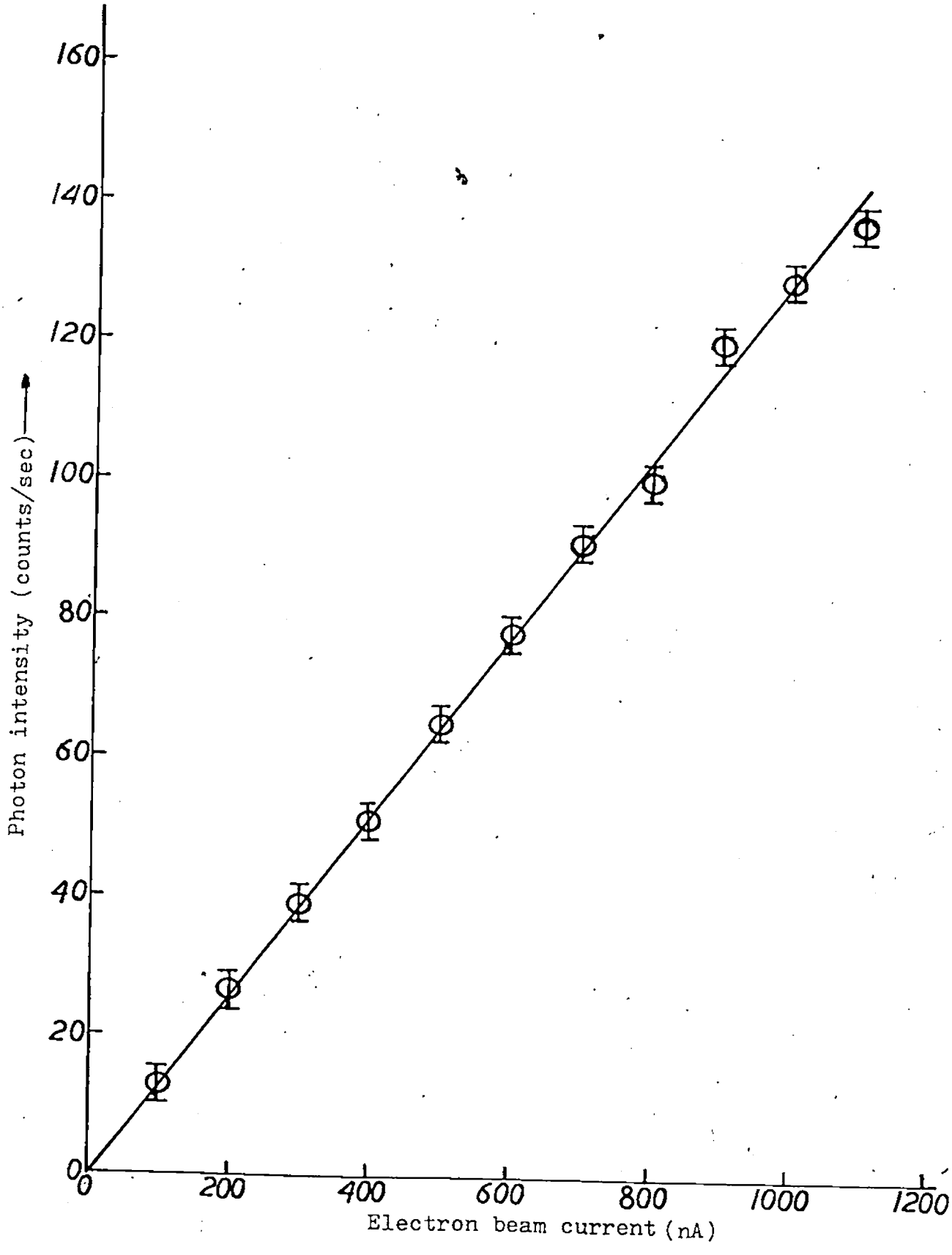

Fig. 2.9. A plot of photon signal intensity versus electron beam current for He 584A line at 40eV.

re-emitted after absorption by a ground state atom, is still correlated in time (within the experimental resolving time) with the scattered electron that caused the initial excitation. The polarization and angular distribution of these photons is, however, no longer related in a simple way to the coherently prepared states. The linear relationship between signal intensity and electron beam current, indicated that only single collision conditions exist in the interaction region. The figure also shows that any change in beam dimensions due to increasing electron current is unimportant.

Electron Gun

The scale drawing of the electron gun is shown in figure 2.10 . The electron gun is divided into two sections, each section composed of four cylindrical lens elements. The reasoning leading to this design is as follows. If two orifices are separated by one lens there is a unique votage ratio that will produce a focus of the first on the second. If a third cylinder is introduced to form a second lens, then, whatever voltages are chosen for the two orifices, it is usually possible to produce a focus by varying the voltage on the middle element. However, you may get magnified image or large beam angle at exit aperture. The introduction of a fourth lens element allows more independent choice of end

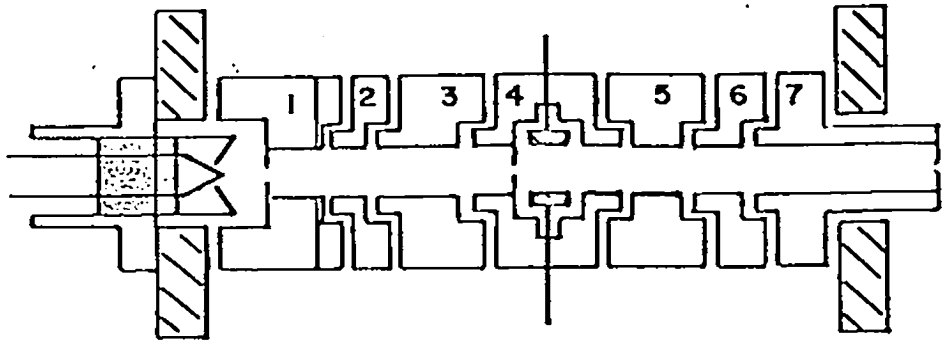

Fig. 2.10. A cross section view of the electron gun (drawn to scale). The lenses are coaxial cylinders of equal diameter separated by distance of 0.25" diameter. The apperture at lenses 1,4 and 7 is 0.020" diameter.

voltages, focus and beam angle and allow operation over wider energy range.

The first section allows electrons to be drawn off the cathode at high energy and then decelerated and focused into slits 4. In the second section deceleration of the electrons occurs and the voltages are controlled in a way that a parallel beam emerges through the exit slit 8. The lens elements are of the same diameter and they are fitted together by sleeves and insulated from each other by ruby balls. Most of them are seen to be the same shape and they may be physically moved around to accomplish any desired experimental need. The interior channel of the electron gun is sooted with acetylene to reduce electron reflection and secondary electron production. The energy spread of the electron beam emerging from this type of gun is typically o.3eV when a tungsten filament is used.

Electron Spectrometer

The scale drawing of the cylindrical electron spectrometer is shown in figure 2.8. The design of the electron spectrometer is based on the paper by Aksela et al (1970). This axial plane focusing cylindrical spectrometer features second order focusing conditions in which the second derivatives of the path length in the direction of common symmetry axis with respect to emission angle vanish. In that case one can use

much larger aperture angles and so get greater transmission and luminosity at the same resolving power than in the case of first order focusing. The optimum performance of this cylindrical mirror analyser is at an injection angle of 42^{o}. The theoretical calculated resolution, is less than 1%, but it was found that the actual resolution is approximately 2%. It was actually observed that the background noise but not the resolution could be improved by reducing the electron beam current and slowing down the electrons prior to analysis. This was done at the expense of losing signal intensity. This is because of the large inherent energy spread in the electron beam.

A typical energy loss spectrum is shown in Fig.(2.11,12). It was obtained by scanning the voltage on the outer cylinder of the analyser. For He , the curve shows that the energy resolution of the system was sufficient to separate the 2P and 2S states despite of the relatively high background noise. (Electrons scattered into the detector after excitation of the $2^{3}P$ state does not decay with the emission of UV light). For Ar, the resolution of our analyser is insufficient to separate the $^{1}P_{1}$ and $^{3}P_{1}$ states due mainly to the large electron beam energy spread.

Atomic Beam and Vacuum System

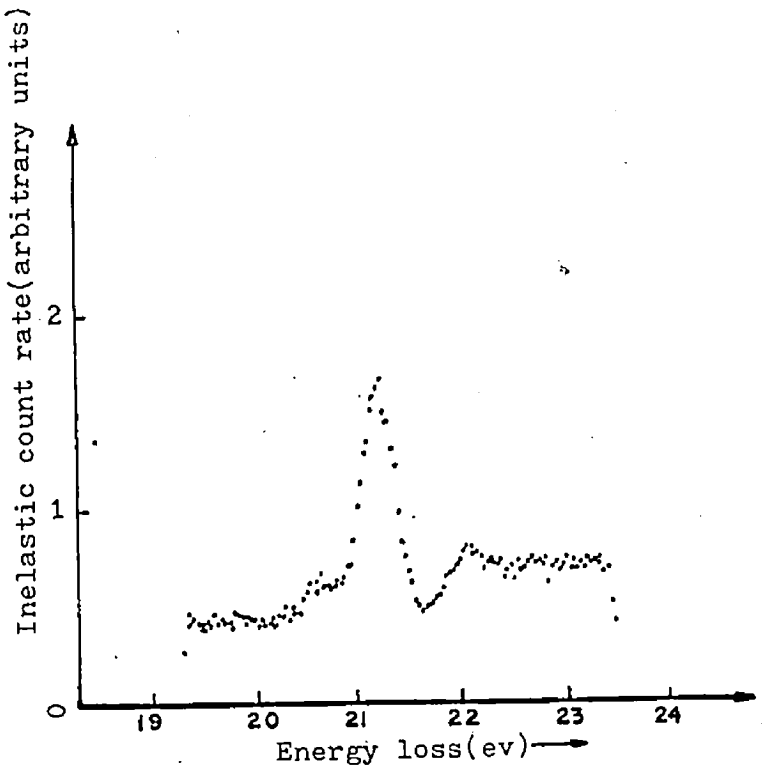

Fig. 2.11. Helium energy loss spectrum at 40eV at an electron scattering angle θ_e=42°.

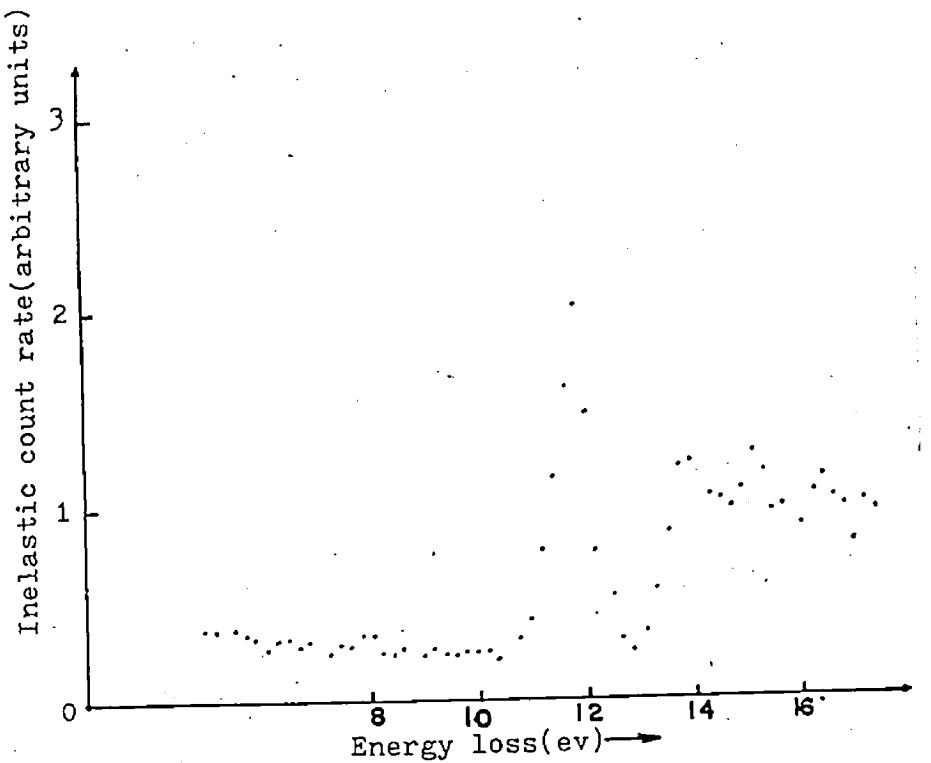

Fig. 2.12. Argon energy loss spectrum at 30eV at an electron scattering angle θ_e=42°.

High purity gas (99.999%) is introduced into the interaction region in a beam formed by a multi capillary array. A leak valve controls the pressure which is measured by a pirani gauge at the input head.

The distance between the interaction region and the end of the multi channel array is about 5 mm . The multi-channel array holder is a push fit into the side of the interaction chamber. The atomic beam is directed out of the interaction region through a hole in the wall. A four inch oil diffusion pump and a six inch liquid nitrogen cold trap were used to maintain a background pressure of 4×10^{-7} torr in the vacuum chamber during operation.

The Detectors and UV Polarizer

Both the electrons and the photons are detected by channeltron electron multipliers (CEM 4039) with an entrance cone of 10 mm in diameter. The relative detection efficiency of the CEM drops from 100 to 1 in the spectral range 500 Å to 1500 Å with maximum detection efficiency of about 25% around 600 Å and 5% around 1050 Å. (Johnson 1969) . The front end of the photon CEM cone is positively biased to prevent positive charged particles entering the CEM, and a grid of 85% transparency is mounted in front of the CEM cone, and negatively

biased to prevent negative charged particles from entering.

In the case of the polarization studies, a gold coated double mirror reflection polarizer is mounted in front of the CEM. The scale drawing of the polarizer with CEM is shown in figure 2.13 A stainless steel tube of 25 mm long and 3 mm in diameter is mounted in front of the polarizer. The dimensions of the tube and the polarizer are chosen in such a way that the CEM detector will not see any photons coming directly from the interaction region or any singly reflected radiation from the polarizer. In other words the detector only detects doubly reflected radiation. The inner part of the tube is sooted with aceythene to prevent de-polarization of the radiation by reflection from the stainless steel wall.

The polarizer together with the CEM detector can be rotated through 360° manually from outside the vacuum system using a rotary feed through. This enables the full angular radiation pattern to be scanned.

With photon (584 Å) incident angle of 70°, the polarization of the double reflected radiation is calculated (See Appendix) to be approximately 80% with 20% transmission. The optimum performance of the gold coated double mirror polarizer is for detection of radiation of wavelength around 550 Å, but it will work equally well around 1000 Å. (See

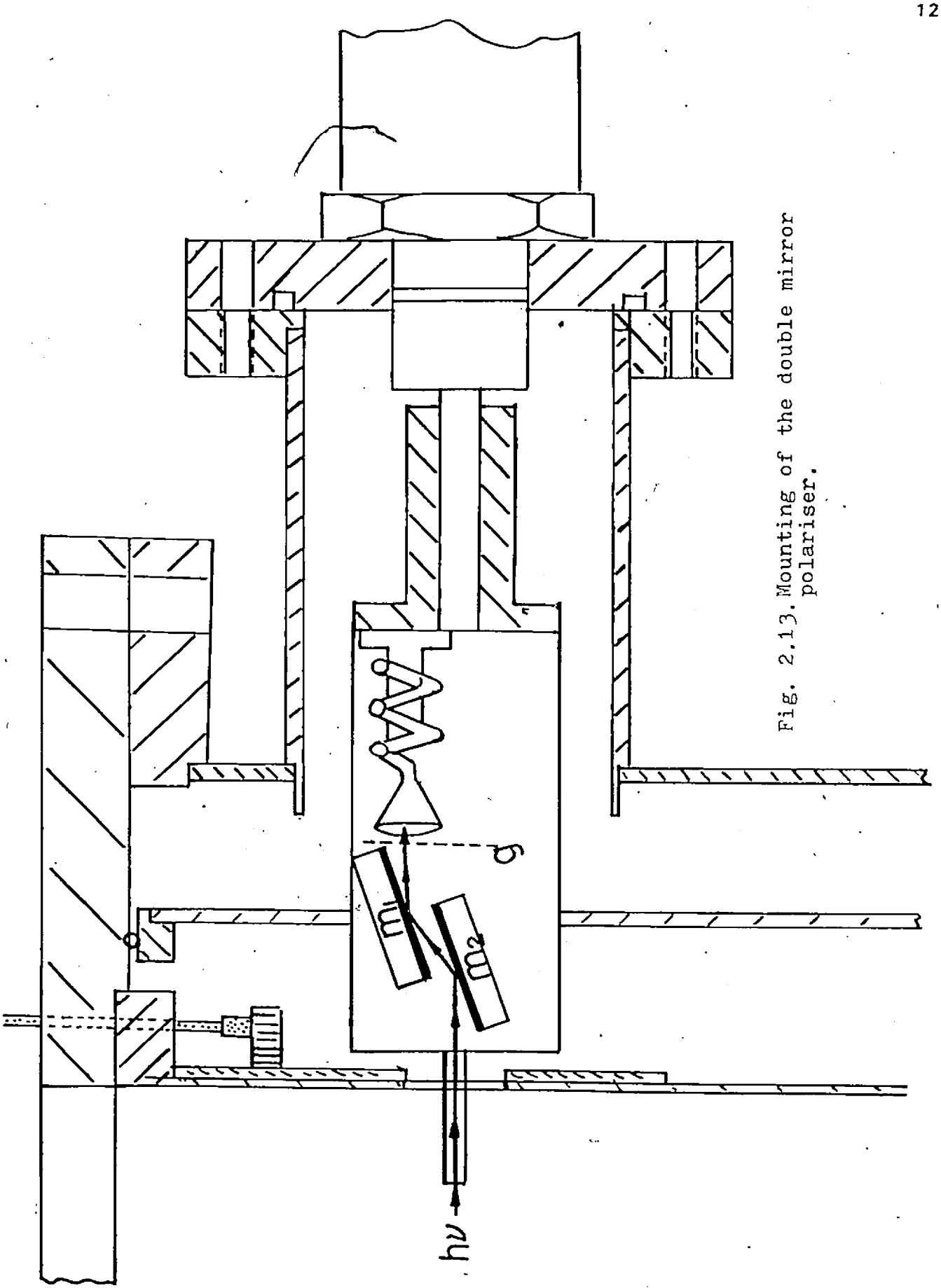

Fig. 2.13. Mounting of the double mirror polariser.

Samson 1967). Gold is chosen for reflecting polarizer material, because it has a uniform polarization characteristic between 600 Å and 2000 Å, see Fig. (2.14) and its reflectance varies little with age (James A. R. Samson 1967, Canfield et al. 1964).

Timing Electronics

The signal from each detector is preamplified, yielding output pulses with decay time of more than 25 μs. These are then fed into a delay line amplifier and the output unipolar or bipolar signal is then fed into a constant fraction timing single channel analyser (SCA) where both the pulse-height and timing are analyzed. The timing electron pulse from the SCA with suitable delay starts the ramp of a time to pulse height converter (TAC), and the photon timing pulse, is used to stop the ramp. The amplitude of the converter output signal is then proportional to the time difference between the start and stop pulses. A multi-channel analyser (MCA) is used to record the resulting pulse height spectrum from the TAC. A coincidence spectrum from the MCA is shown in figure 2.15 The FWHM of 3.3 ns for the curves represents the resolution time of the apparatus when using the polarizer. The resolution time was 10 ns when this was not in use. This is possibly because the interaction region is much better defined when the polarizer is being used.

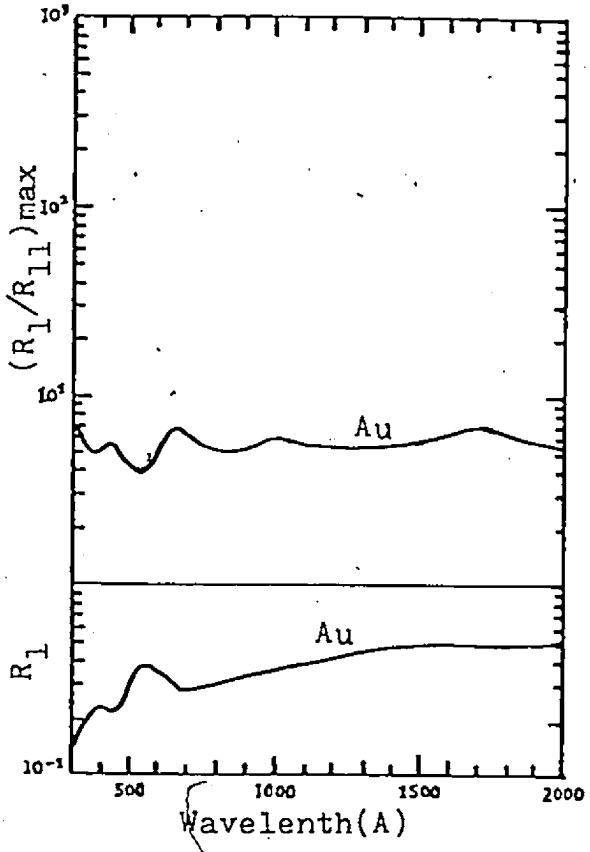

Fig. 2.14. $(R_1/R_{11})_{max}$ and R_1 for Au.

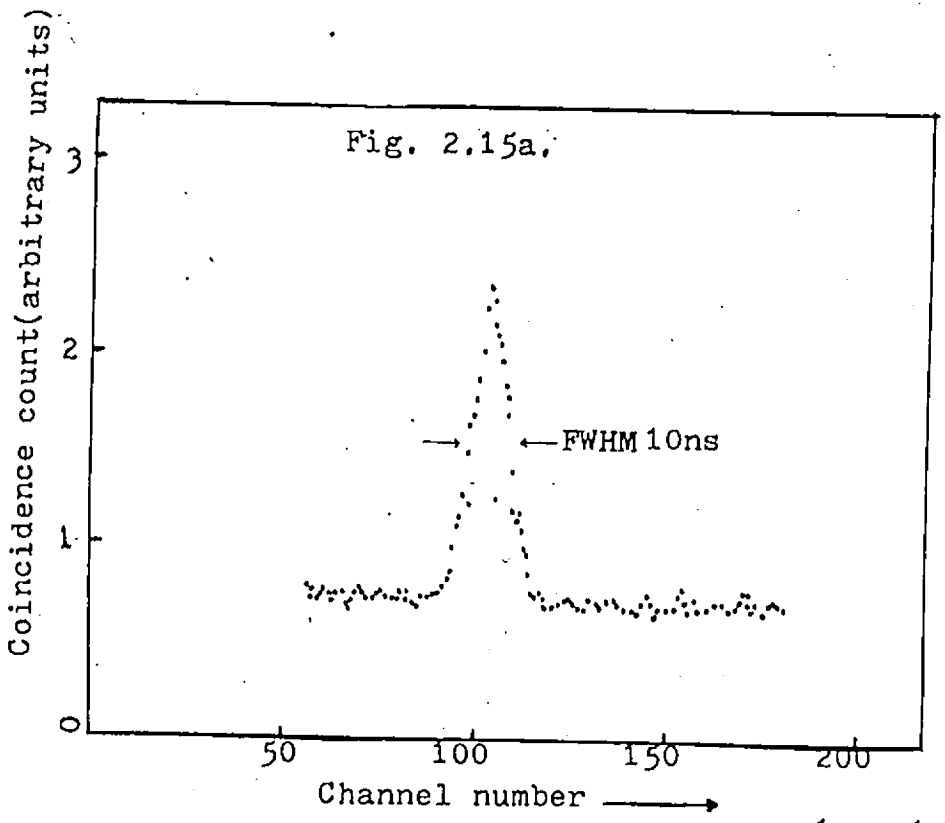

Delay coincidence spectrum for He:2^1P_1-1^1S_o transition for an electron energy of 40eV, electron scattering angle θ_e=42°, photon angle θ_ν=90° and ϕ_e-ϕ_ν=90°, Accumulation time 15 hours, channel width=0.66ns, inelastic rate,190Hz, photon rate,2.5kHz, electron beam current,250nA.

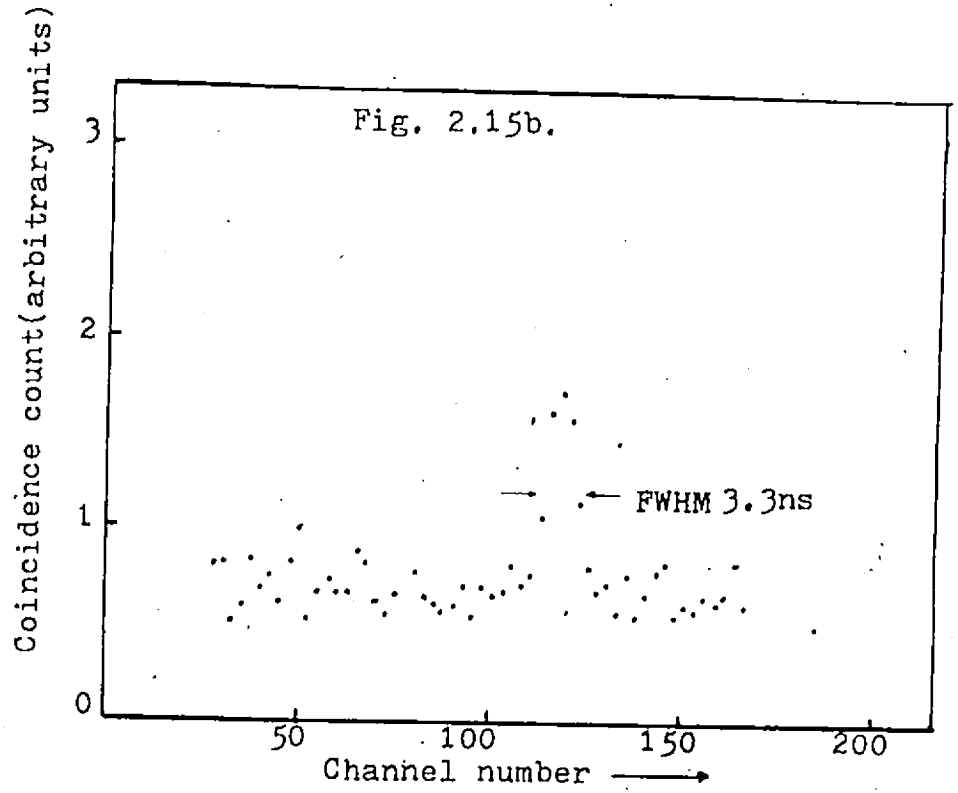

Delay coincidence spectrum for He:2^1P-1^1S_o transition for an electron energy of 40eV, electron scattering angle θ_e=42°, photon angle θ_ν=90° and β=90°, Accumulation time 52 hours, channel width=0.66ns, inelastic electron rate,500Hz, photon rate,100Hz, electron beam current,900nA.

CHAPTER X

DATA ANALYSIS AND SOURCE OF ERRORS

In the actual experiment, photons and electrons from the same scattering event arrive with a definite correlation in time. These genuine coincidences were found to fall into a group of channels of the MCA corresponding to a range of delays Δt. Δt is determined by the life time of the excited state and the resolution time of the apparatus. Chance coincidences occur when the time to amplitude converter (TAC) is started and stopped by electrons and photons from different scattering events. Since the time delays of chance coincidence are randomly distributed, they introduce only a uniform background on the delay time spectrum of the MCA. The number of genuine coincidences collected in time T is obtained by integrating the area under the coincidence peak. The background due to the chance coincidences is subtracted by measuring the average of the base line in about 120 channels outside Δt. The delay time spectrum is recorded over a range much longer than the time spanned by the real coincidences to check for spurious electronic noise which could affect the coincidence rates. The uniformity of the background of random coincidences accumulated during the experiment as shown in figure 2.15.

indicating that spurious events were not a problem in our experiments.

Coincidence techniques free the experiment from many of the usual problems of collision experiments such as cascading from higher states and large background counts. In chapter IX, we demonstrated that both the photon signal intensity and electron signal intensity have a linear relationship with the gas pressure and the incident electron beam current, therefore λ should not be affected by any change of the atomic beam density and electron beam density, and no imprisonment of radiation should occur.

In the evaluation of an actual experiment, instrumental effects as source of systematic errors require careful consideration. In this respect angular correlation and polarization correlation experiments must be discussed separately.

Angular Correlation Measurements

The general pattern of the argument behind the evaluation of the experiment can be the same as in the case of Eminyan et al (1974). In our case the photon detector has a fixed position and therefore the solid angle of photon collection is fixed. Their equation (20) shows noise presents no problem in data analysing if it is small relative to the signal rate

or constant through the experiment. In our experiment however, this is not the case on account of the relatively low energy resolution. Most importantly the solid angle of acceptance in the electron channel or the signal to noise ratio is not independent of the azimuth angle (ϕ) of observation defined by the rotatable slit. This instrumental asymmetry, arising from mechanical construction or the presence of stray fields, affects the solid angle of collection of signal and noise electrons unequally.

It is desired to measure N_c ($\phi = o$) and N_c ($\phi = \pi/2$) in such a way that they are insensitive to the variations in electron beam currents, target density and the efficiency of both the electron and photon detectors. In our experiment $\lambda = N_c(0)/N_c(\pi/2)$, and since the photon channel is fixed, we first scaled the total number of coincidences, N_{real}, collected in time T according to the total number of photon counts that stop the TAC. The coincidence rate is therefore automatically normalized to unit electron current, unit target atom density and also the time variation of the gain or sensitivity of the photon detector if there is any. Hence,

$$N = N_{real}/N_\gamma \qquad \text{-----} \quad (2.59)$$

where N_{real} and N_γ are the total no. of coincidence counts and photon counts collected in time T respectively.

In our case the signal to noise ratio in the electron channel is about 2 to 1 and is ϕ dependent and therefore the background noise, i.e. chance coincidence rate, could be a problem. Thus it is wrong to scale the total no of coincidences according to the total no. of electron pulses N_e that started the TAC. Instead we argue that the number of real coincidences has to come from those electrons that start the TAC after exciting the 2^1P state (He). This is proportional to the area under the peak of the energy loss spectrum excluding the background noise, i.e. the area A as illustrated in figure 2.16.

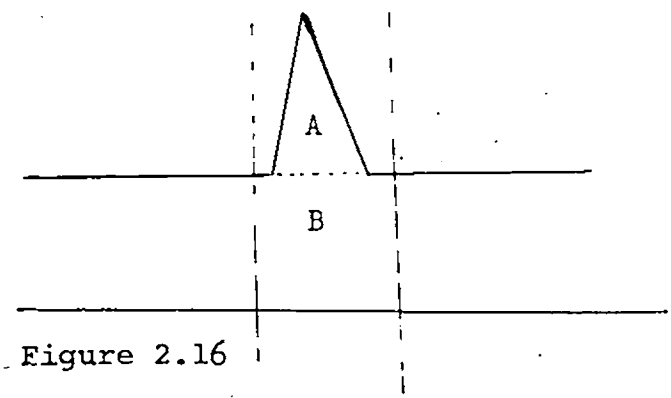

Figure 2.16

We then scaled the total number of coincidence per photon counts according to the area A. Hence,

$$\lambda = \frac{N_c(0)}{N_c(\pi/2)} = \frac{N_{real}(0)/(N_e(0)\cdot A(0))}{N_{real}(\pi/2)/(N_e(\pi/2)\cdot A(\pi/2)} \quad \text{----- (2.60)}$$

This normalization procedure is correct if the electron channels defined by the exit slit encompass the full peak of

the spectrum or more both at $\phi = 0^{\circ}$ and $\phi = 90^{\circ}$ or if the same fraction of the peak is being considered at the two angles. Experiments showed that the shape of the inelastic peak approximated closely to an isosceles triangle with the same base width at each position of the rotatable slit. Under these conditions provided the analyser was set centrally on the inelastic peak then the exit slit passes the same fraction each time: The A's in equation (2.60) represent the average area before and after each coincidence run to account for any time variation of the sensitivity or gain of the electron detector.

In order to account for any drift in λ due to the instability and time variations of the detection efficiency of the apparatus, the experiment was repeated at least once at each electron energy. It was found that the λ values were reproducible within experimental errors. Typically the errors involved are: 3% in evaluating the area A: 5% in evaluating N_{real}, leading to a total uncertainty of about 8% in λ . The statistical error in N_{γ} is negligible for such a long data accumulating time of over 20 hours.

Polarization Correlation Measurements

In polarization correlation measurements, the electron beam is selected once and for all throughout the measurement,

therefore, the problems discussed above do not arise. Systematic errors due to the imperfection of the polarization filter can be determined by calibration and subsequently can be taken into account by appropriate correction factors.

Inevitable error in the construction and mounting of a rotable polarization filter, usually leads to a spurious polarization effect. If the incident light is unpolarized, the transmitted intensity will display a small dependence on the orientation of the linear polarizer.

$$I(\beta) = I_o[1+u(\beta)] \quad \text{-----} \quad (2.61)$$

$$I(\beta+\pi/2) = I_o[1-u(\beta)] \quad \text{-----} \quad (2.62)$$

Thus the instrumental asymmetry factor $u(\beta)$ for any pair of orthogonal polarizer setting can be determined by measurements of the transmitted intensity of unpolarized light. This correction factor $u(\beta)$ is obtained as follows: As can be seen from Vriens and Carriere's (1970) calculation, for He 584 $\mathring{A}$ line the polarization fractions at 300 eV is about 3% and at 400 eV is about - 3%. Therefore we assumed that at 325 eV the polarization fraction is approximately zero, that is, the light is unpolarized. Measurements by Mumma et al (1974) support this. The instrumental asymmetry is shown clearly in figure (2.17) where the photon intensity is plated

against the rotation angle. A circle was drawn through the points and it shows that within experimental uncertainty, at 325 eV the light is unpolarized. And the correction factor $u(\beta) = \left[I(\beta) - I(\beta+\pi/2)\right] \div \left[I(\beta) + I(\beta+\pi/2)\right]$ is then obtained.

Also shown in figure (2.18) is the polarization measurement of He ($\sum$n'P - 1'S) at 40 eV, each point has been divided by the corresponding point at 325 eV to eliminate any spurious instrumental effects. The instrumental asymmetry is again clearly seen.

The polarizer is not perfect in the sense that if the incident light is totally polarized, the maximum and minimum transmitted intensities for two orthogonal setting of the filter is $I_{max} = I_o t_M$ and $I_{min} = I_o t_m$, where $t_m < t_M < 1$. When such a polarizer is used to do coincidence measurements on polarized radiation, the observed intensity or the coincidence rate measured at β and $\beta + \pi/2$, taking into account the instrumental asymmetry is

$$N_c(\beta) = N_c(\beta) t_M\left[1+u(\beta)\right] + N_c(\beta+\pi/2) t_m\left[1+u(\beta)\right] \quad ---(2.63)$$

$$N_c(\beta+\pi/2) = N_c(\beta+\pi/2) t_M\left[1-u(\beta)\right] + N_c(\beta) t_m\left[1-u(\beta)\right] \quad ---(2.64)$$

Hence the polarization ratio is

$$P(\beta) = \frac{P(\beta) - u(\beta)}{q\left[1-u(\beta)P(\beta)\right]} \quad ----- \quad (2.65)$$

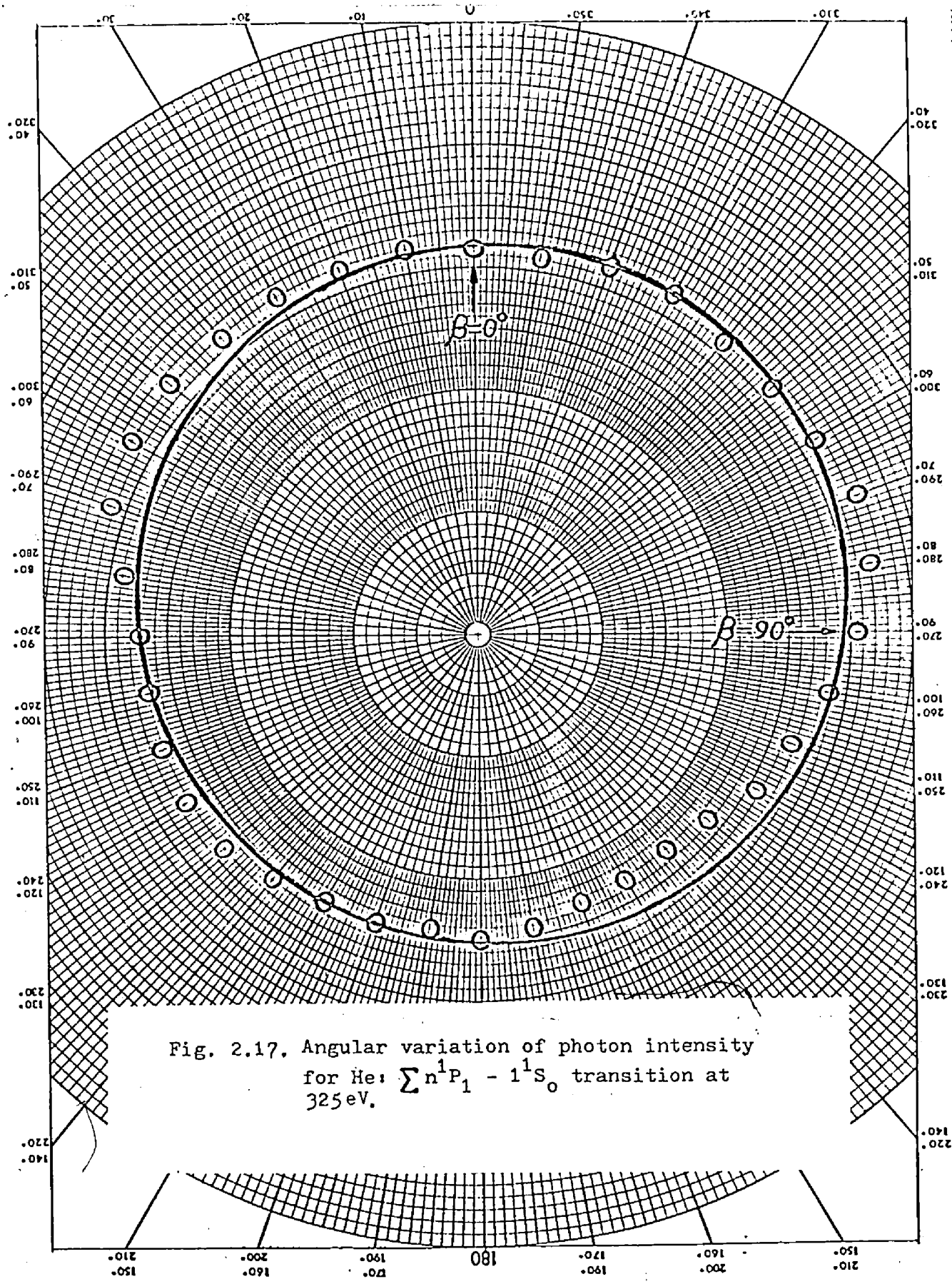

Fig. 2.17. Angular variation of photon intensity for He: $\sum n^1P_1 - 1^1S_o$ transition at 325 eV.

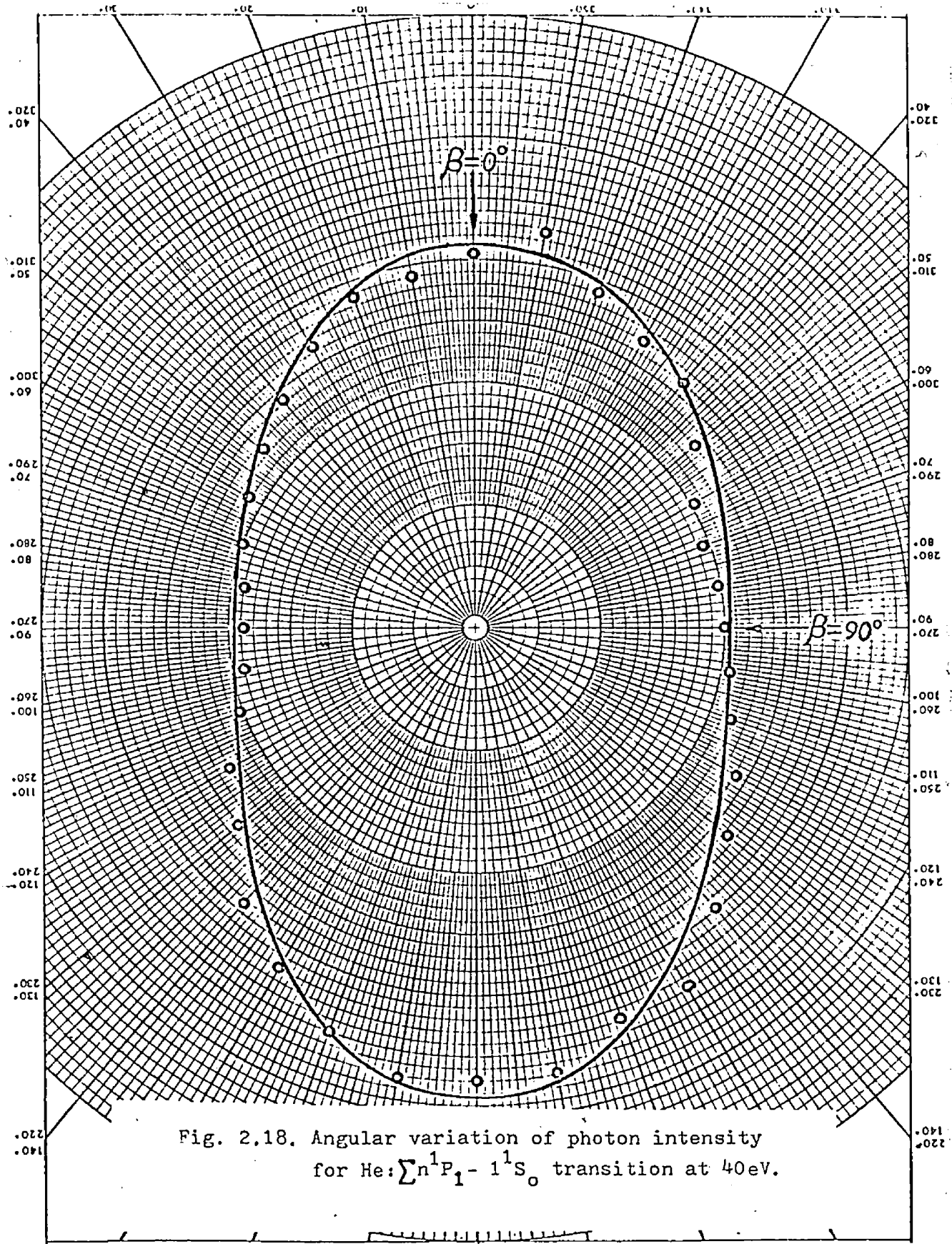

Fig. 2.18. Angular variation of photon intensity for He: $\sum n^1P_1 - 1^1S_o$ transition at 40eV.

where $P(\beta) = \frac{N_c(\beta) - N_c(\beta+\pi/2)}{N_c(\beta) + N_c(\beta+\pi/2)}$ and $q = \frac{t_M - t_m}{t_M + t_m}$ which is the fractional polarization factor of the filter. Therefore we have

$$P(0) = \frac{P(0) - u(0)}{q\left[1-u(0)P(0)\right]} \quad \text{-----} \quad (2.66)$$

$$P(\pi/4) = \frac{P(\pi/4) - u(\pi/4)}{q\left[1-u(\pi/4)P(\pi/4)\right]} \quad \text{-----} \quad (2.67)$$

where, (equation 2.20 and 2.21), $P(o) = 2\lambda - 1$ and $P(\pi/4) = 2\sqrt{\lambda(1-\lambda)}\,\mathrm{Cos}\chi$.

A knowledge of $P(o)$, $P(\pi/4)$, $u(o)$, $u(\pi/4)$ and q is sufficient for determination of λ and $|\chi|$. q can be obtained from calculation or other independent measurement. Typically the errors involved are: 16% in evaluating P's; 5% in evaluating u's; 5% in evaluating q, leading to a total uncertainty of about 12.5% in λ and about 14% in $|\chi|$.

CHAPTER XI

RESULTS AND DISCUSSION

Angular Correlation Measurements

The first measurements of electron photon angular correlations of the helium $1^1S_o - 2^1P_1$ and the argon $^1S_o - 4s'\ ^1P_1$, $^1S_o - 4s^3P_1$ excitation processes were restricted to observation of the photons at 90^o to the incident beam direction. The inelastically scattered electrons are scattered through 42^o from the incidence beam direction. this ejection angle giving optimum performance of the cylindrical mirror analyser. The values of λ's were obtained according to equations (2.8) and (2.9) without any polarization measurement. The information on χ is lost because the photon is detected at right angles to the incidence electron beam direction. The values of λ's obtained were free from any normalization or computer fitting procedures. The results for He are presented in figure 2.19 and in Table 2.1. In Table 2.1 values of λ's are tabulated as a function of electron energy; also included in Table 2.1 are the values of A_o^{col} and $A_{2^+}^{col}$ calculated from equation (2.51) and (2.53). Comparison of λ with various theoretical results is shown in figure 2.19 and in Table 2.1. Each point

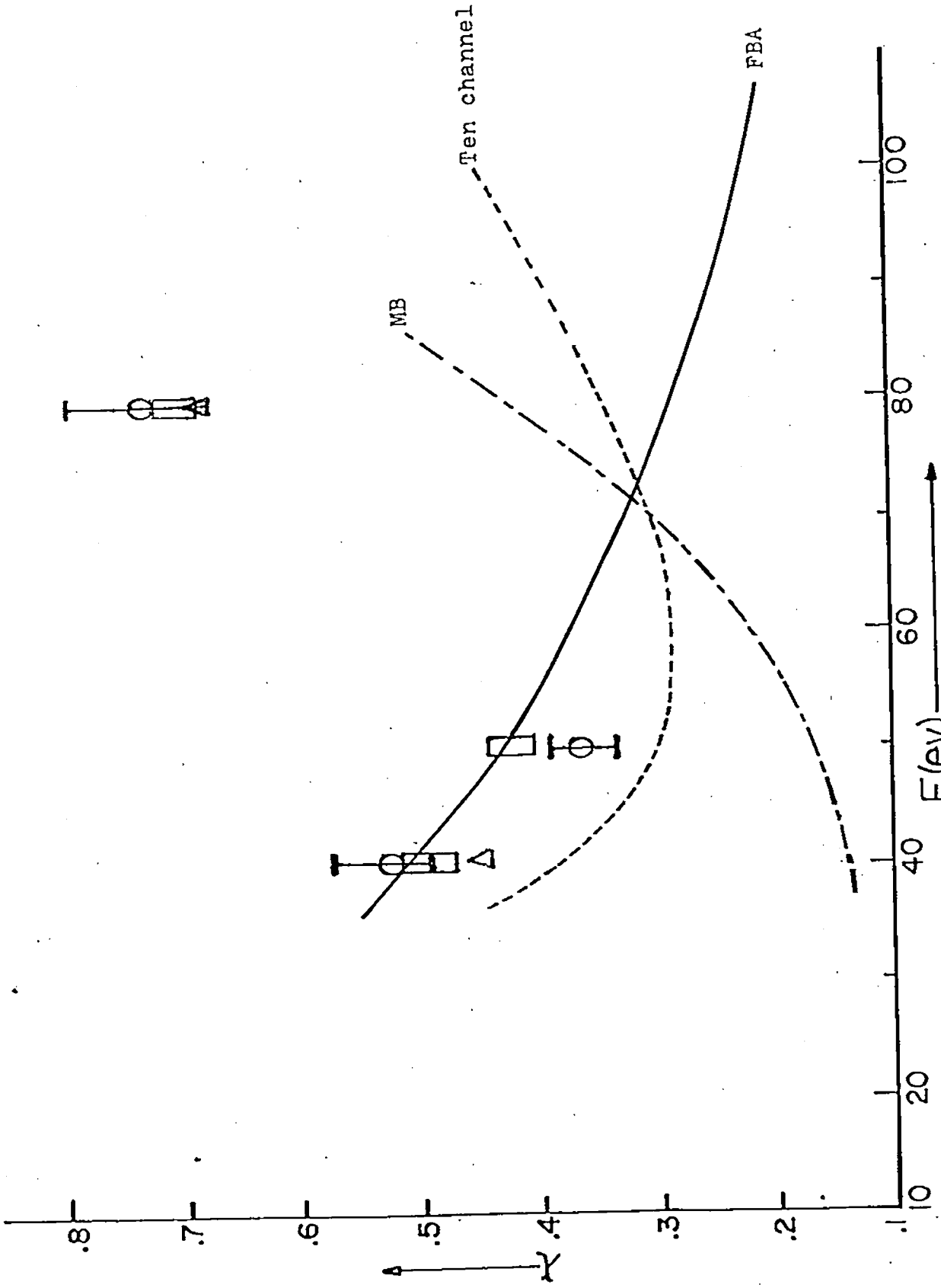

Fig. 2.19. Variation of λ (He; $1^1S_o - 2^1P_1$) with incident electron energy at electron scattering angle $\theta_e = 42^o$. ϕ, present work; Δ, Distorted wave Born approximation (Madison and Shaldon 1973); □, Eminyan et al 1974.

Table 2.1

Experimental results for He $2^1P_1 - 1\ ^1So$ transition (584 Å) at $\theta_e = 42^o$

Energy	λ			$\lvert A_o^{col} \rvert$	$\lvert A_{2+}^{col} \rvert$
	Experiment	Theory	Eminyan et al extrapolated to $\theta_e = 42^o$		
40±.5eV	0.53	0.52 (FBA) 0.46 (DW) 0.40 (E10) 0.13 (MB)	0.51 ± 0.02	0.30	0.24
50±.5eV	0.36	0.43 (FBA) 0.31 (E10) 0.16 (HB)	0.45 ± .06	0.04	0.32
80±.5eV	0.73	0.29 (FBA) 0.70 (DW) 0.34 (E10) 0.40 (MB)	0.70 ± 0.05	0.60	0.14

FBA: First Born Approximation.

DW: Distorted wave calculation of Madison and Shelton (1973).

MB: Many body theory of Thomas et al (1974).

E10: Ten channel treatment of Flannery and McCann (1975).

represents an experimental data accumulation time of 50 hours.

Figure 2.19 shows the variation of λ with electron energy at $\theta_e = 42^\circ$. As can be seen from the graph, the experimental values of λ at this large scattering angle are a more sensitive test of all the theoretical calculations based on different wave functions than are the partial differential cross sections , σ . The first Born approximation, the ten channel treatment of Flannery and McCann and the first order many body approach of Thomas et al cross each other around 70 eV and they disagree with each other both quantitively and qualitatively. According to the simple Born approximation, $\lambda = \mathrm{Cos}^2\theta_K$ where θ_K is the angle between the direction of linear momentum transfer K and the incoming electron beam Z. In accord with the expectation that the first Born approximation should be accurate at small scattering angles and high energies, the FBA predictions of λ at 40 eV and $\theta_e = 42^\circ$ is in perhaps surprising agreement with the experimental data As the electron energy is increased the discrepancies in λ become larger. The inadequacy of FBA is in that it predicts $\chi = 0$. The extrapolation of Eminyan et al's results to $\theta_e = 42^\circ$ are shown. There is a large uncertainty due to the extrapolation because we don't know for sure how fast their curves will rise beyond $\theta_e = 35^\circ$. Also shown in figure 2.19 are the results of the distorted

wave calculation of Madison and Shelton 1973, It is represented by Δ at 40 eV and 80 eV. Madison and Shelton's work is in remarkably good agreement with the experimental data at 80ev. (actual calculation energy 78 eV). The many body theory predicts too small λ's at low energy. It is also worth noting that the accuracy of the many body treatment of the 2^1P differential and total excitation cross section (figures 2, 3 and 4 of Thomas et al 1974) is not maintained for (2^1P) at the larger scattering angles. The 10 channel treatment is reasonable at low energies. However, as pointed out by Flannery and McCann themselves, in order to properly describe large-angle inelastic scattering, the present 10 channel treatment requires modification so as to explicitly include effects arising from electron-exchange and orbit-distortion. It seems that the FBA is more well founded in placing emphasis on the role played by K in the scattering than in its predictions of distribution of the excitation among the sublevels of the excited state. It should be emphasized that the FBA predictions of λ and χ depend only on the kinematics of the collision, i.e. the $\Delta M = 0$ selection rule along K, and do not depend on the particular choice of wavefunctions. It is obvious that none of the existing theories are adequate in predicting λ at such a large electron scattering angle.

For Ar, the assumption that the states involved can be described in terms of L-S coupling is questionable. And secondly, in our experiment, a lack of resolution; both in the electron and photon channels allows only the observation of an overall coincidence rate involving the two processes namely the $4s'\ ^1P_1 - {}^1S_0$ and $4s\ ^3P_1 - {}^1S_0$ transitions. There the two relevant processes can be considered to be incoherently mixed. According to equation 2.12, the experiment only measured a relationship between the $\lambda^{(s)}$ and $\lambda^{(t)}$. We assume that $\lambda^{(s)} = \lambda^{(t)}$. (This assumption is not justified unless we can separate the triplet from the singlet and measure them separately. Work is currently being carried out in this laboratory using a high resolution electron gun to measure $\lambda^{(s)}$ and $\lambda^{(t)}$ separately). A plot of λ as a function of incident electron energy is shown in figure 2.20.together with the Born approximation values. No finer detail calculation has been done for these transition in argon. It is interesting to see that, the same behaviour occurs in argon as in He where the value of λ decreases with increasing electron energy and then increases again. It may be worth noting that Arriola et al (1975) have measured λ for Ar at electron scattering energies of 80.4 eV and 113.4 eV and scattering angles of 8.5^o and 9^o respectively. Their claim that $\lambda^{(s)} = \lambda^{(t)}$ cannot be justified from their measurements

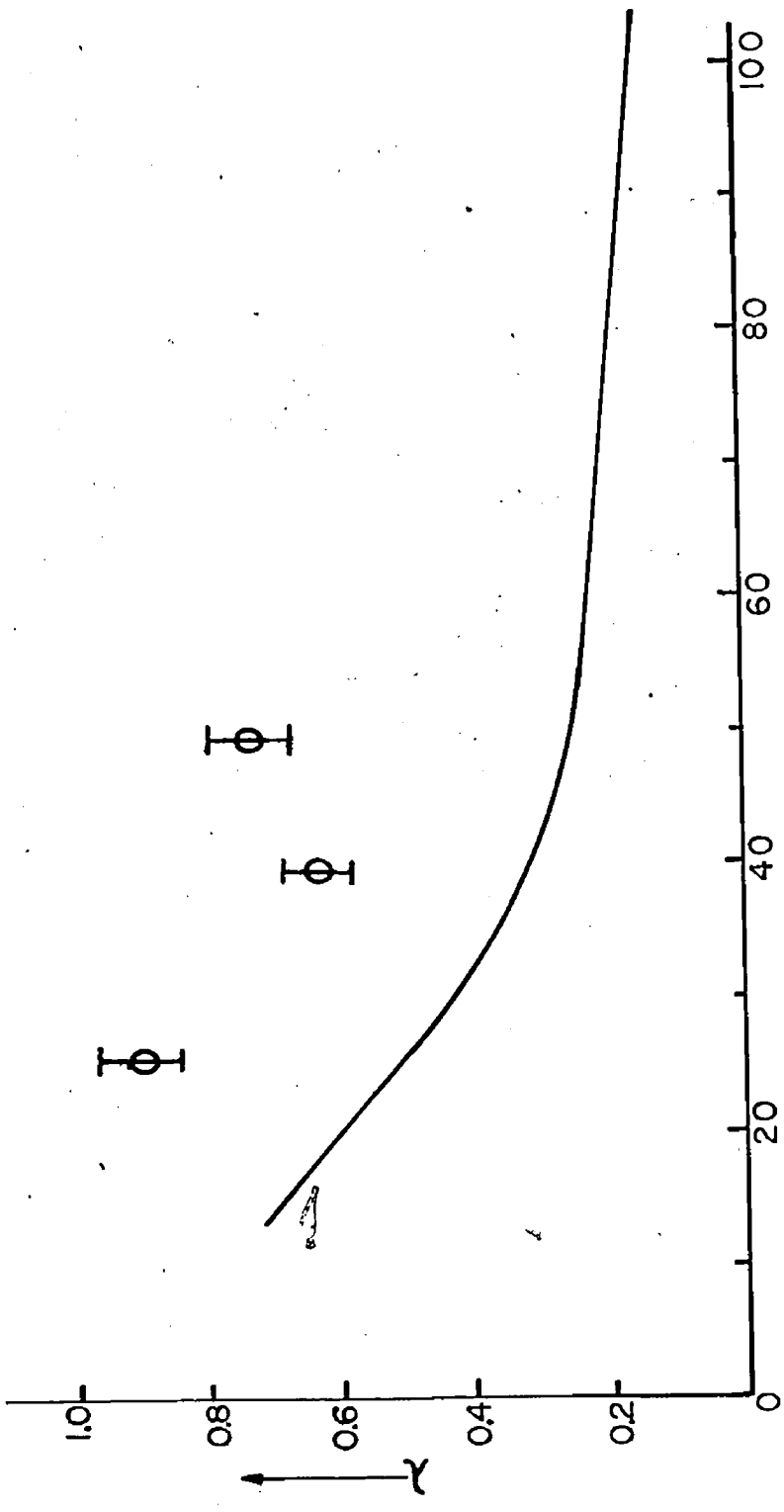

Fig. 2.20. Variation of γ (Ar; ^1S_o - $4s'^1P_1$, $4s^3P_1$) with incident electron energy at electron scattering angle $\theta_e = 42^\circ$. Φ, present work; —— Born approximation.

as discussed previously. This claim cannot be confirmed or refuted experimentally unless the singlet and triplet channels are separated by adequate spectral resolution.

Polarization Correlation Measurements

In order to obtain the phase difference $|\chi|$ between the excitation amplitudes a_o and a_1, we measured coincidences between the polarized photons emitted perpendicular to the scattering plane and the inelastically scattered electrons. According to equations (2.20) and (2.21), a measurement of $P(o)$ and $P(\pi/4)$ is equivalent to a scan of the angular correlation in coplanar observation. A knowledge of these two independent linear polarization values is sufficient for the determination of λ and $|\chi|$, provided $P=1$ ($P^2 = P^2(o) + P^2(\pi/4) + P^2$ (circ)). Circular polarization measurements P (circ) are not feasible for the UV decay of the 2^1P state because of the short wavelength involved, and therefore the sign of χ is still not determined at the present time.

Before going to the coincidence results and discussion of the values of λ and $|\chi|$, let us look at the straight forward linear polarization measurements of the de-excitation radiation perpendicular to the incident electron beam direction. The polarization fractions $P = \frac{I_{\parallel} - I_{\perp}}{I_{\parallel} + I_{\perp}} = \frac{Q_o - Q_1}{Q_o + Q_1}$ yields the ratio of the total differential cross section

Q_0/Q_1 of the magnetic sublevels $M_L = 0$ and ± 1, where $Q_{M_L} = \int_{4\pi} |a_{M_L}|^2 d\Omega_e$. The polarization fractions for He $\sum n^1P - 1^1S$ resonance radiation at 40, 50 and 80 electron volts are given in Table 2.3, using a q value of 0.8 obtained from theoretical calculation (see appendix). These values approximately represent the polarization fraction of the $2^1P - 1^1S$ radiation since this transition is the dominant one observed and since the polarization should be essentially independent of principal quantum number, n (Vriens and Carriere 1970).

For Ar, the measurements showed that 1048 and 1067 Å lines were only slightly polarized at an electron impact energy of 40 eV, though this statement may be misleading since there was a background component of unknown magnitude from other levels .

The experimental results for λ and $|\chi|$ are tabulated in table 2.4 . Values of λ and $|\chi|$ are calculated from equations (2.20), (2.21) and equation (2.66) and (2.67). Also included in Table 2.4 are the values of θ_{min} calculated from equation (2.22) and the orientation and alignment vectors of the excited atom $|O_{1-}^{col}|$, $|A_0^{col}|$, $|A_{1-}^{col}|$ and $|A_{2+}^{col}|$ calculated from equations (2.54), (2.51), (2.52) and (2.53) respectively. Theoretical results and experimental results from other sources are included for comparison.

Table 2.2

λ for Ar ^1S_o - 4S, $^1P_1$, $4S\,^3P_1$ transition (1048+1067Å)

Energy	λ	
	Experiment	Theory(FBA)
26 ± 0.5eV	0.91 ± 0.07	0.47
40 ± 0.5eV	0.63 ± 0.05	0.31
50 ± 0.5eV	0.74 ± 0.07	0.26

Table 2.3

Polarization fraction of He n^1P - 1^1S transtions

Energy	Present work	Mumma et al
40 eV	0.34 ± 0.03	0.53 ± 0.03
50 eV	0.33 ± 0.03	0.52 ± 0.02
80 eV	0.28 ± 0.03	0.41 ± 0.02

Table 2.4

Experimental results and comparison with theories.

$\theta_e = 42^\circ$	λ		
Energy	Experiment	Theory	Eminyan et al extrapolated from 40°
$40 \pm .5$eV	0.56	0.53 (FBA) 0.46 (DW) 0.40 (E10) 0.13 (MB)	0.51 ± 0.02
$32 \pm .5$eV	0.67	0.68 (FBA)	
	χ (rad)		
Energy	Experiment	Theory	Eminyan et al at 40°
$40 \pm .5$eV	1.15	0 (FBA) 0.7 (E10)	$1.14 \pm .01$
$32 \pm .5$eV	0.81	0 (FBA)	
	θ_{min} (degree)		
Energy	Experiment	Theory	Eminyan et al extrapolated from 40°
$40 \pm .5$eV	38	43	43.6 ± 1
$32 \pm .5$eV	31.3	34.5	

Energy	$\lvert A_0^{col} \rvert$	$\lvert A_{1+}^{col} \rvert$	$\lvert A_{2+}^{col} \rvert$	$\lvert O_{1-}^{col} \rvert$ Experiment	Theory	Eminyan et al at 40°
$40 \pm .5$eV	0.34	0.20	0.22	0.45	0.31 (E10)	$0.45 \pm .01$
$32 \pm .5$eV	0.51	0.16	0.17	0.34		

The experimental values of λ and θ_{min} for He (584 Å) are in fair agreement with the FBA and with the results of Eminyan et al extrapolated to $\theta_e = 42^\circ$. It has been noted above that the FBA gives $\chi = 0$, thus $O_{1-}^{col} = 0$. According to Fano and Macek (1973), in the Born approximation, the momentum transfer vector K is the only collision parameter on which alignment and orientation can depend. Since K is a polar vector, no orientation of the atom can occur in this approximation. Furthermore, symmetry about the direction of K implies that $A_{1+}^{col} = A_{2+}^{col} = 0$. In this respect the data clearly shows that any theory, which predicts $\chi = 0$ or π or $\lambda = 0$ or 1, is inadequate.

The value of θ_{min} is very sensitive to λ around 0.5 according to equation (2.22), $\theta_{min} > 45^\circ$ for $\lambda < 0.5$ and $\theta_{min} < 45^\circ$ for $\lambda > 0.5$. According to FBA, θ_{min} is equal to θ_K ; the angle at which the coincidence rate is a minimum, FBA predicts no radiation along K direction, which means that the angular correlation of the emitted photons corresponds to the emission of radiation from a dipole oscillator aligned along the linear momentum transfer vector K.

The physical significance of the data can also be seen in terms of the orientation O_{1-}^{col} which depends on λ and χ. The maximum value of O_{1-}^{col} is 0.5, which corresponds to completely circularly polarized photon emission perpendicular

to the scattering plane. This could be occurring at a particular scattering angle and incident electron energy when the magnetic sublevels $M_L = 0$ and ± 1 are equally populated ($\lambda = 0.5$) and when the phase of the oscillating and rotating dipoles differ by $\pi/2$. We have a value of 0.45 for $|O_{1-}^{col}|$ which agrees fairly well with Eminyan et al's result. This corresponds to a circular polarization of 90% whereas the 10 channels treatment of Flannery and McCann predicts 62% circular polarization. Equation (2.47) and (2.54) show that O_{1-}^{col} has a simple physical interpretation, namely that $-2O_{1-}^{col}$ is the average value of the angular momentum transfer to the atom perpendicular to the plane of scattering in the collision.

CHAPTER XII

CONCLUSION

Electron - photon angular correlation measurements and electron - polarized photon coincidence studies are significant for several reasons. These studies have led to measurements of partial differential cross-section, σ_{m_L}, compared with the measurements of total partial excitation cross-sections, Q_{m_L}, in conventional line polarization studies. They also provided detailed information on the coherence properties of the excitation process, on the orientation and alignment characteristics of the excited atom and on the angular momentum dynamics occurring during the electron-atom collision process. All this information provides a new test of electron atom scattering theories.

The results of the experiment show that electron helium collisions produce considerable atomic orientation, which indicates the degree to which orbital angular momentum is transferred to the atom during the collision. This important feature of the scattering dynamics was precluded in the first Born approximation. The data also indicated that the direction of a principal axis of the alignment tensor for the excited state is shifted away from the momentum transfer axis.

Polarization correlation measurements appear in a much more favourable light than the straight forward electron - photon angular correlations. In addition to being equivalent in yielding λ and $|\chi|$, polarization correlation measurements can prove unambiguously the degree of coherency of the excitation radiation and also the sign of χ by measuring the circular polarization of the coincidence photons. Future development could extend this technique from the visible spectral region where circular polarizers are available to the vacuum UV radiation in the range between 1050 - 1450 Å where circularly polarized radiation can be produced by applying pressure to the edges of a plate of cleaved LiF about 2 to 4 mm thick (Metcalf and Baird 1966).

The influence of resonances on the polarization of line radiation is well known. Future studies might look at the behaviour of λ and χ in the vicinity of some of these resonances. As suggested by Fano and Macek (1973), at resonances, the colliding electron and the one being excited in the atom remain strongly correlated for a time interval sufficient to allow extensive exchange of angular momentum between them.

APPENDIX

A

Angular variation of the polarization of 584Å radiation produced by reflection from a gold coated double mirror polarization.

Incident angle(degree)	$R_{\perp}$	$R_{\parallel}$	P
0	0.0113	0.0113	0.0000
2	0.0113	0.0113	0.0032
4	0.0115	0.0112	0.0127
6	0.0116	0.0110	0.0285
8	0.0119	0.0107	0.0507
10	0.0122	0.0104	0.0791
12	0.0127	0.0101	0.1138
14	0.0132	0.0097	0.1546
16	0.0138	0.0092	0.2010
18	0.0146	0.0087	0.2528
20	0.0154	0.0082	0.3090
22	0.0165	0.0076	0.3689
24	0.0176	0.0070	0.4311
26	0.0190	0.0064	0.4944
28	0.0206	0.0059	0.5561
30	0.0226	0.0053	0.6187
32	0.0246	0.0048	0.6750
34	0.0270	0.0042	0.7279
36	0.0299	0.0038	0.7740
38	0.0331	0.0034	0.8143
40	0.0369	0.0030	0.8481
42	0.0413	0.0027	0.8757
44	0.0463	0.0025	0.8975
46	0.0521	0.0023	0.9141
48	0.0588	0.0023	0.9261
50	0.0665	0.0023	0.9340
52	0.0755	0.0024	0.9385
54	0.0858	0.0027	0.9397
56	0.0977	0.0031	0.9378
58	0.1112	0.0039	0.9308
60	0.1272	0.0050	0.9241
62	0.1455	0.0068	0.9114
64	0.1665	0.0093	0.8941
66	0.1908	0.0131	0.8714
68	0.2187	0.0187	0.8424
70	0.2508	0.0269	0.8064
72	0.2877	0.0388	0.7625
74	0.3303	0.0560	0.7101
76	0.3792	0.0808	0.6487
78	0.4354	0.1164	0.5781
80	0.5001	0.1674	0.4985
82	0.5743	0.2403	0.4105
84	0.6597	0.3436	0.3150
86	0.7578	0.4911	0.2136
88	0.8705	0.7010	0.1079
90	1.0000	1.0000	0.0000

B

Angular variation of the polarization of 1048Å radiation produced by reflection from a gold coated double mirror polarization.

Incident angle(degree)	$R_{\perp}$	$R_{\parallel}$	P
0	0.0158	0.0158	0.0000
2	0.0158	0.0157	0.0031
4	0.0160	0.0156	0.0126
6	0.0162	0.0153	0.0282
8	0.0166	0.0350	0.0502
10	0.0171	0.0146	0.0783
12	0.0176	0.0141	0.1124
14	0.0184	0.0135	0.1525
16	0.0192	0.0129	0.1980
18	0.0202	0.0122	0.2485
20	0.0214	0.0115	0.3032
22	0.0228	0.0106	0.3611
24	0.0245	0.0100	0.4212
26	0.0263	0.0092	0.4820
28	0.0285	0.0085	0.5422
30	0.0309	0.0077	0.6002
32	0.0337	0.0070	0.6548
34	0.0370	0.0064	0.7048
36	0.0407	0.0058	0.7494
38	0.0449	0.0053	0.7881
40	0.0498	0.0049	0.8209
42	0.0553	0.0046	0.8477
44	0.0616	0.0043	0.8690
46	0.0689	0.0042	0.8853
48	0.0771	0.0042	0.8969
50	0.0865	0.0043	0.9045
52	0.0973	0.0047	0.9083
54	0.1095	0.0053	0.9085
56	0.1234	0.0062	0.9052
58	0.1392	0.0075	0.8982
60	0.1572	0.0094	0.8873
62	0.1776	0.0121	0.8721
64	0.2007	0.0160	0.8521
66	0.2270	0.0215	0.8268
68	0.2563	0.0293	0.7954
70	0.2906	0.0403	0.7575
72	0.3288	0.0552	0.7125
74	0.3721	0.0762	0.6606
76	0.4211	0.1053	0.5998
78	0.4765	0.1456	0.5320
80	0.5392	0.2011	0.4567
82	0.6102	0.2776	0.3746
84	0.6904	0.3828	0.2866
86	0.7812	0.5275	0.1939
88	0.8838	0.7264	0.0978
90	1.0000	1.0000	0.0000

REFERENCES

Aksela,S. 1971. Rev. Sci. Instrum. 42, 810.

Aksela,S., Karras,M., Pessa,M., and Suoninen,E. 1970. Rev.Sci. Instrum. 41, 351.

Ariola,H., Teubner,P.J.O., Vgbabe,A., and Weigold,E. 1975.J. Phys. B, 8, 1275.

Bennet,W.R., Mercer,G.N., Kindlmann,P.J., Wexler,B., and Hyman, h. 1966. Phys. Rev. Lett. 17, 987.

Berry,H.G., Curtiss,L.J., Ellis,D.G., and Schectman,R.M. 1974. Phys. Rev. Lett. 32, 751.

Blum,K., and Kleinpoppen,H. 1975. J.Phys.B, 8, 922.

Born,M., and Wolf,E. 1965. "Principle of optics", Perganon Press, 3rd edition.

Clout,P.N.,and Heddle,D.W.O. 1969. J.Opt.Soc.Am. 59, 715.
——— 1971.J.Phys.B, 4, 483.

Cole,T.T., and Oppenheimer,F. 1962. Appl. Optics 1, 709.

Crowe,A., Preston,J.A., and McConkey,J.W. 1972. J.Chem. Phys. 57, 1720.

De Jongh,J.P.,and Van Eck,J. 1971. Physica, 51, 104.

Donaldson,F.G. 1972. Ph.D. Thesis, University of Windsor, Ontario, Canada.

Donaldson,F.G., Hender,M.A., and McConkey,J.W. 1972. J.Phys. B, 5, 1192.

Eminyan,M., Macadam,K.B., Sievin,J., and Kleinpoppen,H. 1973. Phys. Rev. Lett. 31, 576.
——— 1974. J.Phys.B, 7, 1579.

Falkoff,D.L., and Macdonald,J.E. 1951.

Fano,U. 1949. J.Opt.Soc.Am. 30, 859.
——— 1953. Phys. Rev. 93, 121.

Fano,U., and Macek,J. 1973. Rev. Mod. Phys. 45, 553.

Feltsan,P.V., and Povch,M.M. 1970. Opt. Spectrosc. (Eng.Transl.) 28, 119.

Fischer,O. 1933. Z. Phys. 86, 646.

Flannery,M.R., and McCann,K.J. 1975. J. Phys. B, 8, 1716.

Hammer,J.M., and Wen,C.P. 1967. J. Chem. Phys. 46, 1225.

Hippler,R., and Schartner,K-H. 1974. J.Phys. B, 7, 1167.

Imre,A.I., Dashchenko,A.I., Zapesochnyi,I.P., and Keltman, V.A. 1972. J.E.T.P. Lett.(Eng. Transl.) 15, 503.

Johnson,M.C. 1969. Rev. Sci. Inst. 40, 311.

Kleinpoppen,H. 1974. Invited Talk. IVth. Int. Conf. Atom. Phys. Heidelberg.

Kleinpoppen,H., Blum,K., and Standage,M.C. 1975. Invited progress report, IXth. ICPEAC Conference.

Kim,Y.K., and Inokuti,M. 1968. Phys. Rev. 175, 176.

King,G.C.M., Adams,A., and Read,F.H. 1972. J.Phys. B, 5,254.

Kjollerstrom,B., Moller,N.H., and Svensson,H. 1965.Ark. Fys. 29, 167.

Koozekanani,S.H. 1965. IEEE. J. Quantum Electronic. 2, 770.

Koster,G.F., Statz,H., and Tang,C.L. 1968. J. Appl. Phys. 39, 4045.

Latimer,I.D., and St.John,R.M. 1970. Phys. Rev. A, 1, 1612.

Lawrence,G.M. 1968. Phys. Rev. 175, 40.
——— 1969. Phys. Rev. 179, 134.

Lotz, W. 1967. Z. Phys. 206, 205.

Luyken,B.F. J. 1972. Physica 60, 432.

Luyken, B.F.J., De Heer,F.J., and Baas,R.C. 1972. Physica, 61, 200.

Macek,K., and Jaecks,O.H. 1971. Phys. Rev. 174, 2288.

Madden,R.P., Ederer,D.L., and Coding,K. 1969. Phys. Rev.177,136.

McConkey,J.W., and Latimer,I.D. 1965. Proc. Phys. Soc. 86, 745.

McConkey,J.W., and Donaldson,F.G. 1973. Can.J. Phys. 51, 914.

McConkey,J.W., and Preston,J.A. 1973. Abstr. 8th Int, Conf. Phys. Electron. At. Collisions,(Inst. Phys.,Belgrade) 1, 273.

McConkey,J.W., Crowe,A., and Hender,M.A. 1972. Phys. Rev. Lett. 29, 1.

McGuire,E.J. 1971. Phys. Rev. A, 3, 267.

Metcalf,H., and Baird,J.C. 1966. Appl. Optics 5, 1407.

Minnhagen,L. 1963. Arkiv Fysik, 25, 203.

Mumma,M.J., Misakian,M., Jackson,W.M., and Faris,J.L. 1974. Phys. Rev. A, 9, 203.

Peach,G. 1970. J. Phys. B, 3, 328.

Preston,J.A., Hender,M.A., and McConkey,J.W. 1973. J. Phys. E: Sci. Instrum. 6, 661.

Rudko,R.I., and Tang,C.L. 1967. J. App. Phys. 38, 4731.

Schram,B.L. 1966. Physica, 32, 197.

Schram,B.L., Boerboom,A.J.H., and Kistemaker, J. 1966. Physica, 32, 185.

Sharpton,F.A., St. John,R.M., Lin,C.C., and Fajen,F.E. 1970. Phys. Rev. A, 2, 1305.

Shumaker,J.B.Jr., and Popenoe,C.H. 1969. J.Opt. Soc. Amer.,59,980.

Spear,D.P., Fischbeck,H.J., and Carlson,T.A. 1974. Phys. Rev. A9, 1603.

Statz,H., Horrigan,F.A., Koozekanani,S.H., Tang,C.L., and Koster, G.F. 1965. J.Appl. Phys. 36, 2278.

Striganov,A.R., and Sventitskii,N.S. Table of Spectral line of Neutral and Ionized Atoms (Plenum, New York, 1968).

Tan,K.H., and McConkey,J.W. 1974. Phys. Rev. A,10, 1212.
——— 1974. J. Phys. B7, L183.

Thomas,L.D., Csanak,G., Taylor, H.S., and Yarlagadda,B.S. 1974. J. Phys. B: Atom. Molec. Phys. 7, 1719.

Van Raan,A.F.J. 1973. Physica, 65, 566.

Van Raan,A.F.J., De Jongh,J.P., and Van Eck,J.1971 . Abstr. 7th Int. Conf. Phys. Electron At. collisions, (North Holland, Amsterdam), 2, 704.

Van Raan,A.F.J., De Jongh,J.P., Van Eck,J., and Heideman,H.G.M. 1971. Physica, 53, 45.

Vriens,L., and Carriere,J.D. 1970. Physica, 49, 517.

Vriens,L. 1966. Proc. Phys. Soc. 89, 13.

Walker,K.G., and St. John,R.M. 1972. Phys. Rev. A, 6, 240.

Weigold,E., Hood,S.T., and Teubner,P.J.O. 1973. Phys. Rev. Lett. 30, 475.

Zhukov,I.G., Zapesochnyi,I.P., and Feltsan,P.V. 1972. Opt. Spectrosc.(Eng. Transl.), 32, 569.

VITA AUCTORIS

I was born in Malaysia on 9th of May 1944. In May 1968 I graduated from Nanyang University (Singapore) with a B.Sc. in physics. In september 1970, I began graduate work in physics at Lakehead University (Thunder Bay), and I obtained my M.Sc. degree in 1973. In september 1972, I began to work for my Ph.D. degree at the University of Windsor.

PUBLICATIONS

1. Excitation of the $3s3p^6\ ^2S$ and $3s^23p^44s\ ^2P$ Levels of Ar^+ and the 736 Å line of Ne by electrons.
K-H Tan, F.G.Donaldson and J.W.McConkey. Can. J.Phys. vol. 52, No. 9, p786, 1974.

2. Configuration interaction effects in Ar^+.
K-H Tan and J.W.McConkey. J. Phys. B: Atom. Phys., vol. 7, No. 6, L183 (1974)

3. Simultaneous ionization and excitation of Ar by electrons with particular attention to configuration-interaction effects.
K-H Tan and J.W.McConkey. Phys. Rev. A. vol. 10, No. 4, p1212, 1974.

4. Electron impact excitation and ionization of Ar.
K-H Tan J.W.McConkey. Bull. Amer. Phys. Soc. 19, 1194, 1974.

5. Electron-photon coincidence measurements of Rare gas line excitation.
K-H Tan and J.W.McConkey. Phys. in Canada. vol. 31, No. 3, 28, 1975.

6. Electron-photon coincidence studies in He and Ar.
J.W.McConkey, K-H Tan, P.S.Farago and P.J.O.Teubner. IX I.C.P.E.A.C. Seattle, vol. 2, 1144 (1975).